INVESTIGATION OF TEMPORAL AND SPATIAL VARIATION OF CARBON MONOXIDE IN THE SOUTHERN HEMISPHERE

Under the supervision of **Dr. S.H. Mthembu**

Ladis M. Bahige

A thesis presented for the degree of
Master of Science in Physics

School of Chemistry and Physics
College of Agriculture, Engineering, and Science
South Africa
2025

Investigation of Temporal and Spatial Variation of Carbon Monoxide in the Southern Hemisphere

Under the supervision of **Dr. S.H. Mthembu**

Ladis Bahige

A thesis presented for the degree of
Master of Science in Physics

School of Chemistry and Physics

College of Agriculture, Engineering, and Science

University of KwaZulu-Natal

Pietermaritzburg, South Africa

2025

Signature: ..  .....
Ladis Bahige

PREFACE

The research contained in this dissertation/thesis was completed by the candidate while in the Discipline of Physics, School of Chemistry and Physics of the College of Agriculture, Engineering and Science, University of KwaZulu-Natal, Pietermaritzburg campus, South Africa. The research was financially supported by my family.

The content of this work is originally mine and has not been submitted in any form to another University. However, the work of other authors used in this study are duly referenced and acknowledged in the text, while the results reported are absolutely a product of investigations carried out by me.

Signature:[redacted]..... Date:March 20th, 2025

Ladis Bahige

Signature:[redacted].. Date:March 20th, 2025

Dr. Sibusiso H. Mthembu

DECLARATION

I, **LADIS BAHIGE**, declare that

1. The research reported in this desertation, except where otherwise indicated, is my original research

2. This dissertation has not been submitted for any degree or examination at any other university

3. This dissertation does not contain other persons' writting, unless spscifically acknowledged as being sources from other researchers. Where other written sources have been quoted, then:

   (a) Their words have been rewritten but the general information attributed to them has been referenced

   (b) Where their exact words have been used, then their writting has been placed in italics and inside quotation marks, and referenced.

4. This dissertation does not contain, text, graphics or tables copied and pasted from the internet,unless specifically acknoledged, and the source being detailed in the dissertation and in the referencies sections

Signed (Student):..[redacted]..... on this 20th of March 202 5

I hereby certify that this statement is correct.

Signed (Supervisor):..... on this 20th of March 2025

ACKNOWLEDGEMENTS

I would like to express my profound gratitude to my supervisor Dr. Sibusiso H. Mthembu for his fruitful advice and contributions towards the successful completion of this thesis. His wealth of experience, patience, and guidance throughout the period of this research has been of great help. I am also grateful to the University of KwaZulu-Natal for providing a conducive environment for this research work to be carried out.

My immense thanks go to Prof. Jon Rash for his much needed help with editing this work.

I would also like to express my sincere gratitude to my family for their financial and emotional support.

Finally, all glory and praise to the Lord God almighty.

Abstract

Carbon monoxide (CO) is a colourless, odourless, and tasteless gas. It is also poisonous. CO is a trace gas in the Earth's atmosphere, with typical concentrations of the order of hundreds of parts per billion and a lifetime of 2 months. CO concentration, which is monitored by the Terra satellite, varies with location and time. This study focused on the Southern Hemisphere (SH), particularly South America, southern Africa and Australia, between 2005 and 2019. It had two aims: The first was to investigate the sources and seasonal concentrations of CO over these regions, and to analyse whether meridional and zonal winds play a role in CO distribution. It is believed that biomass burning, both natural and anthropogenic, is responsible for the vast majority (99%) of CO emissions. This was tested by comparing distributions of burned areas and CO concentrations. Winter months had more burned areas than summer months, with an average burned area of 1.51×10^7 m^2 compared to 8.19×10^6 m^2. Total column CO concentrations measured by the MOPITT sensor were also found to be higher during winter and spring months. Over southern Africa CO levels reached 36×10^{17} mol/cm^2 in winter, compared to 26×10^{17} mol/cm^2 in summer. Correlation analysis using Pearson coefficients and p-values showed a general positive correlation between CO emissions and burned areas, supporting the earlier conjecture. Trend analysis showed a steady decline in CO concentrations over the study period, likely due to decreases in burned area. Overlaid maps supported the idea that winds play a role in CO distribution in the Southern Hemisphere. For example, westward CO transport from Africa to South America was observed in July-August close to the equator. Then in September-October at latitudes higher than 20° S, eastward transport from South America to southern Africa and from southern Africa to Australia was observed. The second aim of this study was to investigate whether El Niño/La Niña events played a part in the distributions of CO in the SH between 2005 and 2019. These events are climate patterns related to irregular warming/cooling of the ocean surface in the central and eastern tropical Pacific Ocean. A La Niña phase, an El Niño phase and an intermediate neutral phase were identified during the study period, and their CO distributions, burn areas and precipitation levels were compared. In the SH El Niño causes below-average rainfall and the drier conditions lead to increased burning and above-average CO levels. La Niña causes above-average rainfall and the wetter conditions lead to reduced burning and below-average CO levels. The neutral phase displayed near-average conditions as expected.

LIST OF ACRONYMS

CO: Carbon monoxide
ppb: parts per billion
COHb: carboxyhemoglobin
NH: Northern Hemisphere
SH: Southern Hemisphere
ENSO: El Nino -Southern Oscillation
SAM: Southern Annular Mode
CO_2: carbon dioxide
EF: emission factor
ARDS: Acute respiratory distress syndrome
ROS: reactive oxygen species
OH: hydroxide
ppm: parts per million
UNFCCC: United Nations Framework Convention on Climate Change
SAM: Southern Annular Mode
NOAA: National Oceanic and Atmospheric Administration
MERRA: Modern-Era Retrospective analysis for Research and Applications
MODIS: Moderate Resolution Imaging Spectroradiometer
MOPITT: Measurements of Pollution in the Troposphere
IDL: interface definition language
CSA: Canadian Space Agency
CH_4: methane
0_3: ozone
HO: hydroxyl radicals
EOS: Earth Observing System
CDF: cumulative distribution function
SOI: Southern Oscillation Index
IOD: Indian Ocean Dipole
SST: sea surface temperatures

Contents

List of Figures

List of Tables

1 Introduction

Carbon monoxide (CO) is a gas that is odorless, colorless and tasteless. It can however be very dangerous. The Earth's atmosphere contains relatively small amounts of carbon monoxide. In the troposphere, the average concentration of carbon monoxide is approximately 100 parts per billion (ppb), or one hundred molecules of CO in every billion air molecules. However, in particularly clean air, concentrations of CO can be as low as 50 ppb. Carbon monoxide emissions emanate from different sources: biomass burning, burning of propane, gasoline, wood, charcoal, as well as other fuels. Bush fires and other vegetation fires produce CO due to the fuel type and burning efficiency, i.e. the lack of enough oxygen during combustion leads to the production of CO. It is also produced by other natural processes such as biotransformation of halomethanes within the human body [1, 2, 3, 4, 5].

CO can be highly poisonous to humans. When externally exposed to large amounts of CO, negative health effects can occur and can even lead to death. Exposure to high levels of CO leads to the formation of carboxyhemoglobin (COHb) in the human body, which weakens the oxygen-carrying capacity of the blood (hemoglobin), and therefore causes health complications. Some of these include cardiovascular diseases, acute pulmonary diseases, and cerebrovascular diseases. Another major health effect caused by the exposure to CO is carbon monoxide poisoning. It is caused by high levels of carboxyhemoglobin (10 to 30%) in the body. And at levels higher than 50%, carbon monoxide poisoning may cause coma [2]. Carbon monoxide is a stable diatomic gas molecule in the atmosphere. It consist of a triple covalent bond between bond between one carbon and one oxygen atoms. Carbon monoxide is a trace gas that has a lifetime of about 2 months [2, 4, 5].

The focus of this thesis is the Southern Hemisphere region, namely South America (12°N-55°S and 35°W–81°W), Southern Africa (22°S-35°S and 17°E-33°E) and Australia (10°-44°S and 112°E-154°E). This is because the sources and dynamics of CO have received a lot of attention in the Northern Hemisphere while the Southern Hemisphere has received less attention overall. Additionally, because of its distinct characteristics and intricate interplay of its many elements, the Southern Hemisphere is an area of essential relevance in the dynamics of CO around the world. However, investigations on CO concentrations in the Southern Hemisphere are presented with a special mix of difficulties and challenges because of the varied sources and atmospheric circulation patterns that influence it [6, 7]. This thesis seeks to provide a thorough analysis of CO concentrations in the Southern Hemisphere, giving insight into the causes, geographical and temporal fluctuations, and potential implications for both local and global environments.

As a greenhouse gas and contaminant, the colorless, odorless gas CO is essential to the Earth's atmosphere. For the purpose of tackling global environmental concerns, it is crucial to comprehend the concentration and distribution of CO in the Southern Hemisphere. Therefore, in addition to exploring the complex dynamics of CO concentration in the Southern Hemisphere (SH) with a focus on its origins, this thesis also explores the effects of global wind circulations, and the role that the El Nino effect plays in CO distributions in the SH. Due to its unique characteristics and connection to the global climate system, the Southern Hemisphere requires a thorough analysis of CO dynamics in order to better understand and reduce its environmental effects.

1.1 Spatial and Temporal Variations in CO Concentrations

CO levels in the SH vary significantly throughout both time and space. CO concentrations vary spatially with distance from emission sources and are impacted by atmospheric transport processes. Regional hotspots in CO concentration have been identified by high-resolution satellite measurements, such as those over southern Africa and sections of South America during significant biomass burning events. Temporally, CO concentrations are affected by seasonal fluctuations, peaking in the austral winter when biomass burning is more common. Assessing the effect of CO on local air quality and the global climate requires a thorough understanding of these fluctuations [8, 9].

1.2 Remote Sensing and Data Availability

The development of remote sensing technologies has tremendously aided in the study of CO concentrations in the Southern Hemisphere. Global coverage CO level data has been made available by satellite-based equipment, such as those aboard NASA's AURA satellite. Researchers can track CO concentrations at various altitudes and spatial scales thanks to these data sources. These observations provide a thorough understanding of CO dynamics when combined with ground-based monitoring stations. In remote areas of the Southern Hemisphere, data availability and quality might still be problematic, highlighting the necessity of continued study and data validation initiatives [10].

1.3 Sources of Carbon Monoxide in the Southern Hemisphere

In the SH, CO is produced both naturally and artificially, with wildfires being one of the main producers. Because biomass is burned during wildfires, a significant amount of CO is released into the atmosphere. These flames are common in places like Australia, South America, and southern Africa because of the dry, hot weather that encourages the start and spread of wildfires in these areas. High CO concentrations in the atmosphere are also caused by anthropogenic causes, including industrial activities, automobile emissions, and burning biomass for land clearing. The regional and temporal distribution of CO in the SH is influenced by these sources taken as a whole [11, 12].

1.4 Global Wind Circulations and their Effects on CO Distributions

The distribution of CO in the Southern Hemisphere is significantly influenced by the global wind circulations, particularly the zonal (east to west or west to east) and meridional (north to south or south to north) winds. These wind patterns play a key role in the long-distance transfer of CO and other pollutants. The longitudinal transport of CO is influenced by the zonal winds, including the westerlies and trade winds. This affects how the gas is distributed over various longitudes. For instance, the trade winds transport air masses high in CO from the Eastern Hemisphere to the Southern Hemisphere, affecting the overall CO burden there [13].

The north-south transport of atmospheric gases is governed by meridian winds, which are influenced by latitudinal temperature gradients. The polar vortex, which traps air in the polar area during the Southern Hemisphere's winter and affects the distribution of CO, is a distinctive feature of the Southern Hemisphere. The polar vortex decreases during the austral summer, allowing air masses to move between the polar and mid-latitudinal areas. Seasonal and regional fluctuations in CO concentration in the Southern Hemisphere are influenced by the intricate interactions between zonal and meridional winds [14].

1.5 El Niño and its Impact on Carbon Monoxide in the Southern Hemisphere

El Niño is a climate phenomenon that affects the patterns of atmospheric circulation all over the world. It is defined by the recurrent and unusual rising of sea surface temperatures in the tropical Pacific Ocean. CO concentrations are impacted by the El Niño -Southern Oscillation (ENSO), which has extensive influence on the temperature and weather of the Southern Hemisphere. The Southern Hemisphere undergoes a variety of climatic abnormalities, including altered rainfall patterns, protracted droughts, and elevated temperatures, during El Niño occurrences, which irregularly occur every two to seven years. These circumstances foster a climate that is conducive to wildfires, which causes the release of CO and other pollutants into the sky [15].

El Niño also interferes with the Southern Annular Mode (SAM), which can affect CO movement and distribution in the Southern Hemisphere, and other regular atmospheric circulation processes. The movement of air masses between the polar region and mid-latitudes may be impacted by variations in the polar vortex's position and strength, as well as by changes in the southern westerlies. These changes in atmospheric circulation patterns may cause the polar vortex to move further north, perhaps trapping CO-rich air in the Southern Hemisphere. Determining and forecasting variations in CO concentration in the Southern Hemisphere therefore requires an adequate understanding of the El Niño effect [16].

1.6 Importance of Studying CO in the Southern Hemisphere

In addition to being an academic work, researching CO concentrations in the Southern Hemisphere has important ramifications for tackling environmental problems on a global scale. CO can cause air quality to deteriorate, which has an effect on ecosystems and human health. CO is a precursor to the production of ground-level ozone. Additionally, because CO is a greenhouse gas, changes in its concentration can have an impact on the radiative balance of the Earth's atmosphere. Enhancing regional air quality, mitigating the effects of climate change, and informing CO emission reduction policies and plans can all be aided by a better knowledge of CO dynamics in the Southern Hemisphere [17].

1.7 Chemistry

Carbon monoxide is a stable diatomic gas molecule in the Earth's atmosphere. It is made up of one carbon atom joined together with one oxygen atom in a triple covalent bond, as shown in Figure 1 [5].

Figure 1 illustrates four different ways in which CO can be chemically represented. In the models, the gray part represents the carbon atom and the red represents the oxygen atom. CO has a low electric dipole moment of 0.10 debye, a short interatomic distance of 0.123 nm, and a high bond strength of 2072 kJ/mol. Also, CO absorbs radiation in the infrared region that corresponds to the vibrational excitation of its electronic ground state. Table 1 gives additional general properties of CO [2].

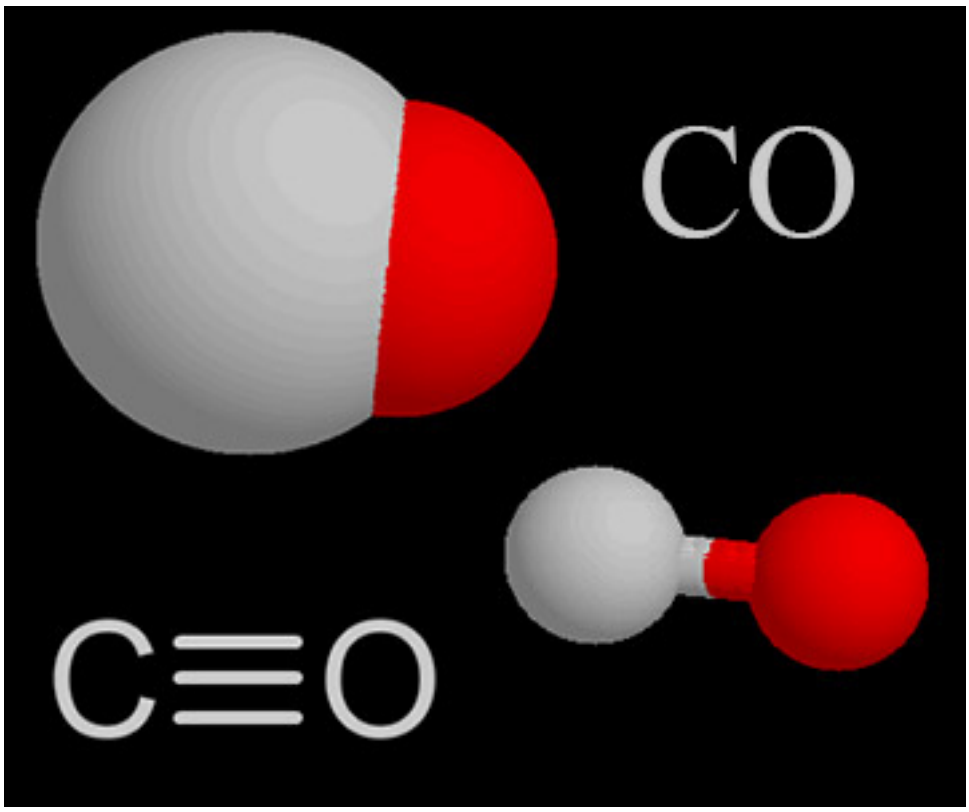

Figure 1: 4 different representations of a carbon monoxide molecule
Credit: UCAR, Center for Science Education

Properties	Value
Molecular weight	28.01
Critical point	140° C at 3495.7 kPa
Melting point	199° C
Boiling point	191.5° C
Density: at 0° C 101.3 kPa at 25° C 101.3 kPa	 1.250 g/litre 1.145 g/litre
Specific gravity relative to air	0.967
Solubility in water: at 0° C at 20° C at 25° C	 3.54 ml/100 ml(44.3 ppmm)[a] 2.32 ml/100 ml(29.0 ppmm)[a] 2.14 ml/100 ml(26.8 ppmm)[a]
Explosive limits in air	12.5–74.2%
Fundamental vibration transition	2143.3 cm^{-1}
Conversion factors: at 0° C 101.3 kPa at 25° C 101.3 kPa	 1 mg/m^3 = 0.800 ppm[b] 1 ppm = 1.250 mg/m^3 1 mg/m^3 = 0.873 ppm[b] 1 ppm = 1.250 mg/m^3

[a] ppmm = Parts per million by mass
[b] Parts per million by volume (ppm = mg/litre)
Table 1: Additional properties of carbon monoxide.

1.8 Sources of Carbon Monoxide

A great debate has been going on for decades about whether most of the CO emitted is produced by natural or human activities. However, it is widely accepted that natural processes contribute to about 40-50% of the CO produced in the non-urban troposphere, while human activities are responsible for the remaining $60 - 50\%$. Combustion processes produce about 40% of CO emitted annually, and oxidation of hydrocarbons, together with other sources such as oceans and vegetation, account for most of the remaining 60%. It is estimated that annually, the total carbon monoxide production from humans and natural sources is between 2 and 5 gigatons (with an average of 2.6 gigatons per year) [2, 5].

In the atmosphere, CO is produced when hydroxyl radicals react with methane and other hydrocarbons, produced by both natural and antropogenic activities. CO is also produced the reaction of isoprene and terpenes with hydroxyl radicals and ozone, and as well by the reaction of alkene with ozone [2]. On earth's surface, CO is produced during the combustion of fuels. Two primary byproducts are produced due to the burning of any carbonaceous fuel: carbon dioxide (CO_2) and carbon monoxide. When the oxygen supply is in excess of the stochiometric need for complete combustion, CO_2 is produced more abundantly. And when the process takes place under fuel-rich conditions with less oxygen than needed, the production of CO is more predominant. There are four basic variables that control the concentration of carbon monoxide produced from all hydrocarbon fuels combustion: Oxygen concentration, combustion chambre turbulence, flame temperature and gas residence time at high temperature [2].
Emission sources of CO are divided into five different categories: Transportation, stationary source fuel combustion, industrial processes, solid waste disposal and miscellaneous. Transportation sources consist of emissions from all mobile sources, highway or onroad vehicles such as cars and motorcycles; off-highway or nonroad vehicles such as aircrafts, locomotives, vessels, farming engines, construction machinery, snowmobiles, etc. [2, 18]

Stationary combustion equipment include fire heating of coal, gas or pil, or power generating plants. They emit carbon monoxide due to improper operating practices or inefficient combustion techniques. The corresponding emission factor (EF) for the stationary fuels combustors depend on the type and size of of the installation and the fuel used, as well as the mode of operation [2]. An emission factor is a coefficient that indicates how quickly greenhouse gases (GHGs) are released into the atmosphere as a result of a specific activity. It is used to estimate a source's emission and is usually expressed by the following equation:

$$\mathrm{EF} = \frac{\mathrm{W}}{\mathrm{A}} \tag{1}$$

where W is the weight of the pollutant and A can either be a unit weight, volume, distance, or duration of the activity emitting the pollutant. As an example, the emission factor of CO can be taken as pounds of CO emitted per ton of coal burned [19].

Industrial processes include emissions from metal, cement, plaster and concrete manufacturing, electricity supply, mining coal and metal ore, land or sea oil and gas extraction, production of chemicals, and food manufacturing. Also, CO is emitted in industrial plants though the combustion of coal and natural gas [20]. Solid waste carbon monoxide emissions are due to the combustion of wastes in municipal and other incinerators, and the open burning of domestic and municipal refuse [2]. Miscellaneous CO emissions are caused by the burning of forest and agricultural materials, as wells as smouldering coal refuse materials and structural fires. For example, fires such as those in the Amazon and the Southeast Asian territory, are a major source of of carbon monoxide emission (and pollution) in many regions in the southern hemisphere

[2, 6].

The biggest source of antropogenic CO is highway vehicles. In the USA for example, an estimated 50% of all CO emitted nationally in 1990, was attributed to highway vehicles [1, 2]. CO sources are also found in indoor settings through emissions from different sources as well as in the infiltration or ventilation air from outdoors. The indoor concentration depends on a complex interaction of a variety of interrelated factors such as the type, nature, number and characteristics of sources. These factors also affect the introduction, dispersion and removal of carbon monoxide. Usually, source emissions from indoor combustion are characterized by emission rates, represented in migrograms per kilojoules, i.e. the mass of pollutant emitted per unit of fuel input [2].

The major sources of indoor CO emissions include coal or wood burning stoves, cigarette combustion, gas cooking stoves, unvented or improperly vented machines such as kerozene space heaters and gas space heaters, and unvented or poorly vented gas appliances [2, 21]. Indoor sources can be accidental or unintentional. Examples of such sources include faulty or leaky flue pipes, poor use of combustion sources such as the use of a poorly maintained kerozene heater, etc.[2].

1.9 Population Exposure to CO and Health Effects

As urban areas constitute one of the numerous sources of CO emissions, people can be exposed to CO in many ways in everyday life: while at their places of work, while using motor vehicles, cooking or heating with wood or other fuel fires, or being around areas that are major combustion sources (areas such as high traffic areas or industrial areas), etc [22, 23] . The typical level of CO in urban areas is approximately 10 ppm, which is around 100 times higher than the overall atmospheric levels (about 100 ppb). But in areas with high traffic, the level can go as high as 50 ppm, and at some workplaces or in some homes, CO concentrations can exceed 100 ppm, usually leading to carboxyhemoglobin levels of at least 10% [2, 5].

CO is not a necessary threat to plants, since it is quickly oxidized into CO_2 which is used for photosynthesis. It is however a very poisonous gas to humans and animals as they primarily need oxygen to breathe. This is because hemoglobin, the protein in the blood responsible for carrying oxygen from the lungs to cells throughout the body, is more than 200 times more likely to bind with CO than with oxygen. Thus, people breathing in high amounts of CO will likely result in their hemoglobin binding with it, hence blocking oxygen from reaching the cells. When hemoglobin binds with CO, a stable complex of CO called carboxyhemoglobin (COHb) is produced in the red blood cells. The normal percentage of COHb is less than $1-2\%$ of total hemoglobin. Because of its inability to carry oxygen, COHb is called dyshemoglobin [2, 5, 18]. A good number of negative health effects, some of which will be discussed next, can result as a consequence of exposure to high amounts of CO, especially exposure taking place in confined spaces. Some of those health effects include cardiovascular, acute pulmonary, cerebrovascular, and behavioral effects.

1.9.1 Cardiovascular Effects

Significant cardiovascular abnormalities can result from prolonged exposure to high doses of CO. The development of COHb, which occurs when CO binds to hemoglobin in red blood cells and lowers the blood's ability to carry oxygen, is a crucial component in CO poisoning. Tissue hypoxia results from this, which sets off a compensatory reaction that raises heart rate and cardiac output to meet the body's oxygen requirements. While there is not a single

CO threshold value that consistently affects cardiovascular health, symptoms typically appear at COHb levels greater than 10% and worsen with increasing COHb levels [24, 25]. Studies have demonstrated that CO exposure can affect blood vessel endothelial function, resulting in endothelial dysfunction. This dysfunction can exacerbate hypertension and raise the chance of having cardiovascular problems like heart attacks and strokes. While there can be variation across people, continuous exposure to CO levels above 9 ppm (8-hour time-weighted average) is linked to a higher risk of hypertension [26, 27].

1.9.2 Acute Pulmonary Effects

Exposure to CO can have immediate respiratory effects, especially in cases of excessive exposure. CO competes with oxygen for binding sites on hemoglobin, making the respiratory system susceptible to its harmful effects. High CO concentrations can cause tissue hypoxia in the lungs, which can cause respiratory discomfort and even severe respiratory failure. COHb levels above 20% may cause symptoms including coughing, shortness of breath, and chest pain, while levels above 30% are more likely to cause serious pulmonary consequences [28, 29]. Additionally, CO's irritating qualities can cause respiratory tract inflammation, aggravating pre-existing lung diseases and raising the risk of infections. Acute respiratory distress syndrome (ARDS) and pulmonary edema can result from exposure to CO at values above 1500 ppm, demanding emergency medical attention [30].

1.9.3 Cerebrovascular Effects

The brain has a high oxygen requirement and is sensitive to hypoxia, making it particularly vulnerable to the consequences of CO exposure. Cerebral hypoxia results from the reduction in oxygen delivery to the brain caused by CO's binding to hemoglobin. This may result in neurological symptoms such as disorientation, vertigo, migraines, and cognitive impairment. Although there is significant individual variation, symptoms frequently appear when COHb levels exceed 20% [31, 32]. In addition to the direct consequences of hypoxia, CO exposure can cause the release of reactive oxygen species (ROS) in the brain, which can cause oxidative stress and damage to neuronal cells. Seizures, loss of consciousness, and even coma may occur as a result of prolonged or severe exposure, along with other more serious cerebrovascular effects. Researchers have discovered that exposure to CO levels as low as 9 ppm might cause minor cognitive impairment, whereas concentrations of 200 ppm can cause confusion and headaches found that CO concentrations above 1000 ppm can result in seizures and unconsciousness. It's crucial to highlight that people who already have neurological problems may be more vulnerable to these effects [33, 34].

1.9.4 Behavioural Effects

Chronic and acute behavioural impacts of CO exposure are also possible. Acute exposure to high CO levels can affect one's mood and cognitive ability. People who have been exposed to CO may exhibit symptoms like irritation, disorientation, and poor judgment. When CO exposure happens in situations requiring quick decisions and focus, like while driving, these behavioural alterations might have catastrophic repercussions. Individual differences exist in the specific CO values linked with acute behavioural consequences, however, symptoms frequently appear at COHb levels of more than 15% [34, 35]. Additionally, persistent behavioural changes might result from prolonged exposure to low levels of CO, such as those observed in indoor environments with defective heating systems. Chronic CO exposure has been linked in some studies to mental decline and a higher risk of psychiatric illnesses like sadness and anxiety.

Despite the fact that there is no exact threshold for chronic behavioural impacts, it is crucial to minimize CO exposure to avoid these long-term effects [36].

1.10 Effects of Biomass Burning on the Environment

Large amounts of pollutants, such as particulate matter, carbon monoxide, nitrogen oxides, and volatile organic compounds, are released into the atmosphere when biomass is burned. Due to their negative effects on air quality, these pollutants can cause respiratory issues as previously mentioned, cardiovascular ailments, and decreased visibility. Due to biomass burning events, the southern hemisphere frequently sees severe haze and smog occurrences [37]. Southern hemisphere biomass burning makes a sizable contribution to global greenhouse gas emissions. It releases powerful greenhouse gases as carbon dioxide (CO_2), methane (CH_4), and nitrous oxide (N_2O). Biomass burning produces carbon dioxide which adds to long-term carbon emissions and is believed to accelerates climate change [38, 39, 40].

The SH's biodiversity and ecosystems are also severely impacted by biomass burning. It causes ecosystems to be destroyed, vegetation to disappear, and species to be displaced. Fires have the potential to change ecological processes, sever ecological connections, and lessen total species diversity [37]. Also, for southern hemisphere societies, the smoke and toxins that result from biomass burning have serious negative health effects. Smoke exposure can lead to cardiovascular problems and respiratory conditions including asthma and bronchitis. The negative effects of biomass burning on health frequently have a disproportionately large impact on indigenous people [34].

1.11 Conclusion

In conclusion, the purpose of this thesis is to advance our understanding of the dynamics of CO in the SH. This study aims to shed light on the intricate CO dynamics in this area by examining the sources, geographical and temporal fluctuations, and the function of atmospheric circulation patterns. Understanding CO behavior in the Southern Hemisphere is of utmost importance given the growing urgency of solving air quality and climate change challenges.

Additionally, the SH serves as a good and interesting focus for research on CO dynamics because of its distinctive features. Wildfires and anthropogenic emissions are just two of the sources of CO in this hemisphere that have a big impact on the level of CO in the atmosphere. The distribution of CO across latitudes and longitudes is additionally influenced by the complex interplay of zonal and meridional wind circulations. The impact of the El Niño effect, a well-known climate phenomenon, on air circulation patterns has a significant impact on CO concentrations. The ultimate purpose of this thesis is to advance our understanding of carbon monoxide in the Southern Hemisphere in order to better solve environmental and climate-related problems. This thesis will delve into these elements to provide a thorough understanding of carbon monoxide in the Southern Hemisphere.

2 Literature Review

2.1 Spatial and Temporal Variations in CO Concentrations

The sources and amounts of atmospheric CO vary in different areas of the world as well as in different seasons. For instance, in Europe, the US, and eastern China, CO concentrations are highest in and around urban areas due to vehicle and industrial emissions. In Africa, CO seasonal shifts are related to the widespread and shifting agricultural burning, which shifts north and south of the Equator with the seasons [4]. In the northern hemisphere, the CO concentration decreases significantly in June, July, and August, which correspond to summer months. Hot temperatures imply that air carries more moisture, resulting in more hydroxide (OH), and hence destroying carbon monoxide faster in summer. But in those same months (June, July, and August) in the SH, which correspond to winter months, CO concentrations are higher than the summer months (December, January, and February) concentrations [4, 41].

Generally, there is an obvious difference in CO concentrations between the northern and the southern hemispheres. The concentrations in the north are higher than those in the south. This is because the north has more sources of emission due to the fact that more fossil fuel emissions occur in the northern hemisphere. And because CO has a short lifetime of about 2 months, it cannot reach fast enough the equator and is consequently destroyed before it equilibrates with the concentrations in the southern hemisphere [41].

CO concentrations have decreased since 2000. The decrease is particularly more noticeable in the NH. This decline in concentrations, according to experts, is due to technological and regulatory progress, meaning that vehicles and industries are emitting less CO. Also, in the Southern hemisphere, where agricultural fires and deforestation are the principal sources of CO, concentrations of CO have decreased. This coincides with satellite observations of declines in the number of small fires and areas burned, noticeably in Africa, implying a decline in deforestation since 2005 [42].

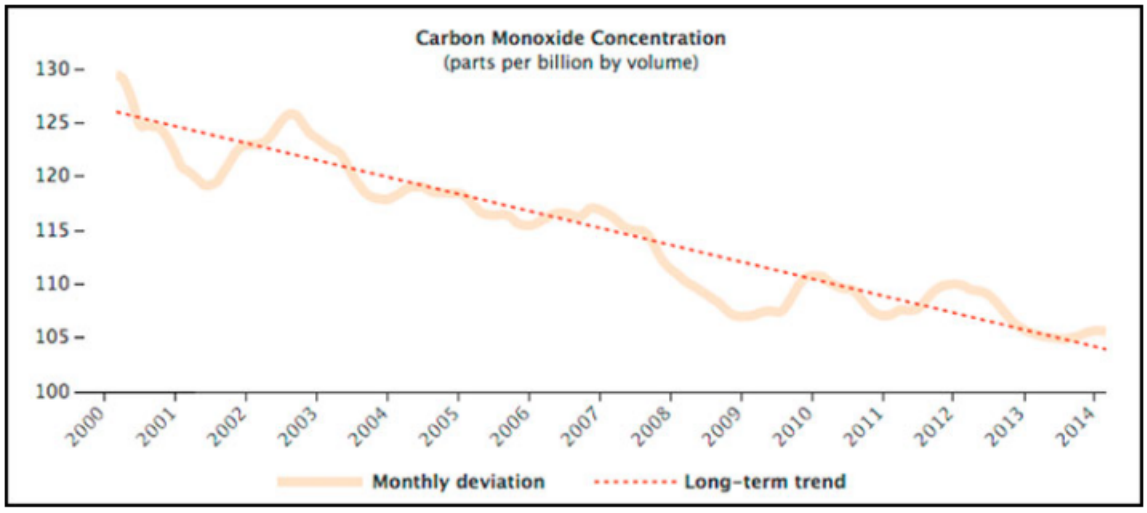

Figure 2: Carbon monoxide concentration in parts per billions from 2000-2014
Credit: MOPITT, NASA

Figure 2 is a line graph showing the global long term trend (dotted red line) and the global monthly deviation (orange line) of CO concentration in parts per billion from 2000 to 2014. On

the line graph, it can be seen that the concentration of CO has been decreasing on average in that period of 14 years. A number of peaks can however be observed, notably the one of 2002 and 2003, which is attributed by some researchers to an "unusual fire season" in the boreal forest in Russia. Also, a dip in CO emissions can be observed from 2007 to 2009, which corresponds to a decrease in global fire emissions and, according to some researchers, it also corresponds to the global financial crisis that began in late 2008, causing a decline in manufacturing output [42]

Tropospheric CO concentrations are typically about 100 ppb (parts per billion), but concentrations in clean air can be as low as 50 ppb. In typical urban areas, CO concentrations are about 10 ppm (parts per million: 1 ppm = 1.1 mg of CO/m^3), but in areas with heavy circulation, CO concentrations can go as high as 50 ppm [5]. CO is not considered a (strong) greenhouse gas because it does not possess the ability to absorb thermal infrared energy strongly enough. However, it has an important but indirect contribution to the build-up of some greenhouse gases in the troposphere: It helps increase the concentrations of methane (CH_4) and ozone (0_3) by reacting with some chemicals (hydroxyl radicals (HO)) that typically destroy CH_4 and 0_3 [5, 43].

2.2 Source of CO

The burning of organic materials, or biomass, has occurred naturally for millions of years. However, due to human activity, the size and intensity of biomass burning have greatly expanded in recent decades. Biomass burning contributes significantly to the world's greenhouse gas emissions and is a key factor to the Earth's climate system. The negative effects of biomass burning on air quality, human health, and ecosystems have made it a significant environmental problem throughout the SH [44]. This section aims to look at burned areas as a result of biomass burning in the southern hemisphere. It seeks to explore the reasons behind biomass burning, evaluate its effects on the environment, look at regional variations, and briefly talk about monitoring and measurement methods.

The term "biomass burning" describes the burning of organic material, such as forest, grassland, and agricultural waste. It can be caused by both natural occurrences and human activity. Lightning strikes and volcanic eruptions are examples of natural causes, whereas deforestation, slash-and-burn farming and land clearance for urban development, and the burning of agricultural waste are examples of man-made causes [45]. The southern hemisphere's biomass burning is influenced by a diversity of variables, including climatic conditions, vegetation species, and human activities. Climate anomalies, including El Nino occurrences, can cause protracted dry spells that make biomass more flammable. The intensity and scope of biomass burning are greatly influenced by vegetation features, such as fuel load and flammability [46].

2.2.1 Biomass Burning Regional Variations in the SH

South America A significant amount of biomass is burned, especially in the Amazon jungle. The high frequency of fires in this area is a result of land removal for agriculture, illegal logging, and environmental variables. The size and effects of the Amazon rainforest fires on biodiversity and the environment, like the major occurrence in 2019 and others, have garnered attention on a global scale [47, 48, 49].

Africa In the African savannas, biomass burning is frequent. There are frequently both natural and man-made fires, with natural fires being a crucial ecological function for preserving savanna ecosystems. However, the deliberate burning of land for agricultural and pastoral

purposes frequently results in uncontrolled fires that harm ecosystems and produce significant emissions [39, 47, 48].

Australia In Australia, biomass burning incidents are common and serious, especially in the dry season. Recent Australian bushfires, like the disastrous 2019–2020 fire season, have had terrible repercussions, including the loss of life, the destruction of property, and significant environmental damage. Australia is becoming more susceptible to severe and protracted fire seasons as a result of climate change and land-use policies [47, 48, 49].

Additional Areas Although this research only focuses on the three previous regions (South America, Africa and Australia), it is important to note that biomass burning occurs in other southern hemisphere regions as well, including Southeast Asia and the Pacific Islands. Forest and peatland fires linked to land clearing and palm oil cultivation have grown to be a significant environmental problem in Southeast Asia. The distinctive ecosystems of the Pacific Islands make them prone to fires brought on by invading species, human activity, and climatic anomalies [47, 50, 51].

2.2.2 Tracking and Measuring Burned Areas

Techniques for Remote Sensing Monitoring and assessing burned areas as a result of biomass burning depends heavily on remote sensing. Satellite-based sensors, like MODIS (Moderate Resolution Imaging Spectroradiometer), offer useful information on the frequency and size of fires as well as their radiative output. Understanding the time and spatial patterns of biomass burning occurences is made easier by these data [52].

Land-based Observations Field surveys and monitoring networks are examples of ground-based observations that add to remote sensing data by giving on-the-ground data about fire behaviour, fuel qualities, and ecosystem responses. For the purpose of strengthening fire models and confirming remote sensing observations, ground-based measurements are crucial [53, 54].

Measurement and Monitoring Challenges Even with improvements in monitoring methods, it is still difficult to precisely quantify the burned areas caused by biomass burning. These difficulties include limited access to remote areas, cloud cover and smoke interference in satellite imaging, and the requirement for better cooperation and data exchange across nations [45, 55].

2.2.3 The Aftereffects of Burned Areas

By lowering the amount of organic matter in the soil, nutrient depletion, and increased soil erosion, biomass burning can cause soil deterioration. The extreme heat from fires changes the physical and chemical characteristics of the soil, altering its fertility and ability to store water [56]. Events involving biomass burning can have a negative effect on water quality and watershed management. Water bodies can become contaminated by ash and debris from burned areas, harming aquatic ecosystems and water supplies for agriculture and human consumption [37].

Biomass burning has serious negative ecological and socioeconomic effects on vegetation and forests. It impairs ecosystem functions, lessens the ability to store carbon, and results in the habitat loss of many plant and animal species. The delayed process of forest regeneration following fires exacerbates the long-term effects [37]. Indigenous peoples in the southern hemisphere frequently have close relationships to the land and depend on healthy ecosystems for

their survival. Events involving the burning of biomass obstruct customary ways of life, damage cultural assets, and can have a significant socioeconomic impact on indigenous populations [37].

2.2.4 Management and Mitigation Techniques

Strategies for managing and preventing fires are essential for reducing the effects of biomass burning. Prescribed burning, early warning systems, fire breaks, and community involvement are included in this. Including indigenous knowledge and practices in the management of fires can be extremely important [57]. To reduce biomass burning in the southern hemisphere, strategic land use planning and policies are crucial. Promoting reforestation and afforestation activities, establishing land-use zoning, and encouraging sustainable agricultural practices can reduce the likelihood of uncontrolled fires [57].

A crucial part of efficient management measures is involving the neighbourhood communities and increasing public knowledge of the effects of biomass burning. Communities are able to actively participate in fire prevention and response activities because to education programs, capacity building, and the involvement of local stakeholders [57]. International collaboration and agreements are necessary to control biomass burning. Cooperation among nations for the exchange of information, know-how, and resources can improve fire management skills. Global efforts to address biomass burning depend on programs like the United Nations Framework Convention on Climate Change (UNFCCC) and regional cooperation platforms [58].

2.2.5 Case Studies of Notable Biomass Burning Occurrences

Due to their severity and effects on biodiversity and the environment, the Amazon rainforest fires, especially the one that occurred in 2019, attracted attention on a global scale. Deforestation, changing land uses, and political and economic factors all have a role in the high frequency of fires in this area [47, 48, 49]. In the African savannas, fires are a normal component of the ecosystem and help to preserve biodiversity and the dynamics of the landscape. However, uncontrolled fires brought on by agricultural practices and land clearing provide problems for ecosystem health and carbon emissions [39, 47, 48]. The 2019–2020 fire season in Australia saw some of the worst bushfires the nation has ever seen. The intensity and size of the flames were influenced by land-use patterns, extended drought, and climate change. The incident made it clear that better fire management tactics and adaptive measures are required [47, 48, 49].

2.3 Atmospheric Winds and their Effects on CO Distribution

2.3.1 Introduction

Global wind circulations are critical in shaping the Earth's atmospheric dynamics, distributing heat, moisture, and atmospheric elements across the world. These worldwide circulation patterns have an impact on the Southern Hemisphere, which is known for its distinct atmospheric features and limited direct sources of CO [6, 13]. Understanding the complex interplay between global wind circulations and CO distributions in the Southern Hemisphere is essential to understanding climate change, air quality, and environmental policies. This section explores how wind circulation impacts CO distributions in this region.

2.3.2 Global Wind Circulation

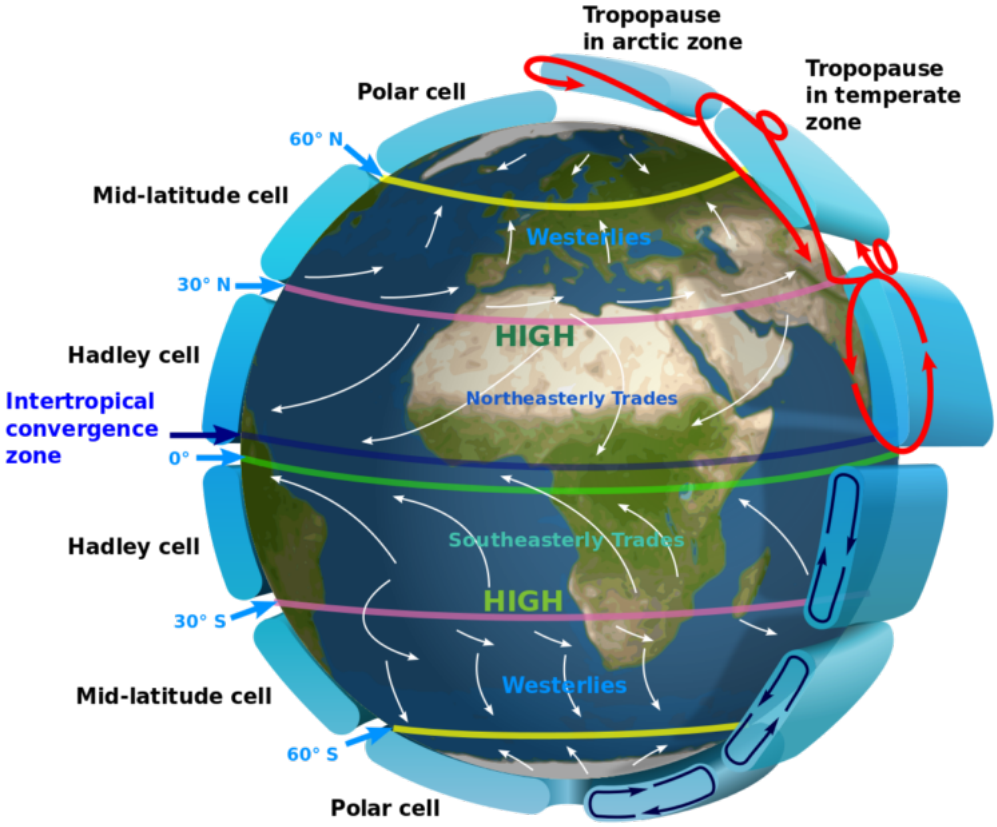

Figure 3: Earth's global wind circulation illustrating easterlies (long arrows) and westerlies (short arrows).
Credit: Lumen, Physical Geography

Global atmospheric circulation patterns are governed by a series of convection cells – with hot air rising nearer the equator and cooler air falling closer to the poles – which cause poleward and equatorward motion of air. These combine with the coriolis effect due to the Earth's rotation, which causes the motion to veer to the right in the northern hemisphere and left in the SH. This accounts for important features such as the easterly trade winds [59].

(i) The Hadley Cell

In these cells, air blows from the northeast to the southwest (NH) and from southeast to northwest (SH), forming the trade winds or easterlies. These winds are indicated by the long white arrows in Figure 3. Hadley cells extend from the equator to between 30 and 40° north and south. The trade winds blow towards and move up near the equator in the form of thunderstorms, forming the Inter-Tropical Convergence Zone (ITCZ), indicated by the blue line in Figure 3. Air flows on top of the storms towards higher latitudes, then descends to create high-pressure regions over the subtropical oceans and hot deserts such as the Sahara [60, 61].

(ii) The Ferrel Cell

In these cells, winds blow from the southwest (NH) and from the northwest (SH). These winds are known as the westerly winds, or simply westerlies, indicated by the middle white arrows in Figure 3. There is a high-pressure zone created at about 30° north and south that drives these winds poleward. Air converges in the Ferrel cell at low latitudes and rises up along the frontier of the cool polar air and the warm subtropical air. This usually occurs between 60 and 70° north and south, for example around the latitude of the United Kingdom. Due to the fact

that the Ferrel cell is driven by the circulations in the polar and Hadley cells, it moves in the opposite direction to the two cells [60, 61].

(iii) The Polar Cell

Polar cells extend from between 60 and 70° north and south, to the poles. At the poles, temperatures are low. Because of this, the air becomes dense and sinks, creating a high-pressure zone. This causes the winds in these cells to travel equatorward, i.e. from the northeast in the northern hemisphere and from the southeast in the southern hemisphere, and are called the polar easterlies, indicated by the short white arrows in Figure 3. In other words, air ascends over the highest latitudes, and then flows towards the lower latitudes [60, 61].

2.3.3 Southern Hemisphere CO Distributions

Compared to the NH, the SH has fewer direct sources of CO emissions. There is less manufacturing, less human density, and a comparatively unspoiled environment, which all contribute to lower CO concentrations. However, local emissions are not the only factor influencing the distribution of CO in the Southern Hemisphere. The Hadley cell and subtropical jet streams, as well as long-range transport and global atmospheric circulation patterns, are important factors that shape CO distributions in this region [62].

2.3.4 Role of the Hadley Cell

One of the main forces behind global wind circulations, the Hadley cell is essential for transferring CO and other elements of the atmosphere. CO and other trace gases are carried by the warm, humid air that ascends close to the equator. Precipitation and cloud formation accompany this upward motion, which helps remove CO from the upper atmosphere. Consequently, at the mid-latitudes, the subtropics' descending dry air makes it easier for CO to be transported toward the Earth's surface. The Southern Hemisphere's CO distribution pattern is influenced by these dynamics [59].

2.3.5 Influence of Subtropical Jet Streams

CO distributions in the Southern Hemisphere are also influenced by subtropical jet streams, which are a part of the Hadley cell circulation. These extremely fast winds in the upper atmosphere move CO and other atmospheric components across latitudes as a means of transportation. During specific times, the subtropical jet streams may contribute to higher CO concentrations in the Southern Hemisphere by helping to spread CO from its sources in the Northern Hemisphere [59].

2.3.6 Seasonal Variations in CO

Shifts in wind patterns impact seasonal fluctuations in CO concentrations. There is an increase in CO movement from the Northern Hemisphere to the Southern Hemisphere during the austral summer, when the Hadley cell moves southward. This can result in higher CO concentrations, which can have an impact on regional air quality. Moreover, fluctuations in the Southern Annular Mode (SAM) or other anomalies in wind circulation patterns can influence seasonal variations in CO [59, 63].

2.3.7 Conclusion

The global wind circulation has a significant influence on how carbon monoxide is distributed throughout the SHe. Subtropical jet streams, the Hadley cell, and seasonal variations in wind patterns all have a substantial impact on the transport and dispersion of CO in this region.

This intricate dynamic has consequences for air quality, climate change, and human health. Evaluating the effects of changes in atmospheric circulation patterns on Earth's environment requires an understanding of the complex link between the global wind circulation and CO distributions in the Southern Hemisphere.

2.4 El Niño Effect on CO Concentration

2.4.1 Introduction

Global climate patterns are significantly impacted by the El Niño phenomenon, which is characterized by the periodic increase in sea surface temperatures in the central and eastern equatorial Pacific. El Niño's influence on atmospheric composition, specifically on CO distributions, is one of the least studied aspects of the climate [64]. This theory explores the intricate relationships between Southern Hemisphere CO concentrations and El Niño events. Learning the wider ramifications for air quality, climate, and environmental management requires understanding these dynamics.

2.4.2 El Niño: An Overview

El Niño, which translates to "The Little Boy" in Spanish, is the term used to describe the cyclical increase in sea surface temperatures in the eastern and central equatorial Pacific Ocean. This meteorological phenomenon is a component of the broader El Niño-Southern Oscillation (ENSO) system, which includes the occurrences of La Niña and El Niño. La Niña refers to the periodic cooling of ocean surface temperatures in the central and east-central equatorial Pacific, generally occurring every 3 to 5 years. It represents the cool phase of the ENSO cycle. El Niño periodically occurs every 2 to 7 years, and it is linked to disturbances in both atmospheric and oceanic circulation patterns, resulting in extensive climate anomalies. La Niña and El Niño occur when the sea surface temperature (SST) anomaly in the Niño 3.4 region over the Pacific (5°N–5°S, 120°W–170°W) varies by at least 0.5°C for up to five consecutive three-month periods [46, 65, 66].

Figure 4 illustrates the ENSO phases between 2000 and 2020. The recent strong ENSO phases can clearly be seen when the SST anomaly in the Niño 3.4 region varies by at least 1.5°C (NOAA Climate Prediction Center). These phases occurred in 2010/2011 (i.e., strong La Niña phase) and 2015/2016 (i.e., strong El Niño phase) and are highlighted by the grey shades. The neutral phase of 2013/2014 is also highlighted in grey.

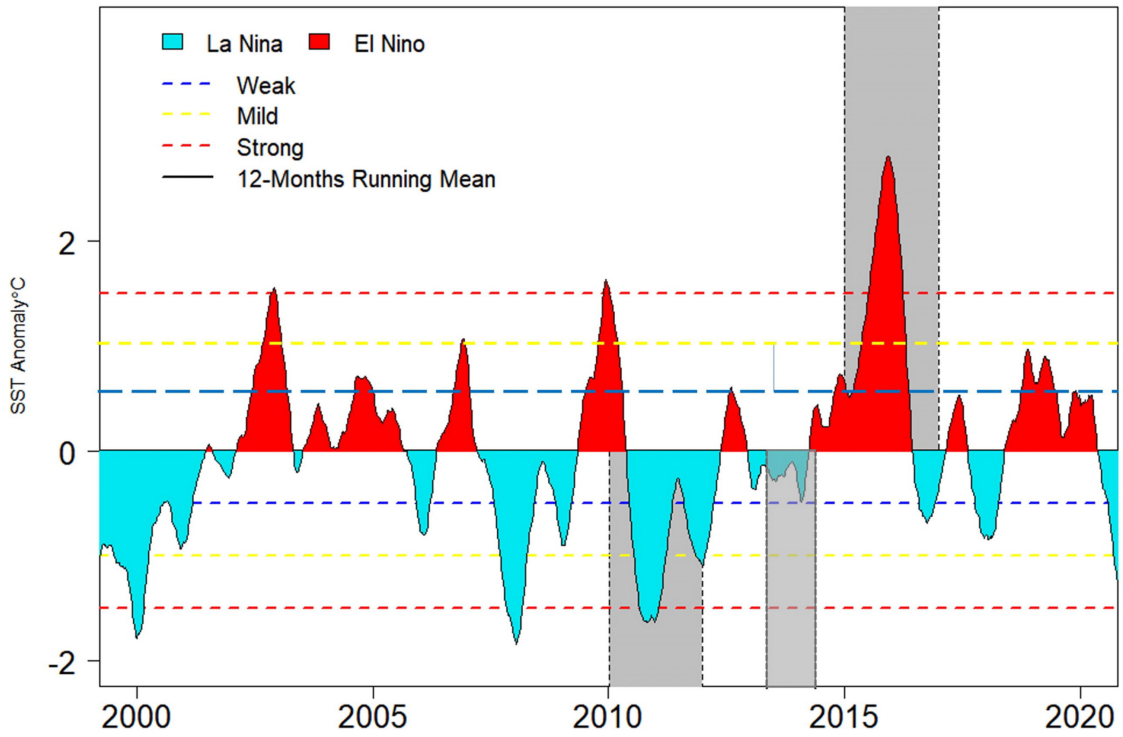

Figure 4: Patterns of sea surface temperature (SST) anomaly in the Niño 3.4 region, showing La Niña and El Niño events between 2000 and 2020. The highlighted periods in grey represent the recent periods of strong La Niña (2010/11), El Niño (2015/16) and Neutral phase (2013/14) Credit: Shikwambana et al.[66]

2.4.3 El Niño's Influence on Atmospheric Circulation

The rising of sea surface temperatures during El Niño occurrences modifies the Pacific Ocean's heat distribution. The usual temperature gradient is being disrupted, which has a domino effect on atmospheric circulation patterns. The subtropical high-pressure systems are moved, and the jet streams change their positions due to the rising warm air over the central Pacific. Together, these alterations are referred to as the "atmospheric bridge," and they have an impact on weather patterns all across the world, including the Southern Hemisphere [46].

2.4.4 El Niño and Biomass Burning

One of the many ways by which El Niño affects carbon monoxide distributions in the Southern Hemisphere is by changing biomass burning patterns. In certain areas, El Niño usually brings drier-than-normal weather, which increases the risk and intensity of wildfires. Significant volumes of CO are released into the atmosphere as a result of the increased frequency of wildfires. During El Niño episodes, biomass burning becomes a substantial source of CO, leading to increased concentrations in affected regions, particularly in parts of South America, Africa, and Australia [67]. El Niño has opposite effects on the eastern and western parts of the Pacific Ocean. El Niño causes higher temperatures and lower rainfall in eastern and northern Australia, increasing the danger of heatwaves, droughts, and bushfires [68]. However, during El Niño, the western coast of South America experiences greater precipitation due to convection over warmer surface waters. Rainfall increases dramatically in Ecuador and northern Peru, causing coastal floods and erosion [69].

2.4.5 Atmospheric Transport and Hemispheric Shifts

El Niño has an impact that goes beyond localized biomass burning. Pollutants such as CO are transported across hemispheres due to El Niño-related changes in atmospheric circulation patterns. Due to its lower population density and lower direct CO emissions, the Southern Hemisphere is more vulnerable to this kind of long-distance transport. Pollutants may be transported from the Northern Hemisphere to the Southern Hemisphere as a result of changing atmospheric circulation patterns, which may have an effect on CO distributions in this region [70].

2.4.6 Southern Oscillation Index and CO Anomalies

The Southern Oscillation Index (SOI) is a crucial gauge of El Niño and La Niña events, as it measures the variation in air pressure between Tahiti and Darwin. La Niña is linked to positive SOI readings, whereas El Niño is indicated by negative values. Research has indicated a connection between increased CO concentrations in the Southern Hemisphere and El Niño occurrences, which are marked by negative SOI levels. The link between atmospheric composition and large-scale climate patterns is highlighted by these anomalies in CO levels during El Niño episodes [71].

2.4.7 Oceanic-Atmospheric Coupling and Climate Anomalies

El Niño's oceanic and atmospheric components combine to produce a cascade of climatic anomalies that affect atmospheric conditions and weather patterns all across the world. In addition to influencing air circulation, rising sea surface temperatures also alter the frequency and severity of extreme weather occurrences. Droughts, heat waves, and changes in precipitation patterns are examples of these events that can further contribute to variations in CO concentrations, particularly in areas where biomass burning and anthropogenic emissions are common [46, 67].

2.4.8 Conclusion

To summarize, the El Niño effect on carbon monoxide distributions in the Southern Hemisphere is the result of a complex interplay of atmospheric and oceanic processes. El Niño has a major impact on CO concentrations in this region through its influence on long-range transport, atmospheric circulation patterns, and biomass burning. It is crucial to fully understand these relationships because of the consequences for weather dynamics

3 Instrumentation, Data, and Analysis Techniques

3.1 Instrumentation and Data: Remote Sensing

3.1.1 Introduction

Climate research, environmental monitoring, and Earth observation depend heavily on remote sensing combined with sophisticated data analysis methods such as MERRA. It greatly improves our knowledge of atmospheric composition, air quality, and climate change when combined with devices like MODIS and MOPITT (Measurements of Pollution in the Troposphere) [52, 72, 73, 74]. This method and instruments were used in this study as follows: Firstly, MOPITT was used to measure CO quantities as total column CO concentration in units of molecules per square centimetre. Secondly, MODIS was used to gather data for burned areas (fires) in square metres. Lastly, MERRA was used to compile data for wind circulations in metres per second. Additionally, data interpretation was made possible using the high-level general-purpose programming languages Python and IDL (interface definition language), as well as Microsoft Excel: Python was used to download the burned area data from the ESA Climate Office website, and he wind, pressure, and CO concentration data were obtained from the Merra (NASA) website. The spacial resolution of the data for CO concentration, wind and pressure is 360 x 180, and the resolutionfor the burned area data is 720 x 1440. Python was also used to convert downloaded files into "*.txt*" files, and to produce Excel spreadsheets of mean values of the appropriate data; IDL was used to generate plots over the Mercator projection using the data from the "*.txt*" files; and Microsoft Excel was used to produce the bar graphs from spreadsheets of the appropriate data. In this in-depth conversation, we will examine the fundamentals and practical uses of remote sensing with MOPITT and MODIS, as well as how MERRA analysis enhances their functionality and how they are employed to gather information.

3.1.2 Remote Sensing with MOPITT

The purpose of the satellite-based remote sensing device MOPITT is to measure trace gases in the troposphere of Earth. The primary goal of MOPITT, which was created in partnership with NASA and the Canadian Space Agency (CSA), is to track atmospheric quantities of methane (CH_4) and CO. This instrument uses thermal infrared radiation that is released by the Earth's surface and atmosphere, working on the basis of passive remote sensing. The absorption of this radiation by the target gases is then measured by MOPITT, which offers important information about their distribution and variability [72].
In atmospheric science, the MOPITT measurements of CO and methane (CH_4) are crucial. As a result of combustion, CO is linked to a number of pollution sources, such as wildfires and industrial operations. Strong greenhouse gas methane has a direct impact on the Earth's radiative balance and climate due to its atmospheric concentration. The data from MOPITT help us understand the sources, sinks, and distribution of these gases, which is useful for modeling climate change and evaluating air quality [73]. MOPITT data was used in this research to track and quantify CO concentrations in the Southern Hemisphere.

3.1.3 Remote Sensing with MODIS

Conversely, MODIS is an adaptable remote sensing tool that is a component of NASA's Earth Observing System (EOS) that functions on both the Terra and Aqua satellites. Among the many high-resolution images and quantitative measurements of different Earth surface and atmospheric parameters that MODIS provides are those in the visible and infrared portions of the

electromagnetic spectrum. These variables consist of aerosol concentrations, cloud characteristics, atmospheric profiles, land cover, and ocean characteristics [52, 55]. MODIS plays a vital role in tracking various facets of the Earth's ecosystem. It can offer data for analysis of land use and land cover change, monitoring of sea surface temperature, detection of wildfires, and measurements of aerosol concentration due to its multispectral and multispatial capabilities. In Earth scientific applications such as ecological studies, disaster management, and climate research, MODIS is essential [52, 55].

3.1.4 MERRA Analysis

NASA created MERRA, or the Modern-Era Retrospective analysis for Research and Applications, a complex method for assimilation of data. It smoothly incorporates readings from equipment like MOPITT and MODIS, among many other remote sensing data sources, into extensive and ongoing records of Earth's atmospheric conditions going back to 1979. MERRA utilizes a cutting-edge atmospheric model and incorporates observational data from multiple sources, such as weather balloons, ground-based instrumentation, and satellite measurements [74]. A critical component of MERRA's operations is the data assimilation process. To provide a consistent and continuous dataset, it integrates observational data with model simulations, thereby minimizing biases and inaccuracies in the models or the observations alone. A comprehensive picture of Earth's atmospheric conditions over an extended time span is provided by MERRA data assimilation, which is a potent instrument for climate research, weather forecasting, and environmental monitoring [74]. This research made use of the MERRA-2 reanalysis data, which are zonal and meridional winds to produce the vector velocity plots.

3.1.5 Complementary Roles and Applications

MOPITT, MODIS, and MERRA have different but complementary functions in atmospheric research and Earth observation. These tools and methods of data analysis, when combined, provide a comprehensive picture of the intricate processes that make up our world. The power of MOPITT lies in its exceptional precision in measuring trace gases, such as methane and carbon monoxide. This feature is especially useful for monitoring the sources of pollution, evaluating the quality of the air, and examining the effects of natural disasters like wildfires on the composition of the atmosphere. Incorporating MOPITT data into MERRA analysis can improve atmospheric modeling quality and provide researchers with new insights into the dynamics of the carbon cycle and pollution dispersion [72, 73]. With its extensive Earth observation capabilities, MODIS complements MOPITT by offering a more comprehensive perspective of the planet's surface and atmosphere. Aerosol concentrations, cloud characteristics, sea surface temperatures, and changes in land cover are all included in MODIS data. These datasets improve the precision of climate simulations and atmospheric modeling when included into MERRA analysis. For example, MODIS imaging and MOPITT data can be combined to determine the position and size of wildfires, which emit significant volumes of carbon monoxide. Subsequently, MERRA analysis can use this data to enhance atmospheric models, enabling more accurate forecasting of the effects on air quality and the distribution of contaminants [52, 75]. Additionally, scientists are able to examine patterns and alterations in the Earth's climate and surroundings across a number of decades thanks to MERRA's long-term and continuous atmospheric records. This historical perspective is required in order to understand the impact that climate change and natural occurrences such as volcanic eruptions and El Niño events have on the Earth's atmosphere. By integrating MOPITT and MODIS data into MERRA analysis, researchers are able to conduct comprehensive investigations into the long-term effects of these events and evaluate their implications for the Earth's climate system [74].

3.1.6 Conclusion

The combination of sophisticated data assimilation methods like MERRA analysis with remote sensing tools like MOPITT and MODIS is an effective approach for Earth observation and atmospheric study. With the use of these instruments, we can learn more about long-term environmental patterns, air quality, climate change, and atmospheric composition. The combination of remote sensing and data assimilation will be crucial in tackling the environmental issues of the twenty-first century as our comprehension of the Earth's intricate processes deepens.

3.2 Data Analysis Techniques

3.2.1 Mean

In data analysis, the mean or average is is the most commonly used measure of central tendency, i.e. the statistical measure used to determine a single value that represents the full distribution [76, 77], or a fundamental statistical measure used to summarize a set of data points into one point. It provides a central value that represents the typical (average) or expected value in a dataset. There are other sorts of means, but the arithmetic mean, weighted mean, geometric mean, and harmonic mean are the the most commonly used. When used without an adjective (just as mean), the mean typically refers to the arithmetic mean [76]. This is the type of mean that was used throughout this research to find the average values of all the data sets.

The arithmetic mean is calculated by dividing sum of all the values in the data set by the total number of observations or data points. It is represented by the symbol $\bar{x}$ for a dataset of n values, i.e. $x_1,\ x_2,\ x_3, ...,\ x_n$, and its formula is given by:

$$\bar{x} = \frac{1}{n}\sum_{i=1}^{n} x_i \tag{2}$$

where x_i represents each data point [76, 78].

The mean is a very useful measure used in many other fields, such as economics, psychology, engineering, etc. for multiple reasons: It is easy to compute and interpret, making it a convenient summary statistic. The mean gives a brief overview of the central tendency of the data, helping to summarize and describe the key characteristics of a dataset by using every available value the dataset [76, 79]. It additionally facilitates simple comparisons between different datasets or groups within a dataset. Furthermore, the mean is a foundational element for more complex statistical methods, such as variance, standard deviation, and hypothesis testing [80]. However, while the mean is a valuable measure, it has some limitations: It can be significantly affected by extreme values (outliers), which may not represent the typical values in the dataset. Also, In skewed distributions, the mean may not accurately reflect the central tendency. In such cases, the median or mode may be more appropriate [78, 79].

In summary, the mean is an essential measure of central tendency in data analysis. It offers important insights into the general behavior of the dataset. Despite its limitations, it is a frequently used statistic in a variety of sectors due to its simplicity and interpretability.

3.2.2 The Pearson correlation coefficient (r)

The Pearson correlation coefficient and p values are two important statistical tools for quantifying and assessing the relationships (or correlation) between variables. Commonly denoted

by the symbol r, the Pearson correlation coefficient measures the strength and direction of the linear relationship between two continuous variables. It is computed as the covariance of the two variables divided by the product of their standard deviations. The Pearson correlation coefficient (r) between two variables X and Y is given by the following formula:

$$r = \frac{\sum_{i=1}^{n}(X_i - \bar{X})(Y_i - \bar{Y})}{\sqrt{\sum_{i=1}^{n}(X_i - \bar{X})^2}.\sqrt{\sum_{i=1}^{n}(Y_i - \bar{Y})^2}} \tag{3}$$

where n is the number of observations, X_i and Y_i are the individual data points, $\bar{X}$ and $\bar{Y}$ are the means of variables X and Y, respectively [81, 82, 83]. The Pearson correlation coefficient ranges from -1 to 1, i.e. from a perfect negative linear relationship (-1) to a perfect positive linear relationship (1). No linear relationship is represented by 0 (null hypothesis) [66, 81, 83, 84]. The two variables that will be tested in this research are CO emissions and burned areas.

3.2.3 The p-value

p values, on the other hand, represent the likelihood of obtaining the observed correlation coefficient or a more extreme value under the null hypothesis of no relationship. In other words, p-values denote how significant the observed correlation is. A small p value (usually equal or less than 0.05) suggests strong evidence against the null hypothesis, implying that the observed correlation is unlikely to arise by solely by chance. In contrast, a large p value (usually higher than 0.05) shows poor evidence against the null hypothesis, implying that the observed correlation may have occurred by random chance. The formula for computing the p value associated with the Pearson correlation coefficient entails converting the correlation coefficient into a t-statistic and then calculating the probability of obtaining a t-statistic as extreme as or more extreme than the observed value [85, 86]. It is given as

$$t = r.\sqrt{\frac{n-2}{1-r^2}} \tag{4}$$

The t-statistic follows a t-distribution with degrees of freedom $df = n - 2$, where n represents the number of observations. The p-value is then determined using the cumulative distribution function (CDF) of the t-distribution. The research hypothesis can dictate whether a one-tailed or two-tailed test is used. In a two-tailed test, either a positive or negative value of r is considered (a priori) evidence against the null hypothesis, and the test is considered nondirectional. A one-tailed test specifies the sign of r in advance, implying that only positive (or only negative) correlation is relevant for rejecting the null hypothesis, thus the test is considered directional [84, 85, 87, 88]. The theory of this research implies that only the positive correlations between CO emissions and burned areas should be verified. The p-value is therefore expected to be equal to or less than 0.05 only for positive correlations. The expressions for the Pearson correlation coefficient and p-value were computed as a python code.

When interpreting the Pearson correlation coefficient and p values, several aspects must be considered, including sample size, effect size, and data assumptions. A statistically significant correlation (i.e., a small p value) suggests a meaningful correlation between variables but does not imply causation. Researchers must take caution when drawing causal conclusions based only on correlation data. Furthermore, large sample sizes can provide statistically significant correlations with little practical significance, highlighting the need of taking effect size into account in addition to statistical significance [84].

3.2.4 Limitations of r and the p-value

The reliability of the Pearson correlation coefficient and p-values is determined by assumptions such as linearity, homoscedasticity (the assumption that Y has equal or similar variability or variance for different values of X. In other words, it describes a situation in which the error term is the same across all values of the independent variables.), and normality. Violations of these assumptions might result in biased estimations and erroneous conclusions. Non-linear correlations between variables, for example, might lead to correlation coefficients that are either understated or exaggerated. Similarly, heteroscedasticity (unequal variance, which describes a situation in which the error term differs across values of an independent variable.) or non-normality of data can impair the accuracy of p values, potentially leading to Type I (False positive) or II(false negative) errors. Therefore, researchers should check the robustness of correlation analyses by reviewing residual plots and doing sensitivity analyses [89, 90, 91].

Despite its extensive use, the Pearson correlation coefficient has limits, especially when dealing with nonlinear correlations, outliers, or categorical variables. In such circumstances, other correlation metrics like Spearman's rank correlation or Kendall's tau may be more appropriate. Furthermore, in order to provide a complete picture of the relationship between variables, p values should be interpreted in conjunction with effect size estimates and confidence intervals. Researchers should also assess the practical implications of correlation findings in real-world settings, taking into account their magnitude and direction [92, 93].

To summarize, the Pearson correlation coefficient and p values are useful statistical tools for quantifying and evaluating correlations between variables. By giving measurements of both strength and statistical significance, these tools allow researchers to make meaningful inferences from empirical data. However, correlation results should be interpreted with caution, taking into account aspects such as sample size, effect magnitude, and data assumptions. Researchers can improve the rigor and validity of their findings in a variety of domains by following basic statistical techniques and supplementing correlation analyses with subsidiary measures.

3.2.5 Coefficient of Determination (r^2)

The coefficient of determination (r^2), also known as the proportion of variance explained, measures how much variance in one variable is predictable from another variable. It goes from 0 to 1, with 0 indicating no shared variance and 1 indicating total shared variance. r^2 can be defined as the proportion of variability in one variable (dependent) that can be accounted for by the other variable (independent) [94, 95, 96]. In other words, the coefficient of determination is a statistical measure that looks at how variations in one variable may be explained by differences in another when predicting the result of an event. This coefficient is very useful in other fields such as market research where it is heavily relied upon when investors are conducting trend analysis as it gives a meaningful assessment of relationship strength between two variables [97]. In this research, r^2 was used when performing the trend analysis of CO concentration to find how much or what percentage of the total variation in annual CO concentrations is explained by the trend (or best fit) line, or how well the best fit line fits the data points (annual CO concentrations).

r^2 is calculated by producing a scatter plot of the data variables with a trend line. This can be achieved in at least two ways: by creating a spreadsheet [97, 98] or by performing a manual

calculation [97]. Manually, r^2 can be obtained by squaring Equation (3):

$$r^2 = \left(\frac{\sum_{i=1}^{n}(X_i - \bar{X})(Y_i - \bar{Y})}{\sqrt{\sum_{i=1}^{n}(X_i - \bar{X})^2} . \sqrt{\sum_{i=1}^{n}(Y_i - \bar{Y})^2}} \right)^2 \tag{5}$$

Also, if the t-test results are available, then r^2 can be calculated from the t-distribution as

$$r^2 = \frac{t^2}{t^2 + df} \tag{6}$$

where t is the t-test value and df is the degree of freedom [99].

It is important to note that while r^2 provides an estimate of the relationship between a dependent variable's movements based on an independent variable's movements, it does not tell whether the chosen model is good or bad, or whether the data and predictions are biased. A high or low value of r^2 is not necessarily good or bad; it does not indicate the model's reliability or whether or not the correct regression has been chosen, i.e. it is possible to obtain a high r^2 for a poorly fitted model, or a low r^2 for a good model, and vice versa [98].

4 Results and Discussion

4.1 Spatial and Temporal Variation of CO Concentration and Burned Area

As stated previously, winter months tend to have larger loads of pollutants due to more potent biomass burning which are favoured by and intensify in dry winter months. Consequently CO levels tend to be higher during those dry months [100]. This section therefore aims to investigate the seasonal variations as well as spatial (continental) distributions of SH CO concentrations, the seasonal variation biomass burning or burned areas in the southern hemisphere, and to investigate if biomass burning is a possible source of the CO concentration. The data covers the period from 2005 to 2019, and the SH areas include Southern Africa, South America and Australia. The seasons are summer (December to February), autumn/fall (March to May), winter (June to August), and spring(September to November).

4.1.1 Spatial and seasonal variation of CO concentration and Burned area

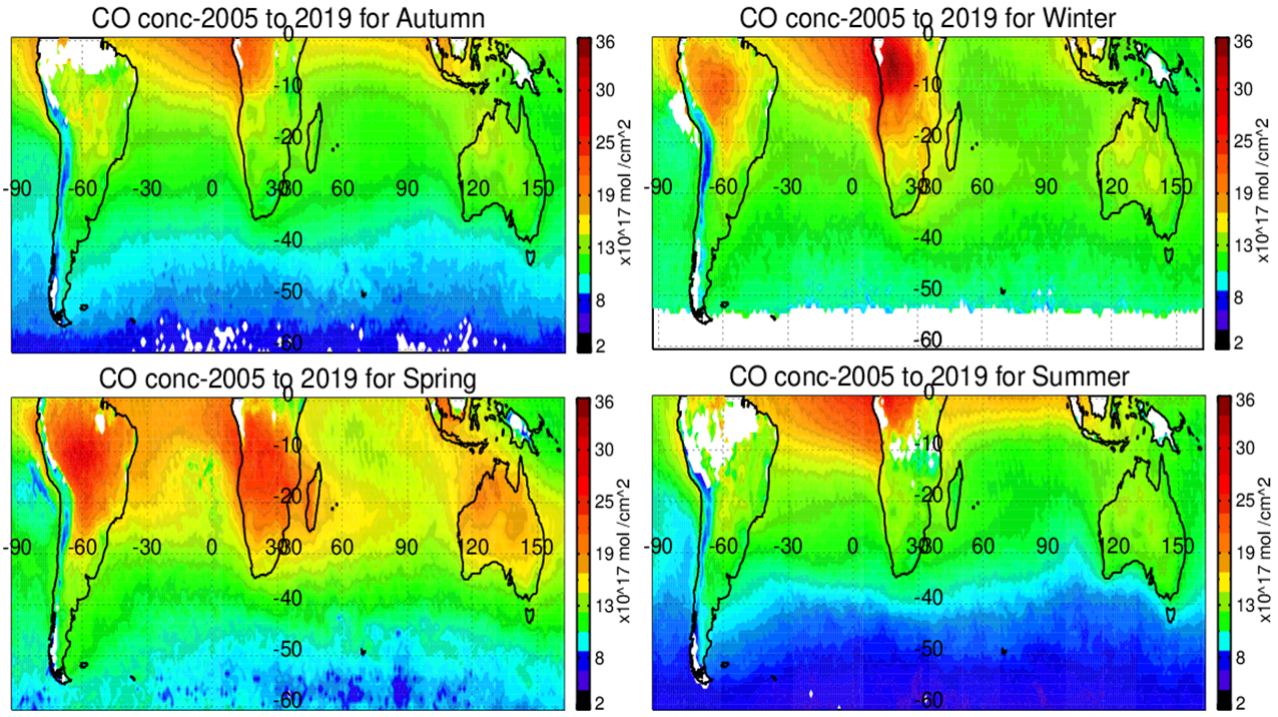

Figure 5: CO concentrations 2005 to 2019 seasonal average (MOPPITT).

Figure 5 gives a layout of the seasonal variation of CO concentration in the SH in mol/cm^2. The CO concentration includes the total emissions from various possible sources, such as biomass burning, industrial processes, combustion engines, etc. Winter has higher CO concentration than summer, with the highest concentration of $\sim 34 \times 10^{17}$mol/cm^2 in winter seen in the northern part Southern Africa at latitudes and longitudes between 0° and 10° South and 9° and 30° East, respectively, i.e. in parts of Angola, Zambia, and the Democratic Republic of the Congo. The highest concentration in summer is $\sim 30 \times 10^{17}$mol/cm^2, around the same region. The highest CO concentrations in Australia, South America, and the central and southern parts of Southern Africa are seen in spring, with Australia reaching $\sim 20 \times 10^{17}$mol/cm^2 in the northern and central parts, and South America reaching $\sim 30 \times 10^{17}$mol/cm^2, covering parts of Brazil, Peru and Bolivia, i.e. between 5 and 20° South and 50 and 75° West. The central and southern regions of Southern Africa reaches a maximum CO concentrations of $\sim 26 \times 10^{17}$mol/cm^2

(Mozambique, Malawi, Zimbabwe, Botswana, and Namibia) and $\sim 19 \times 10^{17}$mol/cm^2 (Madagascar, Swaziland, South Africa, and Lesotho), respectively. Autumn has generally a modereate concentration of $\sim 15 \times 10^{17}$mol/cm^2 in all three regions.

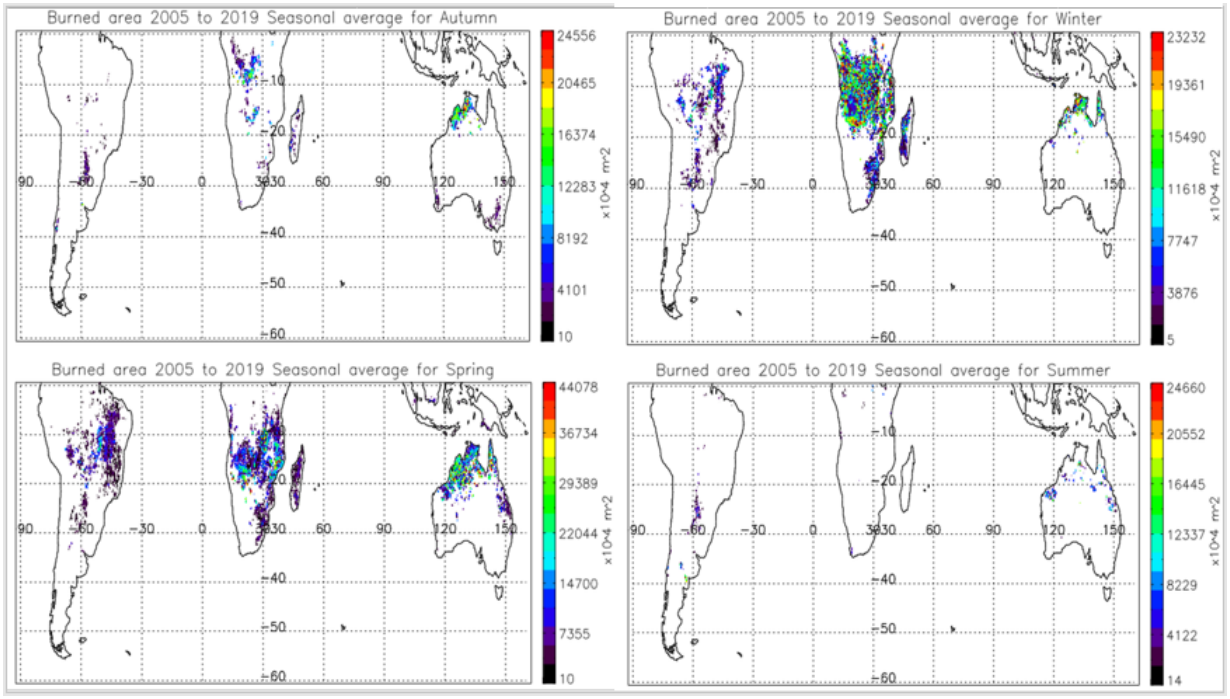

Figure 6: Burned area 2005 to 2019 seasonal averages (MODIS).

Figure 6 gives a layout of the SH seasonal average burned areas in square metres.This figure, as well as other burned area figures used in this study, do not give any information about fire intensity or the amount of biomass burned (fire counts). These figures do not give the types of biomass burned either, since they represent burned areas in general. Burned areas in different vegetation classes will be discussed later. Given that Figure 6 only show locations of fire sources in a general way, it should be used carefully in order to understand CO emissions [100]. Figure 6 shows that winter has once again more burning than summer, with the most burned areas being in Southern Africa. The vast majority of burned areas in Southern Africa is seen between $\sim 5°$ to $20°$ South. Again, maximum burning in both Australia and South America takes place in spring, mostly in the northern parts of both regions.

When Figure 5 is compared to Figure 6, it can generally be seen that there is a possible positive correlation between CO concentration and burned area, i.e. a higher burned area seems to result in a higher CO concentration: In Southern Africa, the northern part sees maximum burned areas in winter, which also corresponds to the season with highest CO concentration in the same region. Australia, South America, and the southern part of Southern Africa register their maximum burned areas during spring, which also yet again corresponds to the season with highest CO concentrations in those regions. Burned areas are moderate during autumn, and so are CO concentrations in the same season. Summer has the minimum burned areas, which corresponds to the lowest CO concentrations in both South America and Australia. However, Southern Africa, especially the northern part, shows some inconsistency, with a very high CO concentration of $\sim 29 \times 10^{17}$mol/cm^2, showing an appearance of a negative correlation, likely due to CO transport from the Northern Hemisphere. Additionally, CO concentrations can be seen over sea surfaces, also likely due to wind circulation. These similarities between CO concentration and burned area will be quantified in Section 5.1.3, and the apparent inconsistency will be further investigated in Section 5.2.

As biomass burning constantly takes place in the SH in majority due to deforestation, cultivation and savanna grazing, among other factors, it constitutes a major source of pollution in the region. Consequently, most of the emitted gases caused by the burning contain carbon, almost 90% are either CO_2 or CO, in amounts depending on burning efficiency and fuel type. The average lifetime of two months in the atmosphere makes CO an excellent tracer of pollution from fire sources and allows the measurement of CO over a fairly long time period [101]. It has been found that in Southern Africa, August and September are often the months with maximum emissions, coinciding with the main austral fire season, while April is usually the month with minimum emissions. In South America, the maximum is likewise reached in August-September, and begins to decline from October to December. Australian CO emissions peak around October and reach minimum levels in February-March. The CO levels throughout the southern hemisphere coincide with the fire intensity in the region. Peak CO levels tend to occur during intense fire activities, while minimum levels tend to occur during periods of suppressed fires [102, 103, 104, 105]. This consistent with was is presented in Figures 5 and 6.

Distinct patterns in CO levels have been observed from the measurements taken by satellite observations (MOPITT) during the years looked at for this study (i.e. between 2005 and 2019). Biomass burning in the regions of Southern Africa, South America and Australia results in considerably higher CO concentrations throughout winter and spring. Due to changes in land use and agricultural techniques, there is a significant and continuous rise in the combustion of biomass, which releases carbon monoxide into the atmosphere, and last until the end end of spring. These cyclical CO peaks throughout the winter and spring months in the SH highlight the way in which emissions from burning biomass affect local air quality [73, 106].

In contrast, the SH has lower CO concentrations throughout summer, which runs from December to February. During this time, there is less burning of biomass and more air dispersion as a result of increased atmospheric vertical mixing, i.e. the upward and downward movement of air that occurs due to the temperature gradients (temperature differences between layers of the air). The overall visible seasonality (the apparent predictable annual fluctuation or pattern) is influenced by the Southern Hemisphere's comparatively pure environment and lower direct CO emissions than the Northern Hemisphere. In addition, the Hadley cell and subtropical jet streams, two atmospheric circulation patterns, have an impact on CO distribution and contribute to these seasonal fluctuations through CO transport [73, 107].

Large-scale biomass burning is an annual occurrence in Africa. In the NH, burning occurs from December to April (or from December to February) in the savanna south of the Sahara desert (the Sahel) and in the tropical rain forest located just north of the equator. As the dry season gradually moves south in the continent, so does the location of the burning regions. Consequently, in the SH, burning takes place from around May (or June). It begins in western central Africa, over the southern part of the Democratic Republic of the Congo (D.R.C.) and Angola, before spreading in the south-eastern direction and down the east coast. An estimated 90 % of the biomass burned in Africa emanates from savanna fires, the majority of which are not wildfires but rather agricultural burning linked with ranging livestock and subsistence farming [100, 108].

Annually in South America, burning begins in around June and takes place in the Cerrado grasslands and drought-deciduous forests that make up the vast majority of the biomass of the South, and the temperate rain forests along the coast in eastern Brazil. Burning also takes place along the southern edge of the Amazonian rain forest [100]. By September, the burning

can be seen in Brazil, Bolivia, Paraguay and northern Argentina. In South America (Brazil), contrary to the situation in Africa, it was observed that regular thunderstorms over the burning areas are generated by the frontal systems in Brazil. Consequently, a deep convection occurs and lifts the burning emissions to the free troposphere, which results in greater levels and higher variability in measured CO [100]. More on this will be discussed later.

Edwards et al.[100] state that in Australia, wildfires usually occur from about September to January, mostly along the northern and eastern coasts. The fire location determines the direction of where the resulting biomass burning plumes is transported. For example, MOPITT and MODIS showed that generally the emissions from the southeast of the continent are transported over the Pacific towards New-Zealand [100].

4.1.2 Burned Area in Vegetation Classes

The previous section looked at a generalized aspect of the average burned areas, which are comprised of four sub-areas viewed in terms of their vegetation classes, which consist of forest, grassland, cropland and shrubland. In this section, the burned areas in each of the four vegetation classes in Southern Africa, South America, and Australia will be looked at to identify in which vegetation class burning occurs the most.

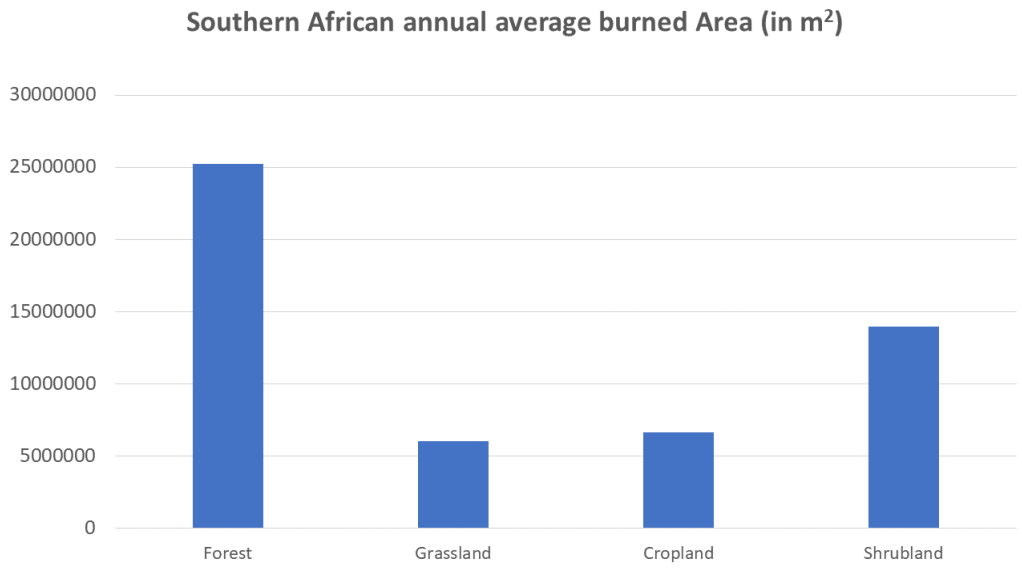

Figure 7: Southern African annual average burned areas from 2005 to 2019 in different vegetation classes.

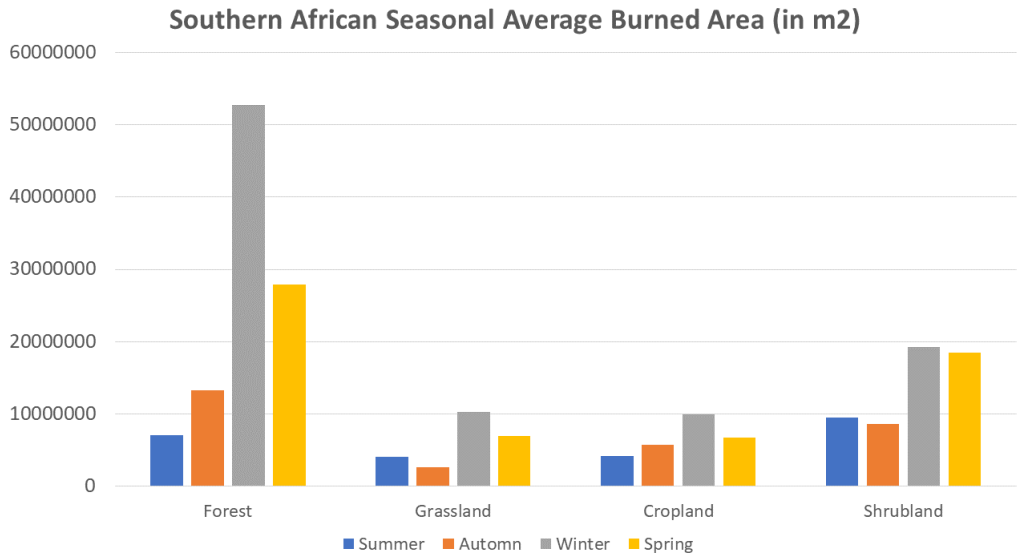

Figure 8: Southern African seasonal average burned areas from 2005 to 2019 in different vegetation classes.

Southern Africa Figure 7 is a bar graph showing the annual average burned area in different vegetation classes in Southern Africa. Figure 8 shows the seasonal average burned area in the same vegetation classes, also in Southern Africa, measured in m^2. Figure 7 shows that forest has the highest burned area of 2.52×10^7 m^2 and grassland has the lowest burned area of 6.01×10^6 m^2. Figure 8 shows that winter has the highest average burned areas in all vegetation classes, followed by spring. Summer has the lowest burned area in forest and cropland, and autumn has the lowest burned area in grassland and shrubland.

The dynamics of the vegetation, human activity, and climate patterns in the Southern African forest are closely related to the seasonal fluctuations observed in burned areas. There are two different major seasons in the Southern Hemisphere: a rainy season in the austral summer and a dry season in the austral winter. The rainy season, which is marked by heavier rainfall, normally lasts from November to April in Southern Africa. Vegetation is at its peak during this time, and there is less chance of wildfires. But when May brings with it the start of the dry season, the vegetation becomes more flammable and wildfire frequency and intensity increase. The mid-dry season, especially in July and August, is when the burning season peaks most frequently because of the fast-moving, dry flames that spread quickly over the terrain. A mix of natural elements, such as lightning strikes, and man-made activities, like land-use changes and agricultural practices, affect the seasonal variability in burned areas [109, 110].

During the dry season in the Southern African grassland, which normally lasts from late fall (Autumn) to early spring, the vegetation gets dehydrated, creating ideal conditions for fire ignition and spread. During this time, grasses and other combustible flora amass (or turn into) dry biomass, resulting in a fuel-rich environment that is easily ignited. Human activities, such as agricultural operations and land clearance, also peak during the dry season, contributing to increased fire occurrences [111, 112]. The moisture-rich soil and plants during the rainy season serve as a natural fire barrier. Southern African grasslands are less likely to have fires because of the abundance of green vegetation and higher humidity, which also limit the availability of combustible materials. Depending on the location within Southern Africa, this wet season usually lasts from late spring to early autumn (during the summer months) [111, 112].

In the SH, the majority of agricultural fires occur in the late dry season (July-October) or from late fall to early spring in Southern Africa. In this region, maize is a winter crop that is often harvested after August, when agricultural fire activity peaks. Millet, cassava, wheat, sorghum, cotton, and sugar cane are among other important winter crops. Farmers in various parts of Southern Africa use the long-standing technique of slash-and-burn agriculture to clear fields and get them ready for planting after harvest. This intentional burning causes an increase in burned areas during this time [113, 114, 115]. Furthermore, due to increased soil moisture and lower vegetation flammability, the rainy season in Southern Africa, which normally occurs in late spring and summer, sees a decrease in burned areas. Rainfall is abundant during this time of year, which lessens the chance of uncontrolled wildfires, and agricultural methods are less dependent on fires [112, 116].

Similarly to all other vegetation classes analyzed previously, the African shrubland's seasonal variations follow a pattern shaped by a confluence of anthropogenic causes, vegetation dynamics, and climate. The African shrubland is marked by a combination of grasslands, savannas, and habitats dominated by shrubs, and it is characterized by notable seasonal variations in temperature and precipitation. Because there is less moisture in the vegetation during the dry season, this region is more prone to wildfires. Burned areas expand at this time as wildfires become more frequent and propagate throughout the surface [112, 117]. The peak of burned areas typically occurs near the end of the dry season when vegetation becomes extremely flammable and there are more natural (lightning) and anthropogenic (agricultural) ignition sources [112].

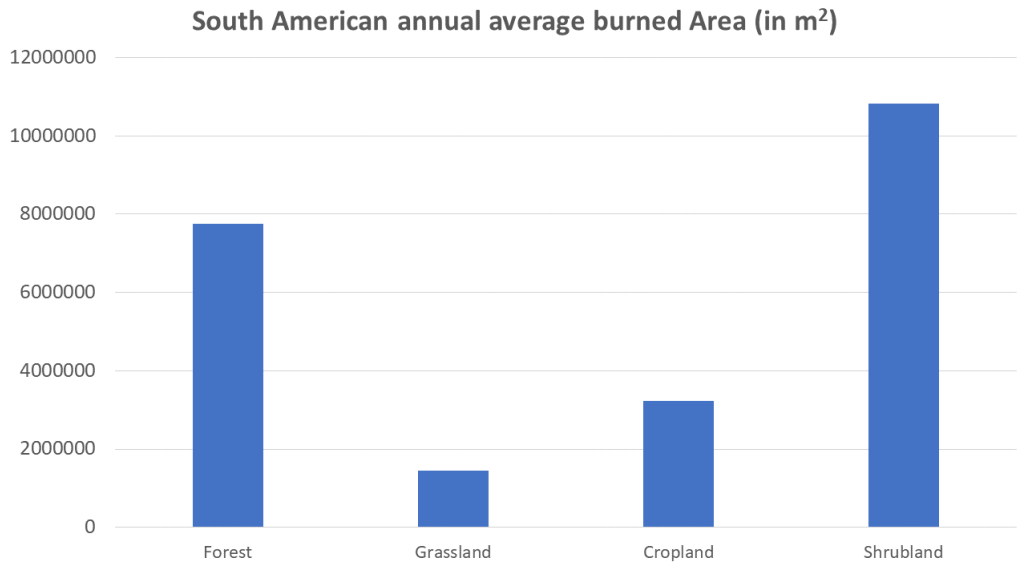

Figure 9: South American annual average burned areas from 2005 to 2019 in different vegetation classes.

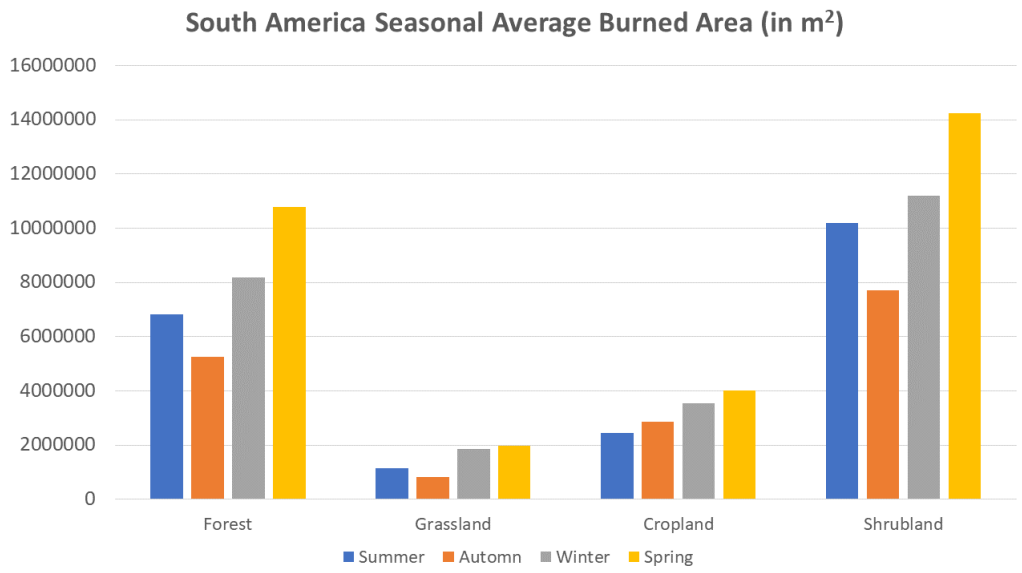

Figure 10: South American seasonal average burned areas from 2005 to 2019 in different vegetation classes.

South America Figure 9 is a bar graph showing the annual average burned area in different vegetation classes in South America. Figure 10 shows the seasonal average burned area in the same vegetation classes, also in South America, measured in m^2. Figure 9 shows that shrubland has the highest burned area of $1,08 \times 10^7$ m^2. Forest has the second highest burned area, and grassland has the lowest burned area of 1.45×10^6 m^2. Figure 10 shows that spring has the highest average burned areas in all vegetation classes, followed by winter. Autumn has the lowest burned area in all vegetation classes except for cropland, in which summer has the lowest burned area.

Climate patterns, land use practices, and natural vegetation cycles all have a substantial influence on seasonal variations in burned areas in the South American forest. The dry and wet seasons in South America are closely associated with the annual cycle of burned regions. The region's dry season, which usually lasts from May or June to October, is a crucial time for fire activity. This time of year, there is less precipitation and a higher temperature, which makes it easier for wildfires to start and spread. During the dry season, human activities like deforestation and agricultural practices further increase the risk of fire. The greatest increase in burned areas frequently happens during the transition from the dry to rainy seasons, when vegetation becomes drier and more prone to wildfires. This trend is especially noticeable in the Amazon rainforest, where a combination of agricultural practices, such as slash-and-burn farming, which uses fire to clear land and cultivate crops, and environmental factors lead to increased fire activity during these months [118, 119, 120]. Furthermore, seasonal changes in burned areas are influenced by natural vegetation cycles. Some South American ecosystems are fire-adapted, with particular plant species reliant on periodic burning for regrowth. The occurrence of wildfires during the dry season is a normal element of the ecological process in these fire-adapted ecosystems, resulting in seasonal changes in burned areas. However, in this region, excessive human activities have disrupted the balance between natural fire patterns and anthropogenic impacts in many locations, resulting in increasing fire frequency and intensity [119, 120, 121].

The South American grassland is characterized by the Pampas. They are flat, fertile plains that stretch from the Atlantic Ocean to the Andes Mountains and span an area of at least

760,000 square kilometers. They are mostly found in Argentina, although they also exist in Uruguay. The Pampa biome, with its large grasslands and heavy agricultural activity, is known for its intense burning, which is mostly caused by agricultural practices including deforestation and pasture management. Seasons in the Southern Hemisphere are a major factor in these changes. Agricultural activities ramp up throughout the austral autumn and winter (March to August), which increases the frequency of planned fires for clearing land and reviving pastures. However, as vegetation grows back and the weather becomes wetter, the amount of burned land decreases over the austral spring and summer (September to February). The meteorological patterns of the area affect the flammability of the grassland ecosystem as well as the sources of ignition, and this seasonality is closely related to those patterns [122, 123, 124].

Spring is a transitional phase that is characterized by rising temperatures and shifting precipitation patterns. The frequency of dry conditions during this time period creates an ideal atmosphere for the ignition and spread of wildfires. Because of the abundance of dry plants and grasses, the South American grassland, notably the enormous areas of the Brazilian Cerrado, is vulnerable to fire outbreaks. Natural factors such as dry weather and the accumulation of flammable biomass increase the likelihood of wildfires starting and spreading over grassland ecosystems [125, 126].

Similarly to Southern Africa, most agricultural fires in South America occur during the dry season. Maize and soybean agriculture predominate in the northern regions of the continent, as well as in southeastern Brazil, but wheat cultivation predominates in Argentina and Chile. During the dry season, which normally lasts from June through September, farmers use fire to clear fields, remove agricultural residues, and prepare the soil for the upcoming planting season. This intentional burning contribute to the increase in burned areas during these months [115, 127, 128].

The South American shrubland is significantly characterised by the Gran Chaco. Covering regions in Paraguay, Bolivia, Argentina and Brazil, the Chaco, specifically the western Chaco, is an arid region made of a number of forests and shrublands with many vegetations shared between them. A decreased soil moisture and an increased dry vegetation make for ideal conditions for wildfires throughout the dry season. Human activity, such as slash-and-burn farming practices and ranching, and natural elements like lightning are common causes of these fires. Subsequently, fire activity tends to peak during the driest months in the South American shrubland [47, 129, 130, 131].

However, some summers tend to have high burned areas due to an interplay of both changes in climate patterns and human activity: During the wet season, some parts of the Gran Chaco may receive moderate to substantial rainfall, while other parts may experience lengthy dry spells. The South American monsoon system affects the region's climate, and the semi-permanent Chaco low-pressure system causes different precipitation patterns. The South American shrubland is mostly located in the western and dry Chaco, and rainfall is usually heavier in the eastern parts of Gran Chaco and gets progressively lighter in the western parts. Additionally, wildfire propagation can be facilitated by changing landscape structure brought about by changes in land-use and land-cover patterns, such as deforestation and increased agricultural production [131, 132, 133, 134].

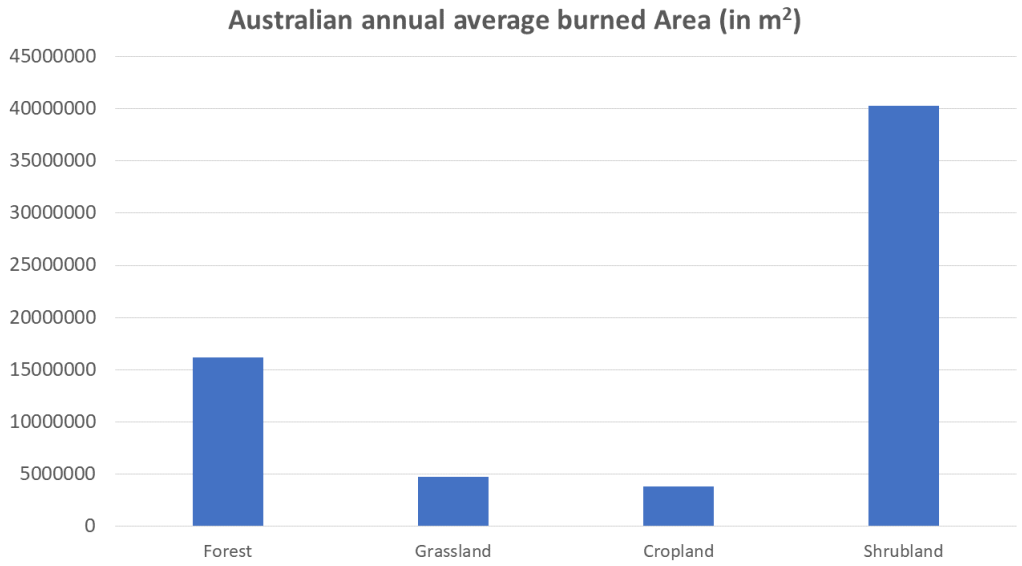

Figure 11: Australian annual average burned areas from 2005 to 2019 in different vegetation classes.

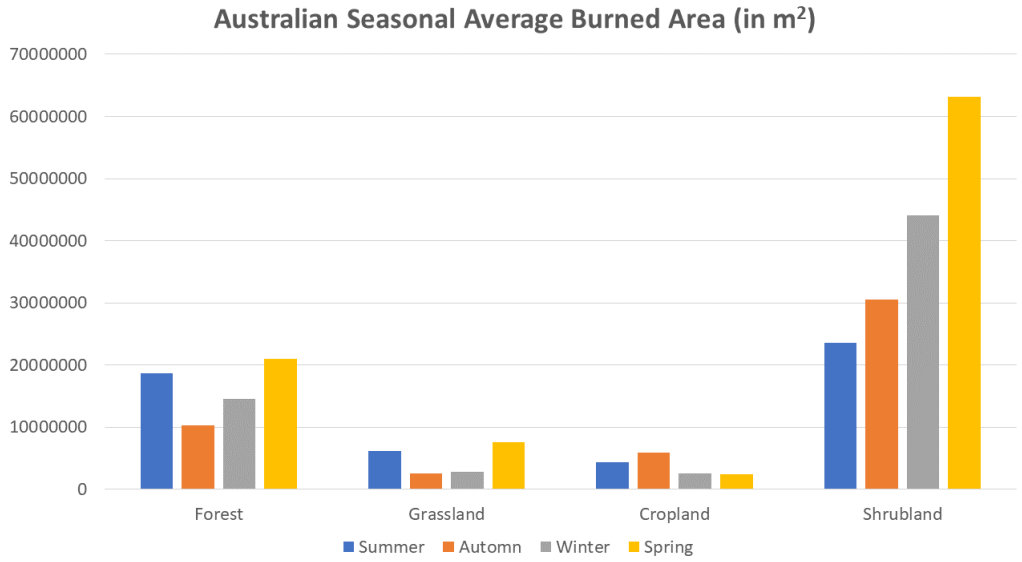

Figure 12: Australian seasonal average burned areas from 2005 to 2019 in different vegetation classes.

Australia Figure 11 is a bar graph showing the annual average burned area in different vegetation classes in Australia. Figure 12 shows the seasonal average burned area in the same vegetation classes, also in Australia, measured in m^2. Figure 11 shows that shrubland has the highest burned area of 4.03×10^7 m^2. Forest has the second highest burned area, and cropland has the lowest burned area of 3.81×10^6 m^2. Figure 12 shows that spring has the highest average burned areas in all vegetation classes except for cropland, which has the highest burned area in autumn. Summer has the second highest burned area in all vegetation classes except for shrubland, where it has the lowest burned area, with winter having the second highest burned area in that vegetation class. Autumn has the lowest burned area in both forest and grassland, and spring has the lowest burned area in cropland.

Summer in Australia is a significant period for wildfires. High temperatures, lengthy dry spells, and strong winds produce ideal circumstances for fire ignition and rapid spread throughout the summer months. The heightened flammability of plants during this time of year increases the possibility of wildfires across the country. Natural climate phenomena such as the Southern Oscillation Index (SOI) and the Indian Ocean Dipole (IOD) also influence Australia's climate patterns, impacting the frequency and intensity of wildfires [135].

Summers and springs have relatively high seasonal burned area values possibly due to the fact that seasonal fluctuations in burned areas are also influenced by land management methods and human activities. Controlled burns are commonly used during cooler months to lower fuel loads and reduce the risk of more extensive and catastrophic wildfires during hotter, drier months. The efficacy of these approaches, however, is dependent on proper timing, weather conditions, and adherence to land management laws. Human activities, such as accidental ignitions and deliberate arson, can lead to increasing burned areas, particularly during fire-prone seasons [136].

Summer, which normally lasts from December to February, is a significant period for fire activity in the Australian grassland. Elevated temperatures, dry weather, and the prevalence of flammable vegetation all contribute to a heightened danger of wildfires during this season. The oscillation in the Southern Oscillation Index (SOI), especially during El Niño events, can intensify these conditions, resulting in larger scorched regions. La Niña occurrences, on the other hand, tend to bring colder and wetter conditions, which suppresses fire activity [137, 138]. Spring months also have high average values, likely due to the fact that, just like in the forest vegetation class, controlled burning is done in the Australian grassland during cooler months to cut fuel loads and lessen the possibility of wildfires becoming more catastrophic during summer months [137, 138].

Australia's agricultural environment is diversified, and the burning of agricultural wastes, also known as stubble burning, is a frequent practice in this country. The cropping cycle can be associated with the seasonality of burned areas in Australian croplands. Following the harvest season, farmers frequently engage in controlled burns to clear fields of post-harvest leftovers, reduce weed development, and prepare the soil for the forthcoming planting season. This technique causes a significant increase in burned areas during this specific period. Agricultural burning in Australia takes place predominantly from March to April in the wheat-producing regions of southwestern Western Australia and the eastern parts of the wheat belt that spans from southern South Australia to central Queensland. Furthermore, weather factors may influence the timing of the burns, with farmers trying to perform controlled burns during times of lower fire danger, such as when weather conditions are generally mild and there is less risk of fire spreading to unintended areas [115, 139, 140].

Australia's fire season normally lasts from December to May in the south, from May to October in the north, and from August to March in the center, with the southeast of the country being one of the most fire-prone regions on earth. Several shrublands such as the Lignum shrublands are spread across inland Australia. Lignum shrublands are found across both semi-arid and arid regions within inland Australia. In these regions, shrub fires occur when a long dry season comes after a good rainfall rich season. Above average rainfall seasons boost lush growth, which becomes a fuel load that increases fire risks during dry seasons [141, 142, 143, 144].

4.1.3 CO Concentration Trend Analysis

The trend analysis was performed by producing scatter plots of average annual satellite-observed total column CO concentrations from 2005 to 2019 in South America, Southern Africa, and Australia. The plots are shown as Figures 13, 14, and 15 below.

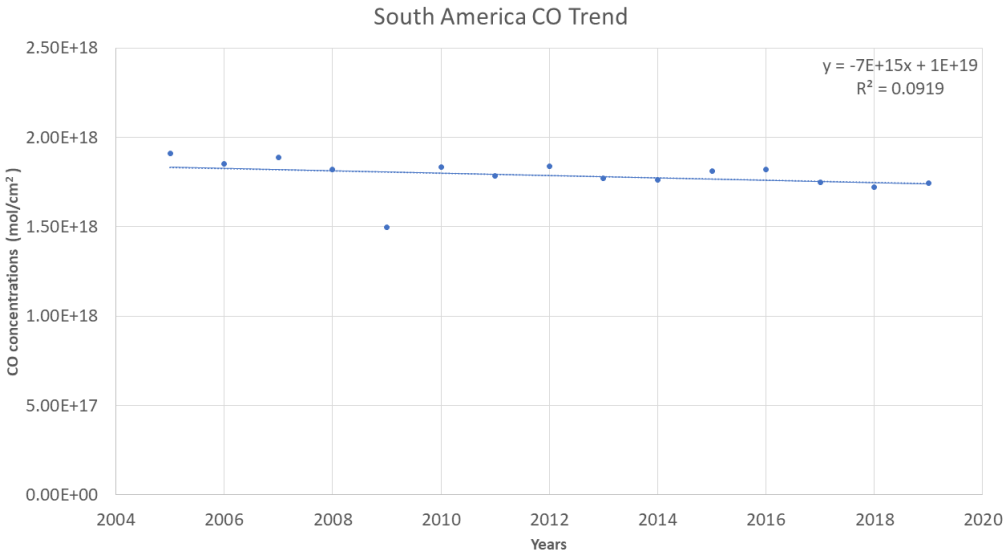

Figure 13: South America annual CO concentration trend from 2005 to 2019

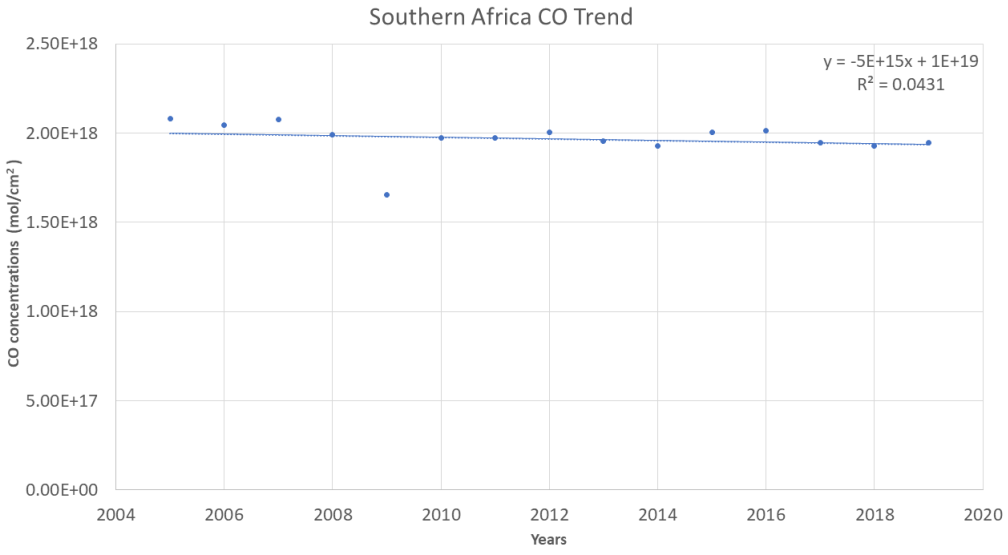

Figure 14: Southern Africa annual CO concentration trend from 2005 to 2019

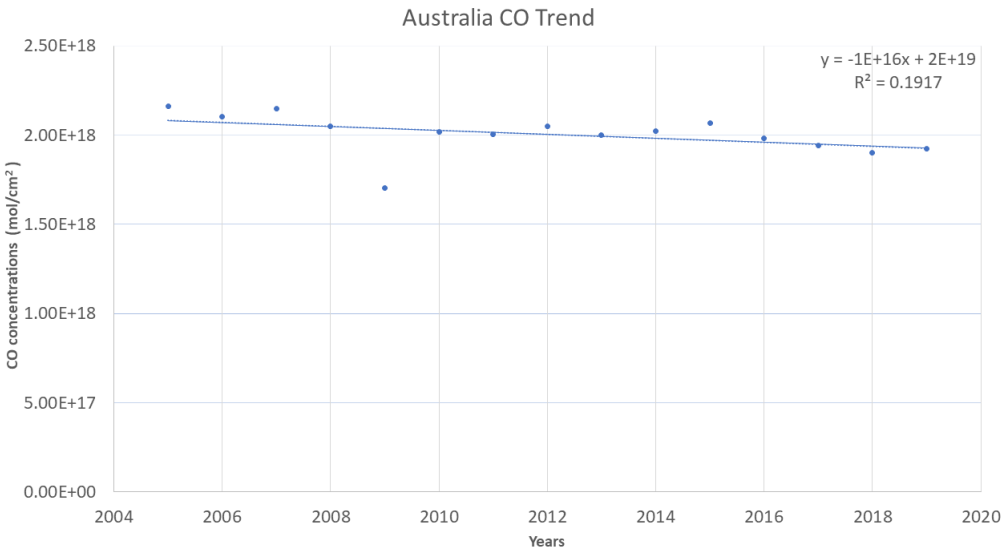

Figure 15: Australia annual CO concentration trend from 2005 to 2019

Figures 13, 14, and 15 show the annual CO concentrations in South America, Southern Africa, and Australia, respectively, measured in mol/cm^2. The scatter plots and trend (best fit) lines are shown with their corresponding equations and coefficients of determination (r^2). All three equations have negative gradients, consistent with the downward trending best fit lines. This annual trend show a decrease in annual CO concentrations in all three regions: South America has a 0.59% (1.13×10^{16} mol/cm^2) annual decrease, Southern Africa a 0.42% (8.67×10^{15} mol/cm^2) annual decrease, and Australia a 0.74% (1.60×10^{16} mol/cm^2) annual decrease. The coefficients of determination are 0.0919, 0.0431, and 0,1917, suggesting that 9.2%, 4.3%, and 19.2% of the annual CO variations in South America, Southern Africa, and Australia, respectively, are described by the variations of years. However, recall that this does not necessarily mean that the model is not reliable, or whether or not this is the right regression. Additionally, in all three regions, there is a deep CO minimum in 2009 and a near-maximum in 2015.

As previously established, biomass burning is the principal source of CO emissions in the SH. More burning tends to lead to higher CO levels [145]. Other factors that influence CO distributions are anthropogenic emissions, transport and oxidation by reaction with the hydroxyl radical (OH) [146]. The decreasing CO trends shown by Figures 13, 14, and 15 would then lead to presume a a favorable change in at least one of those factors, such as a decrease in biomass burning intensity. A previous study that focused on the CO concentration trend between the years 2000 and 2017 found a global annual decline of $0.32 \pm 0.05\%$ or ($5.6 \times 10^{15} \pm 0.9 \times 10^{15}$ mol/cm^2) in MOPITT CO columns, with a global CO source (anthropogenic and biomass burning) decline of $0.32 \pm 0.23\%$ per year [147]. Another study found that between 1998 and 2015, there was a decline in global burned of $24.3 \pm 8.8\%$ which translated to $1.35 \pm 0.49\%$ per year. There was an annual burned area decline of 1.68% and 1.27% in South America and Africa, respectively, with large burned area decreases notable in the tropical savannas of of those two regions, and other regions with low and intermediate levels of tree cover [148]. A third study which was conducted for the period between 2005 and 2016 also found declining trends in CO concentration in South America, Africa, and Australia, and associated those trends to decreases in anthropogenic emissions and biomass burning events. This study found a negative trend in fire counts in the three regions and linked it to the negative CO trends for the period studied [149].

4.2 Correlation Between CO concentration and Burned Area

Total column				
Regions	Emissions	Seasons	r	p-values
South America	Forest	Annual	0.72	0.00
		Summer	-0.07	0.80
		Autumn	0.12	0.68
		Winter	0.74	0.00
		Spring	0.87	0.00
	Cropland	Annual	0.67	0.04
		Summer	0.02	0.94
		Autumn	0.54	0.04
		Winter	0.55	0.04
		Spring	0.84	0.00
	Grassland	Annual	0.66	0.01
		Summer	-0.02	0.95
		Autumn	0.21	0.44
		Winter	0.75	0.00
		Spring	0.91	0.00
	Shrubland	Annual	No Data	No Data
		Summer	No Data	No Data
		Autumn	No Data	No Data
		Winter	No Data	No Data
		Spring	No Data	No Data
Southern Africa	Forest	Annual	0.29	0.29
		Summer	0.51	0.05
		Autumn	0.60	0.02
		Winter	0.43	0.13
		Spring	0.04	0.89
	Cropland	Annual	0.15	0.60
		Summer	0.16	0.56
		Autumn	0.75	0.00
		Winter	0.45	0.10
		Spring	0.36	0.20
	Grassland	Annual	0.02	0.94
		Summer	0.33	0.23
		Autumn	0.55	0.03
		Winter	0.07	0.81
		Spring	0.01	0.96
	Shrubland	Annual	No Data	No Data
		Summer	No Data	No Data
		Autumn	No Data	No Data
		Winter	No Data	No Data
		Spring	No Data	No Data

Table 2 (a): Correlations between CO concentrations and burned areas, and their p-values. Accepted values are highlighted in Red, showing correlations that are unlikely to have occurred solely due to chance.

Total column				
Regions	Emissions	Seasons	r	p-values
Australia	Forest	Annual	-0.02	0.95
		Summer	0.38	0.16
		Autumn	-0.11	0.71
		Winter	0.36	0.21
		Spring	0.31	0.28
	Cropland	Annual	-0.03	0.92
		Summer	0.00	1.00
		Autumn	-0.54	0.04
		Winter	0.34	0.23
		Spring	0.45	0.11
	Grassland	Annual	0.15	0.58
		Summer	0.44	0.10
		Autumn	-0.27	0.33
		Winter	0.02	0.97
		Spring	0.09	0.76
	Shrubland	Annual	No Data	No Data
		Summer	No Data	No Data
		Autumn	No Data	No Data
		Winter	No Data	No Data
		Spring	No Data	No Data

Table 2 (b): Correlations between CO concentrations and burned areas, and their p-values. Accepted values are highlighted in Red, showing correlations that are unlikely to have occurred solely due to chance.

The expectations from this research are to show, as the theory suggests, that there is a relationship between CO emissions and burned areas, i.e. when burning is high, CO is high, and when burning is low, CO is also low. So far, for the most part, results seem to show that this is the case: There is a relationship between CO emissions and burned areas. However, this relationship is not always clear. In certain months in some regions in the SH, there appears to be (little or) no relationship between the two variables, even if that relationship exists. This is what will be explored in this section, using the Pearson correlation coefficient statistical analysis (and p-value). The correlations between seasonal and annual CO emissions and burned areas, with their p-values, will be compared.

Table 2 (a) and (b) display the annual and seasonal correlations between CO concentrations and burned areas, along with their p-values, in three different vegetation classes in the SH. A few observations can be made from those tables: First, All the correlations with magnitudes that are less than 0.50 have p-values greater than the accepted maximum of 0.05, The lowest magnitude is 0.00 with a p-value of 1.00. Second, All the correlations that have magnitudes greater than 0.50 (i.e. moderate to very strong correlations) also have p-values that fall within the accepted range of 0.05 or lower. The highest correlation is 0.91 with a p-value of 0.00, seen in the spring of the South American grassland. Third, as the correlation decreases, the p-value increases; as the correlation increases, the p-value decreases. Fourth, all but one of the correlations with accepted p-values are positive. The negative correlation is -0.54 with a p-value of 0.04, seen in the autumn of the Australian cropland.

What these statistical results seem to suggest, at least in general, is that there is a positive relationship between CO concentrations and burned areas: All moderate-to-weak correlations

(below 0.50) have p-values greater than 0.05 which suggests that the relationship very likely occurred due to random chance. On the other hand, all moderate-to-strong correlations (above 0.50) have p-values equal to or less than 0.05, suggesting that the relationship is unlikely to exist solely due to chance.

Statistical results appear to show a general consistency, which seems to endorse the theoretical expectations of a positive correlation between CO emissions and burned areas. Weak correlations had higher than accepted p-values, and strong correlations had accepted p-values. However, not all accepted correlations were positive, as can be seen in the Australian cropland. This may be explained by different factors, such as wind circulation, which will be discussed in the next section.

4.3 Global Wind Circulation and its Effects on CO Distributions

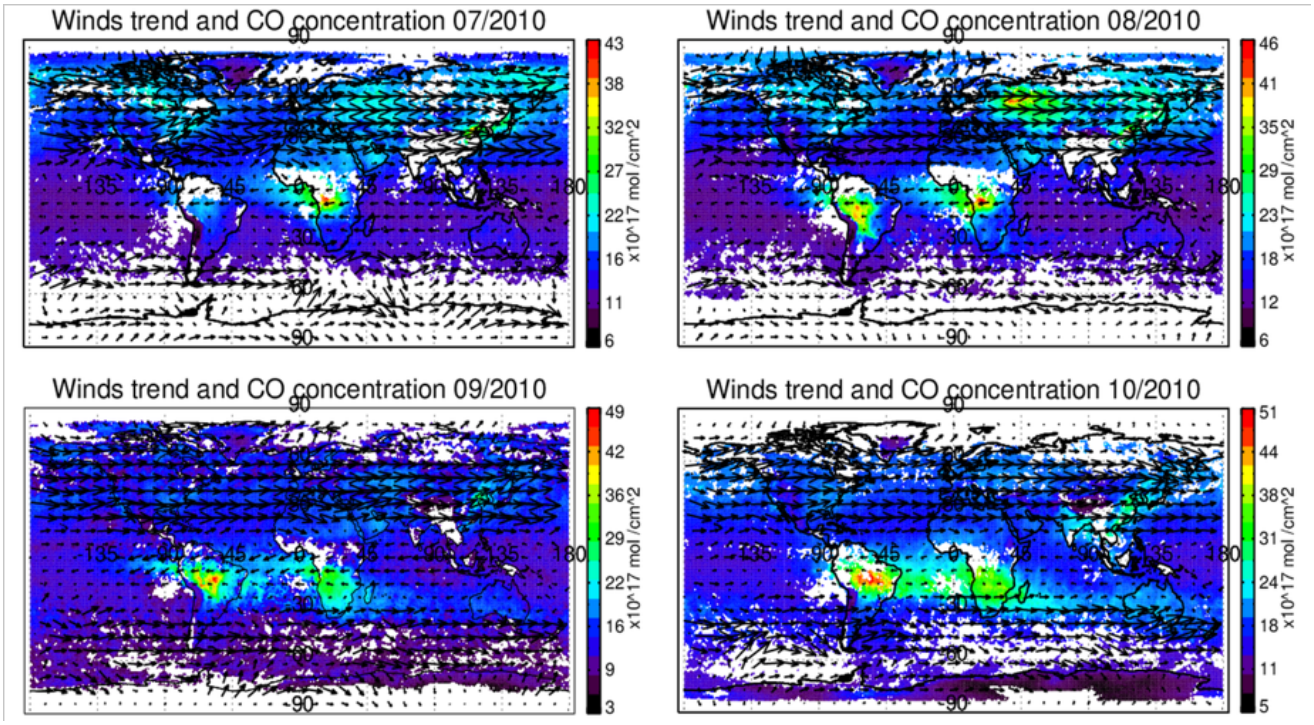

Figure 16: Winds trend and CO concentration from July to October 2010. Transport of CO from South America to Southern Africa and Australia is clearly visible.

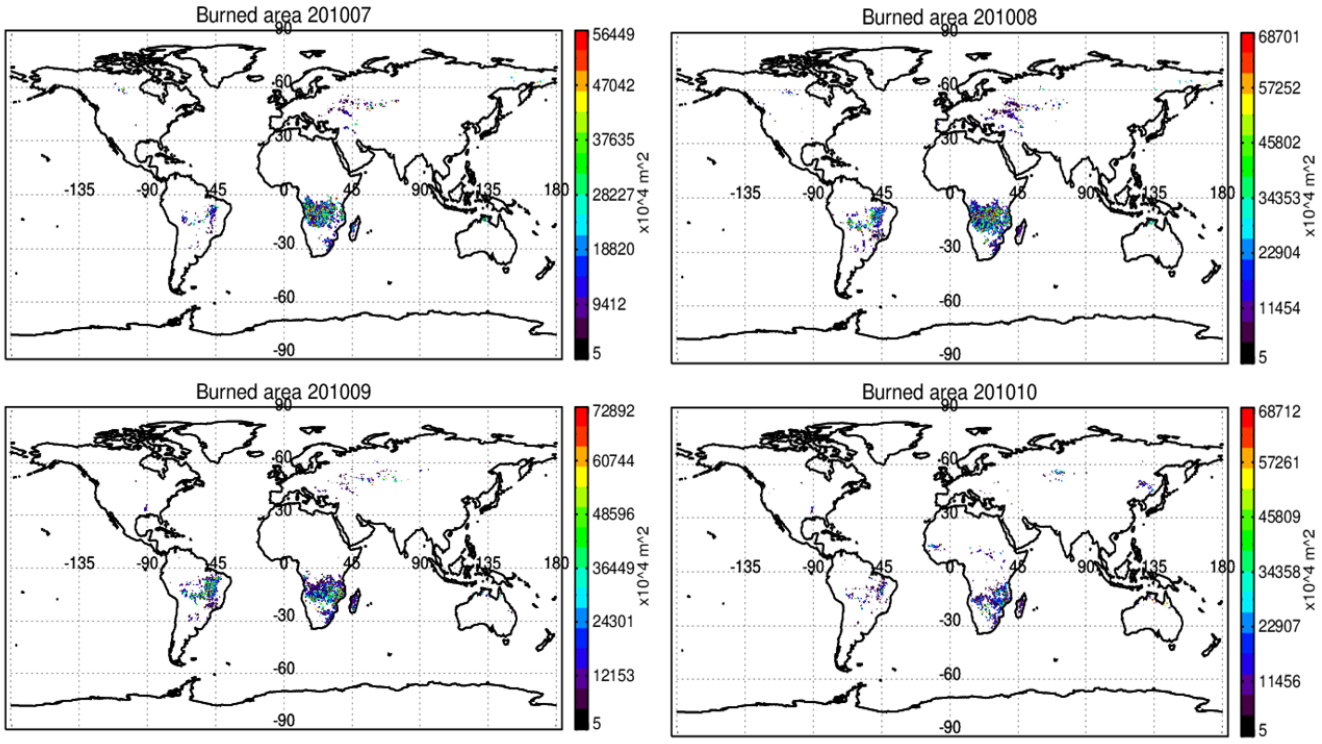

Figure 17: Burned area from July to October 2010

Figures 16 and 17 seek to demonstrate a case in which global winds affected CO distributions throughout the SH. Figure 16 shows the global winds trend and CO concentrations from July to October 2010 and Figure 17 shows burned area, also from July to October 2010. CO concentration in Southern Africa is high in July (reaching $\sim 43 \times 10^{17}$mol/cm^2) and increases in August to as high as $\sim 46 \times 10^{17}$mol/cm^2, coinciding with the high burned area in July which is also higher in August. However September has lower CO concentration than October despite having a higher burned area. South America and Australia also have the highest regional CO concentrations out of the four months (July-October) in October (reaching $\sim 51 \times 10^{17}$mol/cm^2 and $\sim 23 \times 10^{17}$mol/cm^2, respectively), despite having the lowest regional burned areas in the same time period. This suggests a possible CO transport between those three regions due to winds circulation. In fact, in July and August, CO transport appears to be westward, especially in the lower latitudes (0° to 20°S). The movement can be seen from Africa to over the Atlantic ocean, and the CO levels in Australia are still low. In September and October however, the transport appears to have shifted eastward, especially in higher latitudes (21°S and above). By October, while South America still has a very CO concentration, CO transport from South America to Australia over the Atlantic and Indian oceans can be clearly seen.

Global wind circulation has a significant impact on the distribution of atmospheric elements such as CO (CO) around the world. The SH, which has a comparatively clean atmosphere with fewer direct CO emissions, is prone to long-distance pollution transport caused by global wind patterns. Winds from the east, like the trade winds or easterlies, and the west, such the westerlies, have been shown to influence the long-distance transfer of pollutants as well as the movement of air masses over the Atlantic and Indian oceans and between continents. At about 30 degrees South, the Hadley cell from the tropical region and the Ferrell cell from the middle latitude converge to generate a subtropical jet-stream over Southern Africa. The jet stream stretches up to the tropopause area. This tropospheric air stream from the west has a high speed of about 25 m/s and serves as a channel for moving and carrying air masses and pollutants to the east. It has been previously demonstrated that emission from South America can

be advected into the Atlantic and reach southern Africa; consequently, emission from Southern Africa can likewise be transferred to Australia across the Indian Ocean [150, 151].

CO columns over Australia often peak in October, whereas biomass burning emissions in South America typically reach a maximum in September. Southern Africa reaches its peak in in August-September, or in September-October, depending on the location. It has previously been shown that South American emissions can be advected in Australia within a few weeks [152, 153].

4.4 El Niño, La Niña Effects on CO Concentrations

As previously stated, depending on how they were monitored, five El Niño events occurred between 2005 and 2019. Similarly, five La Niña occurred during the same time period. The strongest El Niño occurred in 2015/16, and the strongest La Niña occurred in 2007/08. However, this section aims to investigate and show the 2010/11 and 2015/16 ENSO events, by measuring the average sea surface temperatures (SST) in the central and eastern equatorial Pacific Ocean. In addition, this section also aims to investigate the effects of those ENSO events on rainfall and compare their CO concentrations to those of the neutral period of 2013/14. The time periods of 2010/11 and 2015/16 were chosen because they are respectively the closest strong La Niña and and El Niño periods to the neutral period of 2013/14.

The comparison was done as follows: the average values of monthly Data from 2005 and 2019 (of SST, precipitation and CO levels) were computed, then they were compared with monthly values of the years in focus by subtracting the later from the former to obtain fluctuations (or deviations from the mean) that were plotted as the figures that are used in this section. A positive fluctuation means higher than average and a negative fluctuation means lower than average. For example, the average SST values of all the September months can be calculated and stored in a grid, say Grid A. Also, the SST values for September 2010 can be stored in Grid B of the same dimension as Grid A. Then, Grid B is subtracted from Grid A to obtain fluctuations which can also be stored in Grid C. Finally, Grid C can be plotted as a figure. The same process can be repeated for other months, years, and also for precipitations data and CO emissions data.

4.4.1 ENSO Event: La Niña

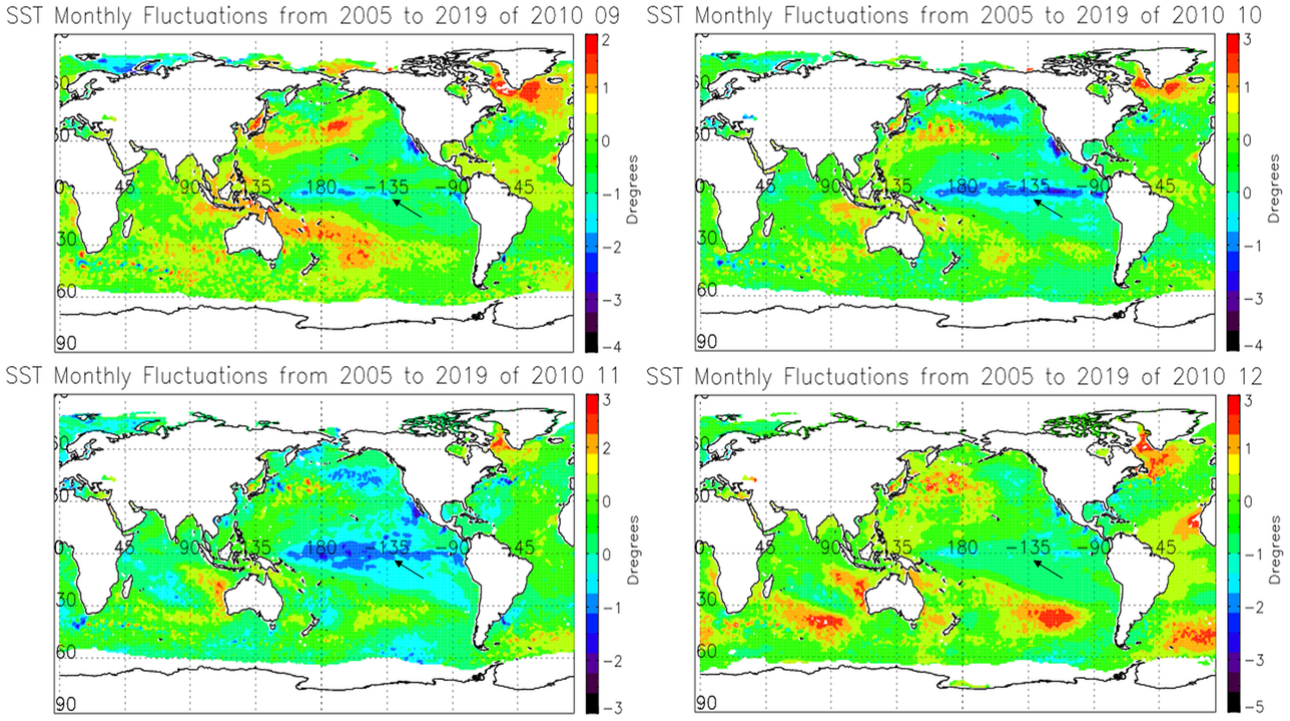

Figure 18: Sea surface temperature fluctuations for the last four months of 2010 in degrees Celcius

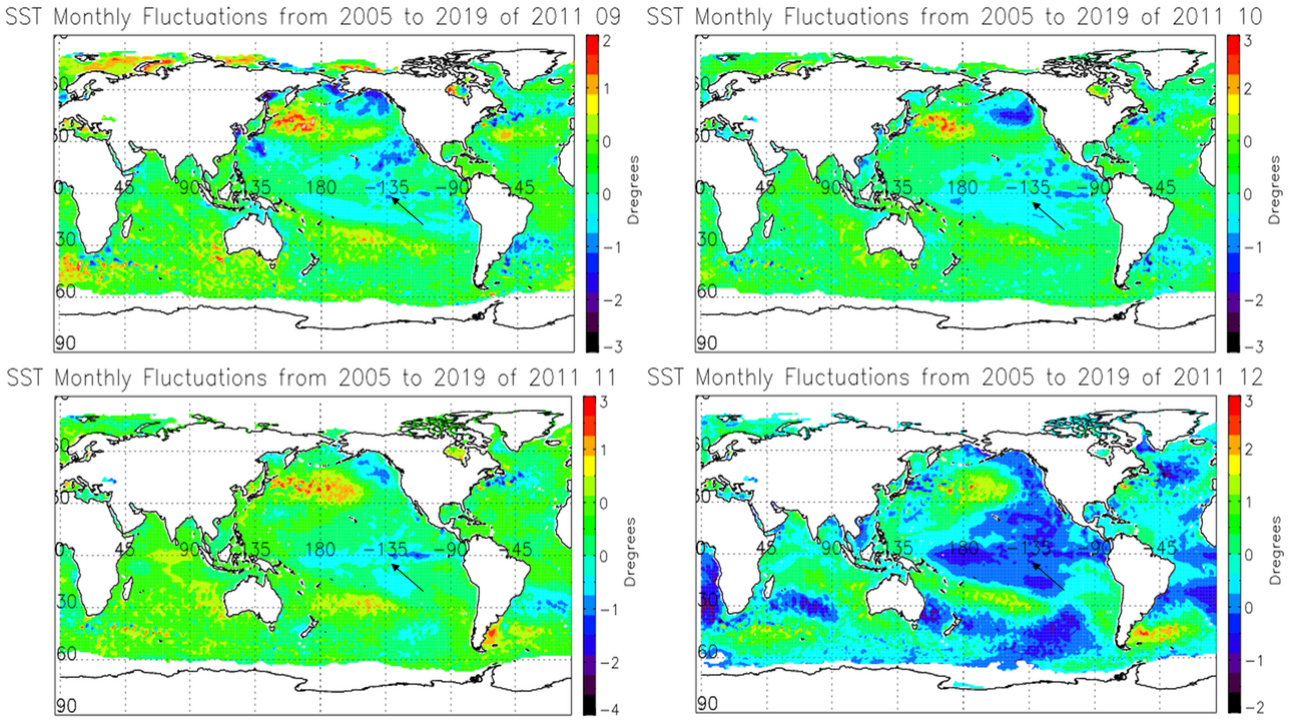

Figure 19: Sea surface temperature fluctuations for the last four months of 2011 in degrees Celcius

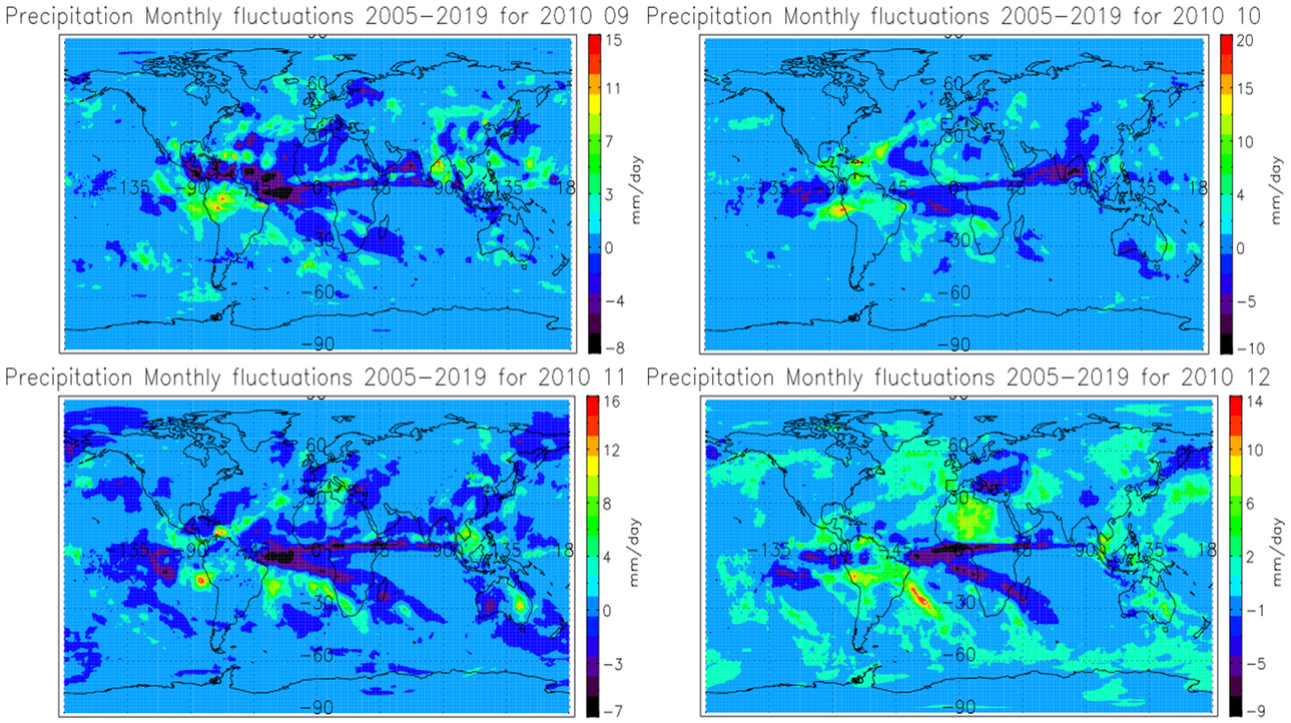

Figure 20: Precipitation fluctuations for the last four months of 2010

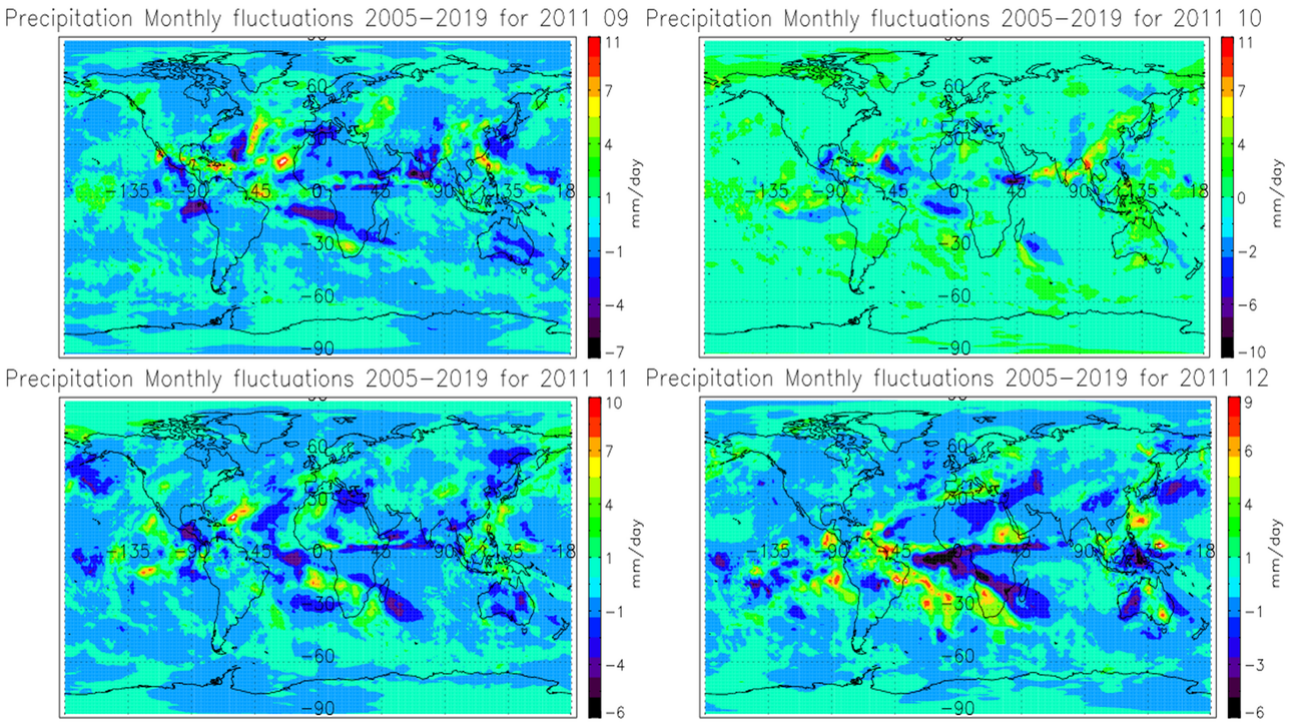

Figure 21: Precipitation fluctuations for the last four months of 2011

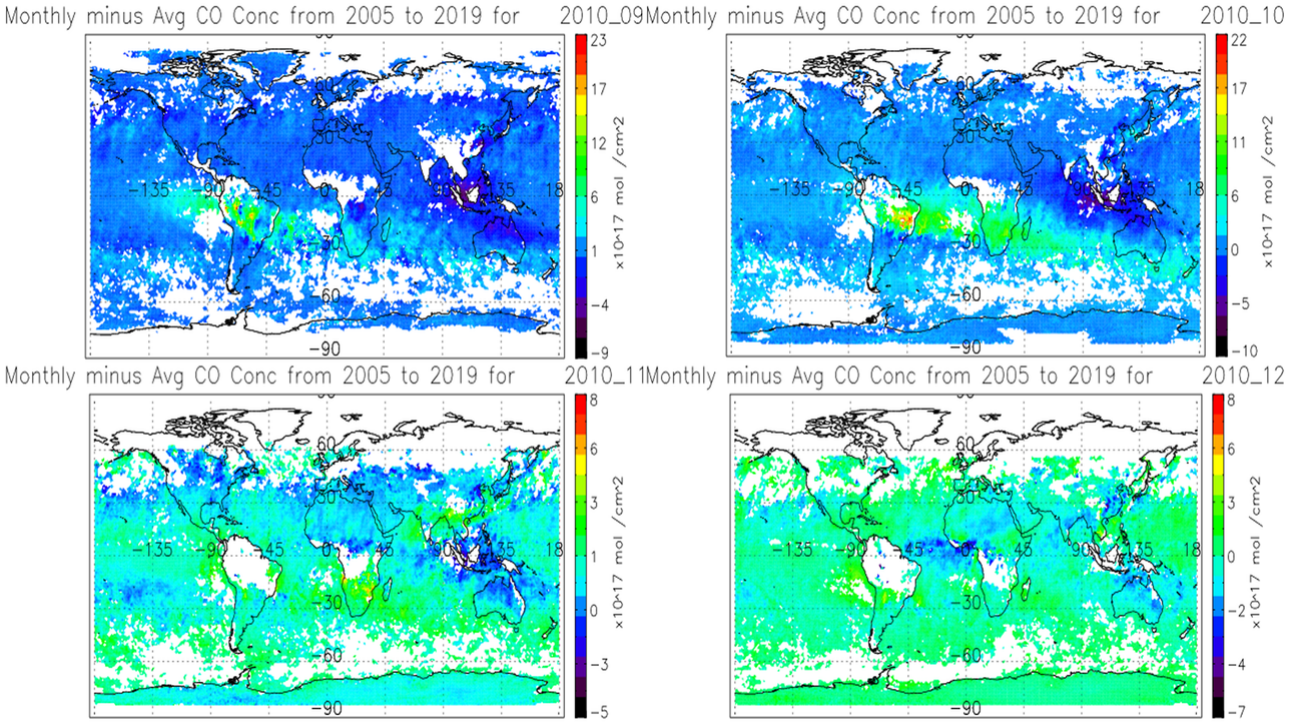

Figure 22: CO emissions fluctuations for the last four months of 2010

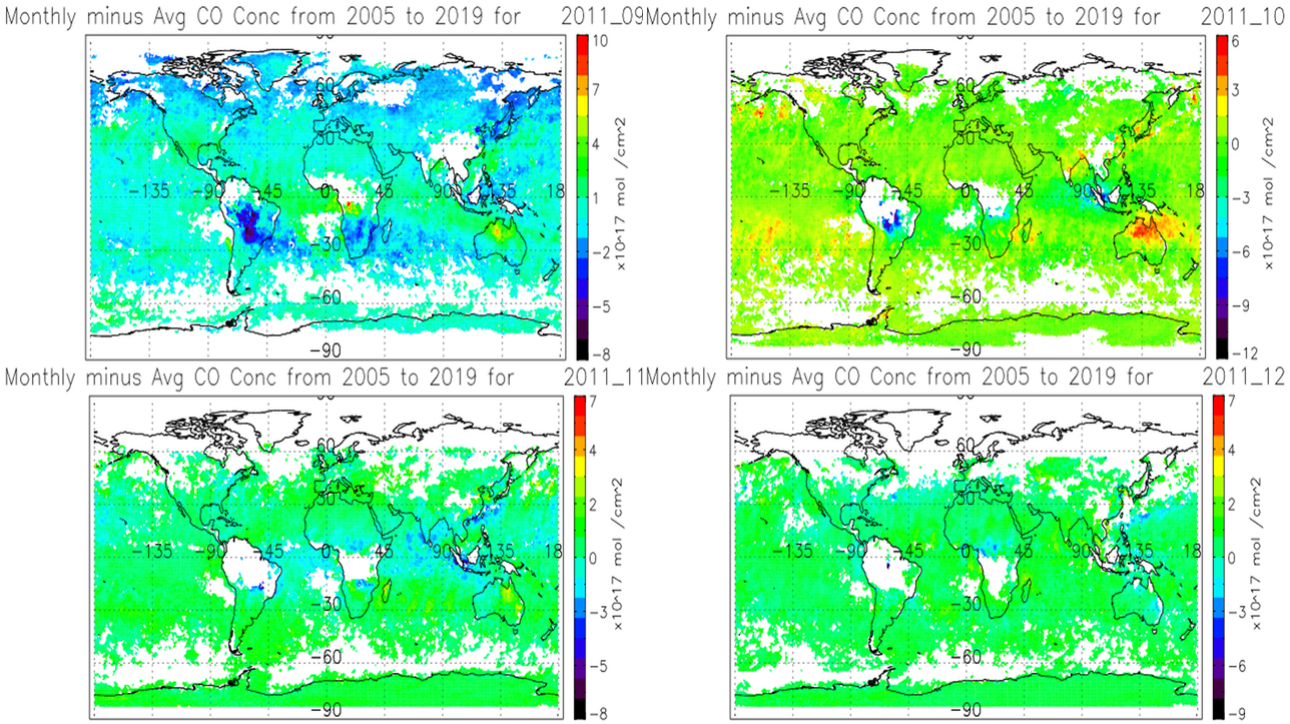

Figure 23: CO emissions fluctuations for the last four months of 2011

It was previously noted that a La Niña event is characterized by the cooling of the SST by at least 0.5 degrees Celsius in the Niño 3.4 region (5°N–5°S, 120°W–170°W). Figures 18 and 19 show the SST fluctuations from September to December 2010 and 2011, measured in degrees Celsius. The black arrows in these figures, as well as in all other SST figures in this section, point to the Niño 3.4 region. The mean temperature in the Niño 3.4 region can be seen to be more than 1.5 degrees below average, hence showing a strong La Niña phase, especially in 2010. In 2011, temperature in the region seems to have slightly risen, although still

being more than 0.5 degrees Celsius below-average. Figures 20 and 21 show the precipitation fluctuations from September to December 2010 and 2011, measured in mm/day. Precipitation levels in 2010 can be seen to be near or above-average for the most part in the South America, southern Africa, and Australia. However, some parts in southern Africa can be seen to reach below-average levels by up to 6 mm/day (November and December). In 2011, precipitation levels in the SH have risen, even as La Niña has weakened during the same period. Figures 22 and 23 show the CO fluctuations also from September to December of both 2010 and 2011, measured in mol/cm^2. Southern Hemisphere CO levels can be seen to be consistently near or below-average, as expected during La Niña.
When cold water rises from the deep ocean to the surface in the eastern Pacific Ocean, atmospheric circulation patterns are altered, impacting global weather conditions. These changes may result in varying weather effects in the Southern Hemisphere, such as changes in the distribution and intensity of rainfall [154, 155].

In Australia, La Niña events typically lead to higher-than-average rainfall in the northern and eastern regions due to the enhanced convection and cloud formation caused by the warm water near Australia. For instance, Australia had one of its wettest periods ever during the 2010–2011 La Niña event, which led to extensive flooding [156]. The effect of La Niña on rainfall varies by region in South America. La Niña typically brings more rain to the southeast of the continent, which includes parts of Brazil, Uruguay, and Argentina. This is mostly because of the change in atmospheric moisture patterns and jet streams, which favours wetter conditions in these regions. On the other hand, La Niña can provide drier-than-average weather in western countries like Peru and Ecuador because the amount of evaporation and ensuing precipitation are lowered due to the cooling of ocean surface [157, 158, 159]. Changes in rainfall patterns during La Niña events are also visible in Southern Africa. La Niña typically corresponds to above average precipitation levels in the region, particularly in the summer. Although there are concerns such as flooding, this can also have positive effects for agriculture. In certain regions of South Africa, Botswana, and Zimbabwe, for example, the 2016–2017 La Niña effect led to increased precipitation and subsequent flooding [66, 160]. Also, in some regions in the SH (especially in Southern Africa), the wet episodes can still take place even during the first few months post-La Niña [66].

The cooling of the average SST in the eastern equatorial Pacific Ocean during a La Niña event has an impact on other global weather trends, causing changes in phenomena such as wildfires and human activities. Consequently, those alterations may indirectly have an impact on CO emissions in the Southern Hemisphere [161]. As previously seen, wildfires and biomass burning are a primary source of CO. A La Niña event can have a significant impact on their intensity and frequency, by causing an increase in precipitation in some regions. In Australia, for example, it has already been shown that La Niña usually brings more rainfall, which can lower the frequency of wildfires. When there are fewer wildfires, biomass burning produces less CO emissions. During the 2010–2011 La Niña event, as Australia saw significant rainfall, wildfire activity was also significantly reduced, thus making the Australian landscape a large carbon sink [162].

Southern Africa also typically sees above-average rainfall during La Niña events, particularly during the summer months. During the 2010–2011 La Niña, Southern Africa had a significant decrease in wildfire activity because of above-average rainfall, which led to lower atmospheric CO levels [163]. On the other hand, La Niña can have mixed effects in South America. A previous research have found that during La Niña events northern Brazil experiences rainier-than-normal conditions. With the characteristic of higher-than-normal pressure

over the central and eastern Pacific, La Niña also results in decreased cloud production and rainfall in that region. The west coast of tropical South America and the pampas region of southern South America experience Drier-than-normal conditions. These conditions may make wildfires more frequent and severe, which would increase CO emissions [164].

4.4.2 Neutral Period

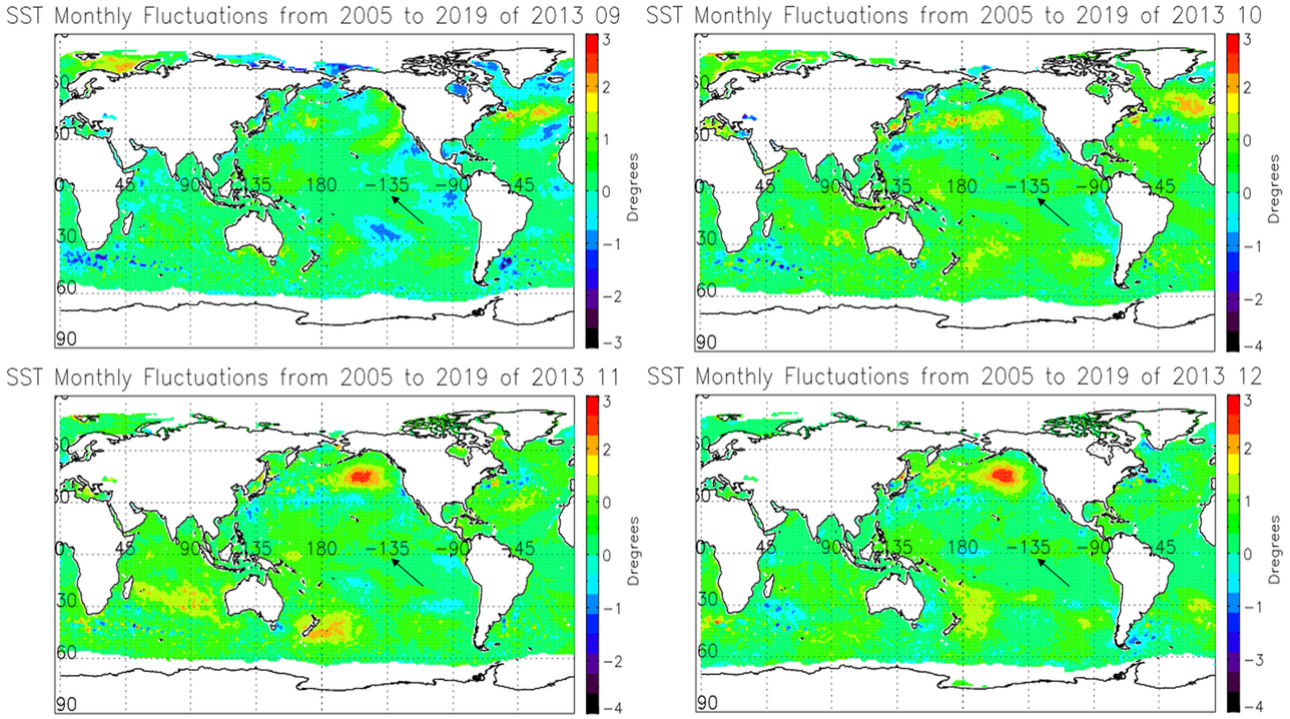

Figure 24: Sea surface temperature fluctuations of the last four months of 2013 in degrees Celcius

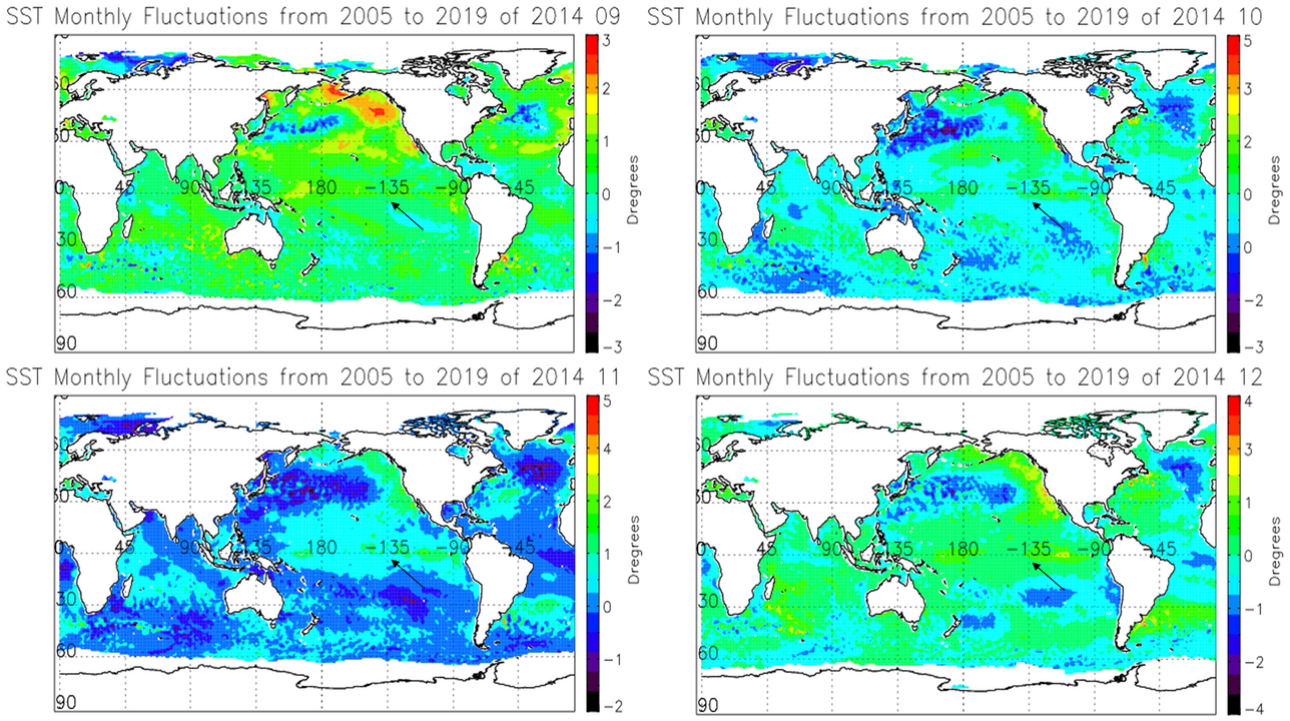

Figure 25: Sea surface temperature fluctuations of the last four months of 2014 in degrees Celcius

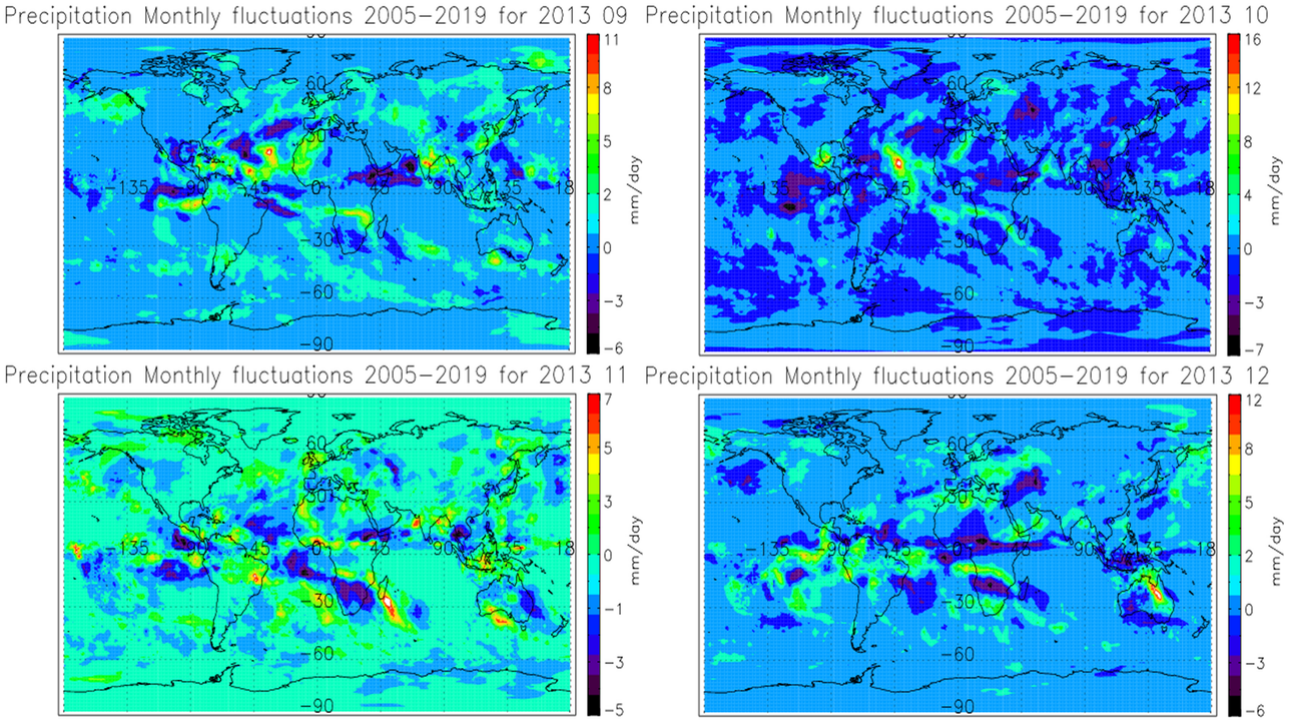

Figure 26: Precipitation fluctuations for the last four months of 2013

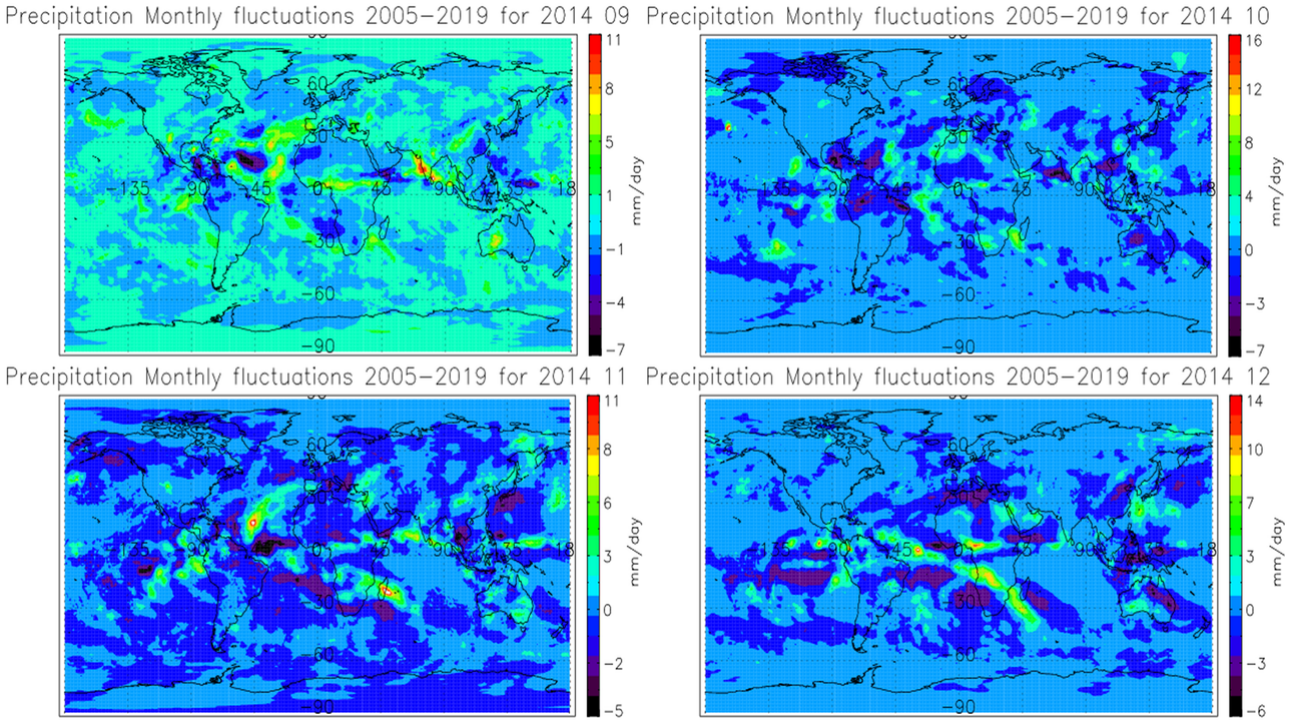

Figure 27: Precipitation fluctuations for the last four months of 2014

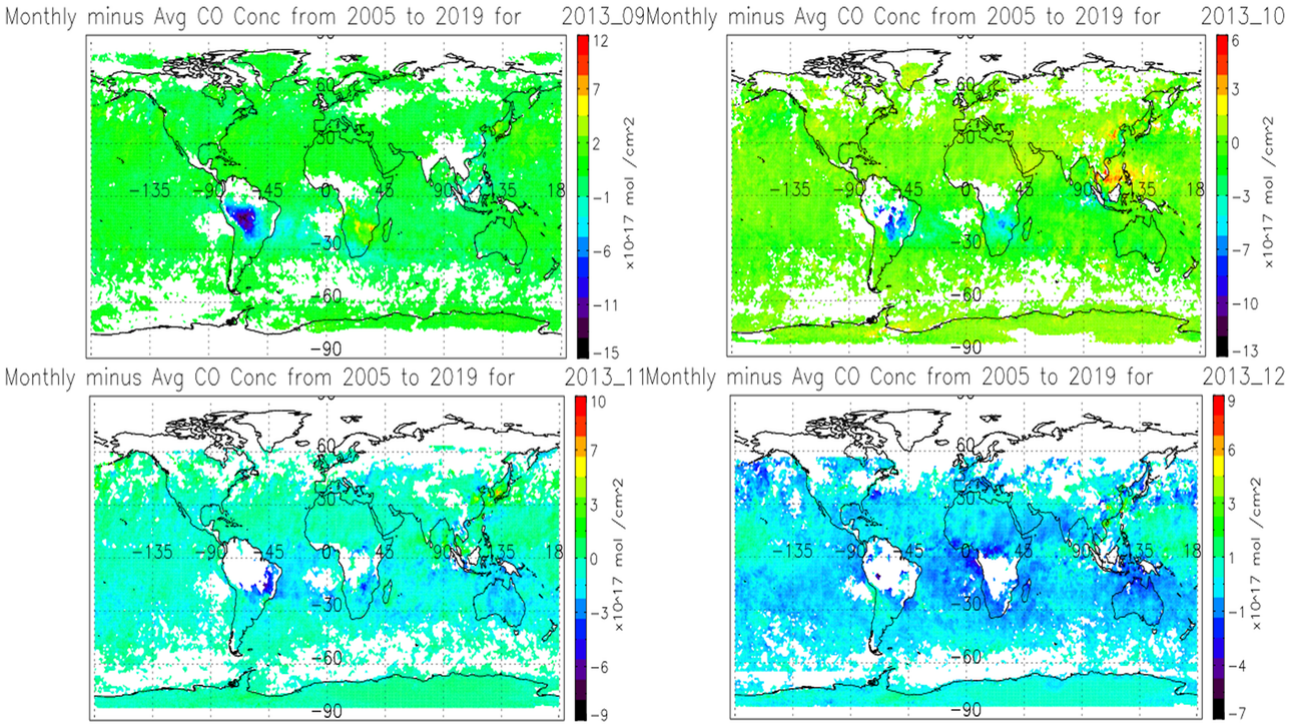

Figure 28: CO emissions fluctuations for the last four months of 2013

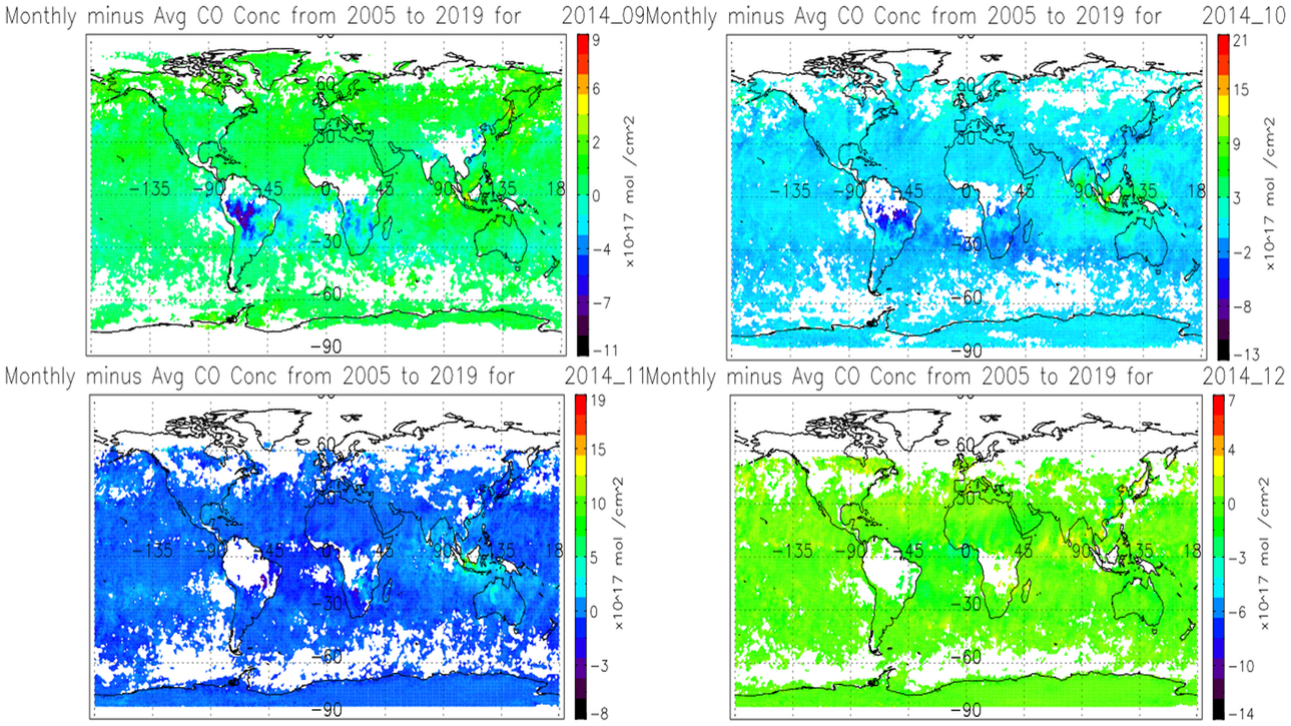

Figure 29: CO emissions fluctuations for the last four months of 2014

Figures 24 and 25 show the SST fluctuations for 2013 and 2014 from September to December, measured in degrees Celcius. The average temperature in the Niño 3.4 region can be seen to remain below the magnitude of 0.5 degrees Celsius throughout the last quarter of 2013, thus making it a neutral period. In 2014 however, the mean temperature in the Niño 3.4 region is more than 0.5 degrees Celsius above-average. The transition attribute of a neutral phase would then suggest that there are higher CO concentrations and lower rainfall during a neutral year than during a La Niña year. Figures 26 and 27 show the precipitation fluctuations for 2013 and 2014 from September to December, measured in mm/day. Figures 28 and 29 show the CO levels fluctuations for 2013 and 2014 from September to December, measured in mol/cm^2. Both Southern Hemisphere precipitation and CO levels can be seen for the most part to remain near-average, as expected.

Concentrations of CO in a year without ENSO effects (a neutral year) can be very different from those in years with El Niño and La Niña. Without ENSO in the SH, namely in regions of Australia, Southern Africa, and South America, the weather patterns are more stable, and CO emissions are generally expected to be near-average. This is because the neutral phase is the transition between ENSO's warm and cold phases, and during this period, sea surface temperatures, wind patterns, and tropical precipitation are all near-average [165].

4.4.3 ENSO Event: El Niño

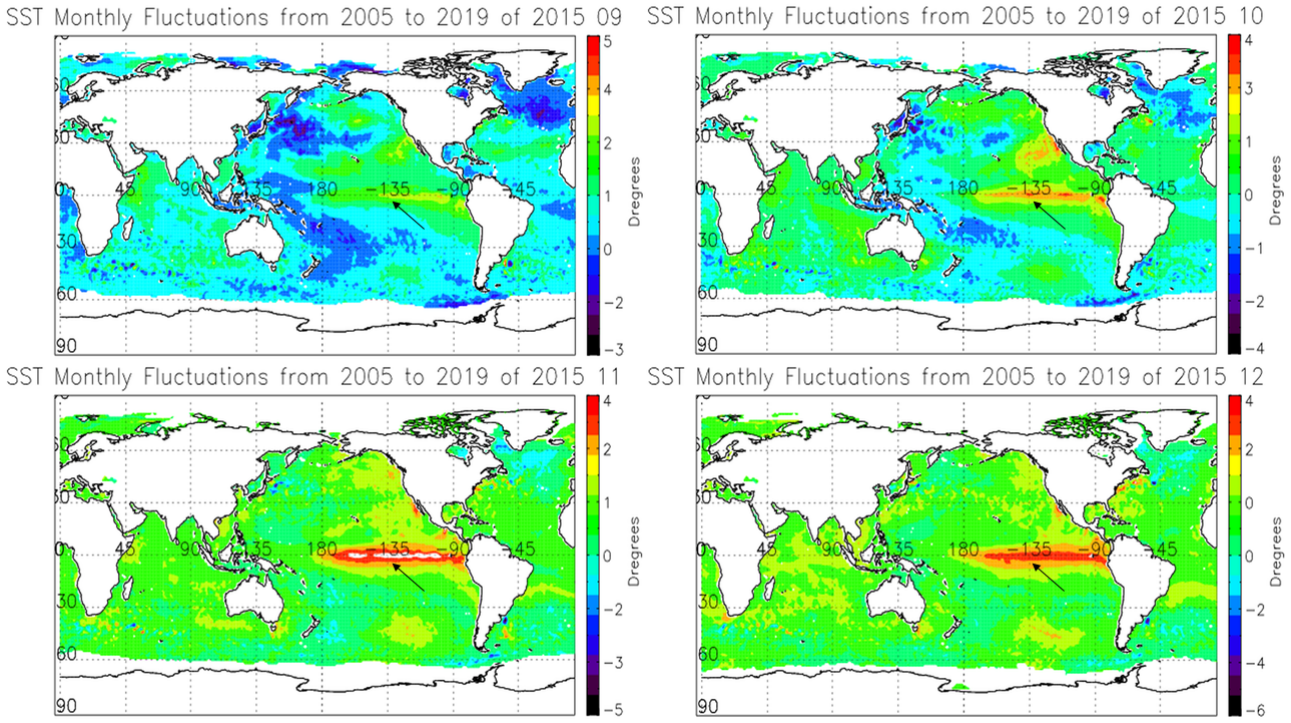

Figure 30: Sea surface temperature fluctuations of the last four months of 2015 in degrees Celcius. The mean temparature in the Niño 3.4 region suggests a strong El Niño phase

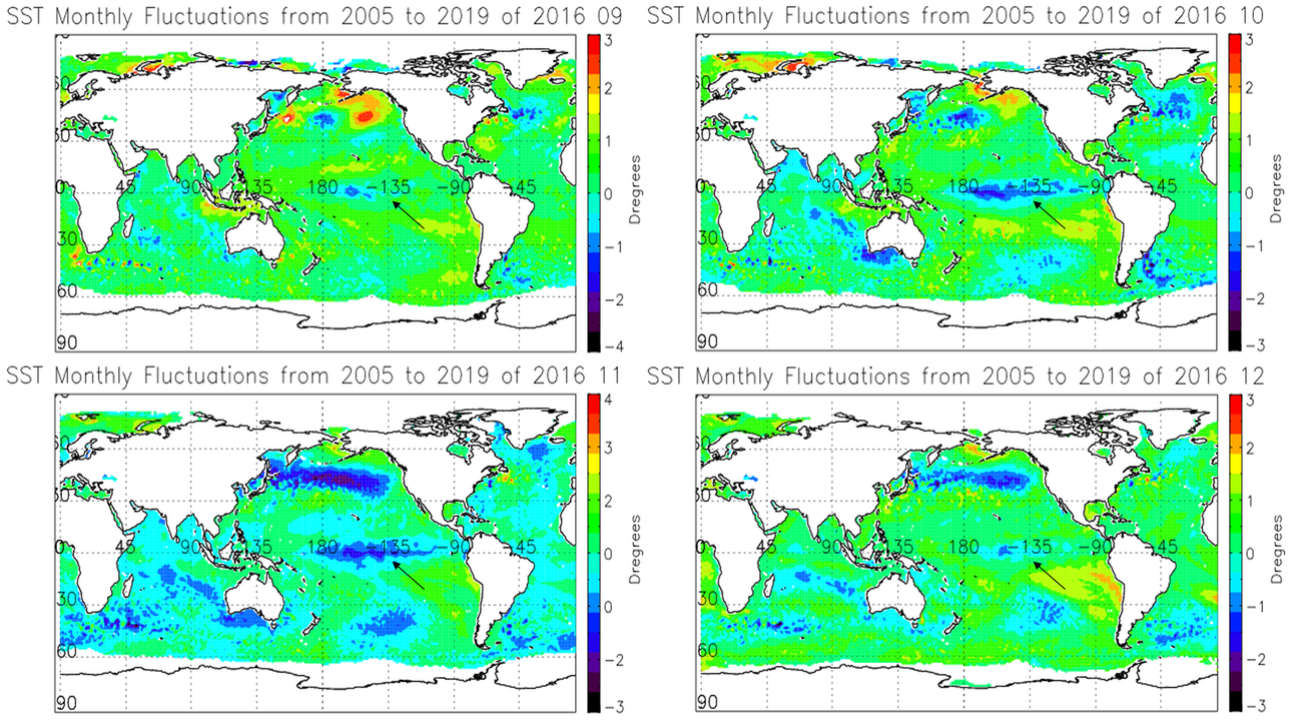

Figure 31: Sea surface temperature fluctuations of the last four months of 2016 in degrees Celcius. The mean temparature in the Niño 3.4 region suggests that the 2016-17 weak La Niña phase is already taking place

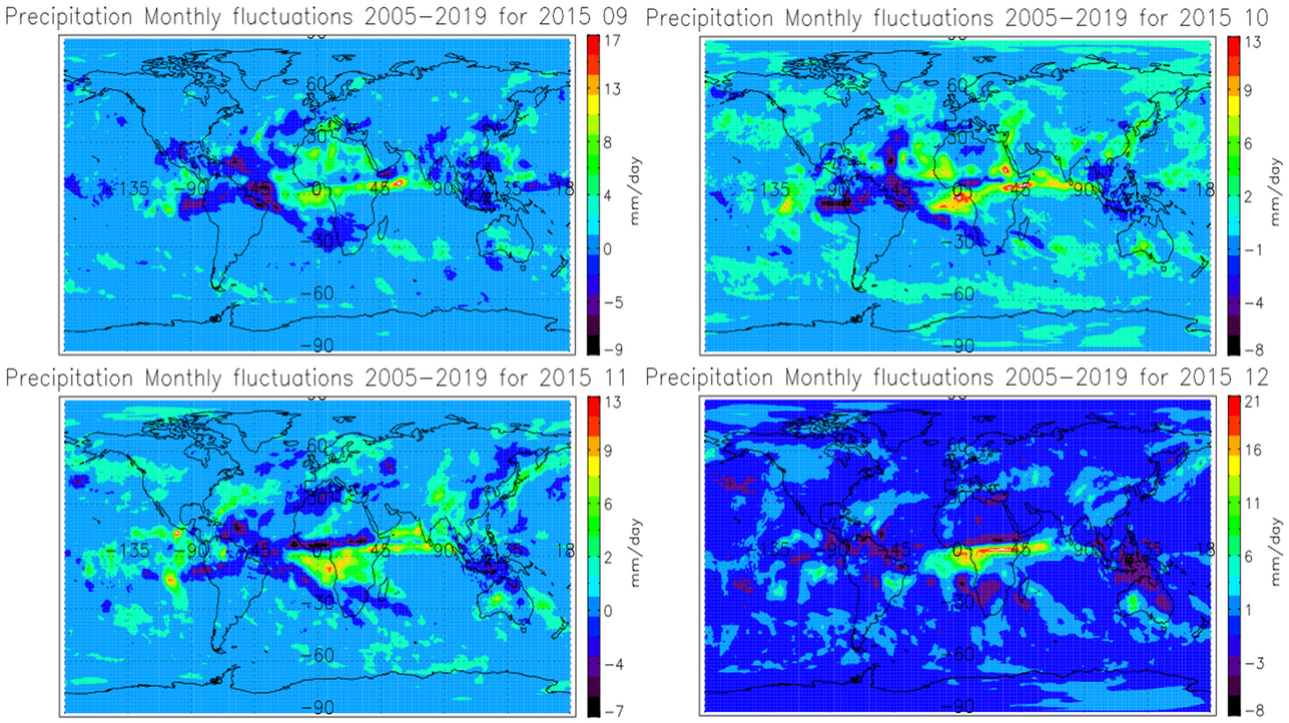

Figure 32: Precipitation fluctuations for the last four months of 2015. Precipitation levels are near or below average for the most part in the South America, southern Africa, and Austrlia

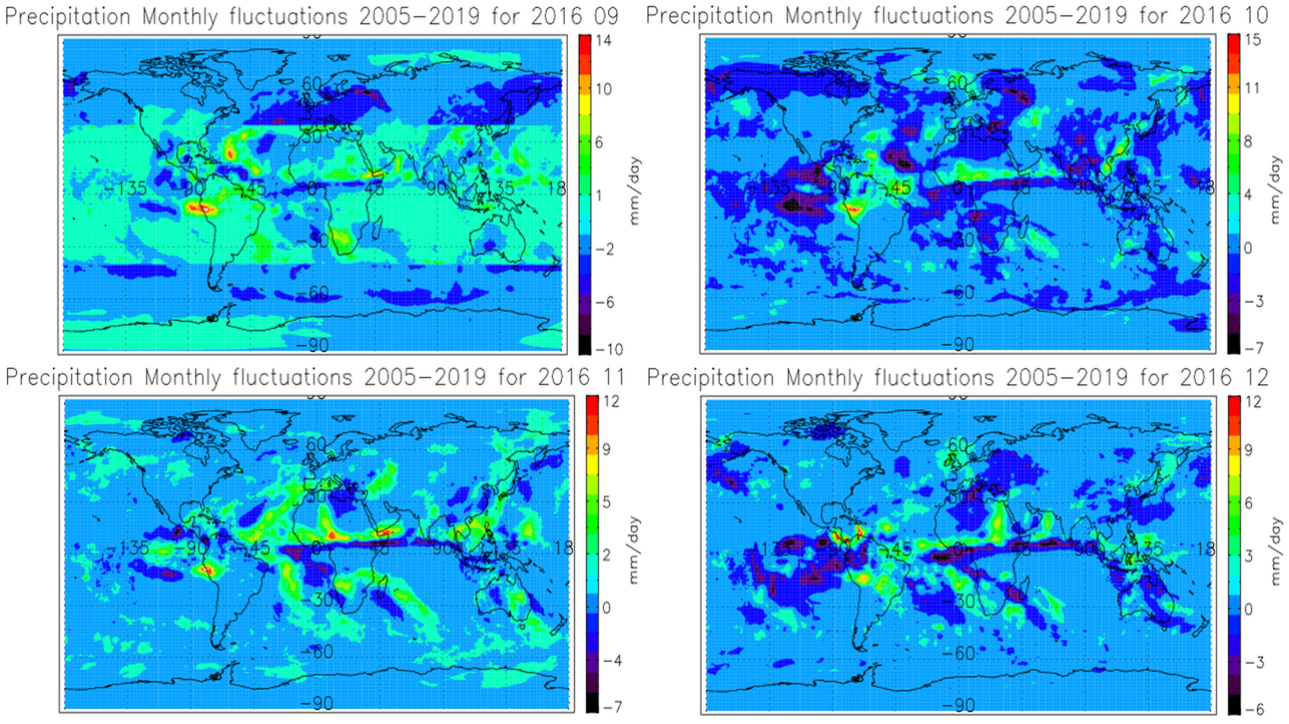

Figure 33: Precipitation fluctuations for the last four months of 2016, precipitation levels South of the equator seem to have risen, likely due to La Niña

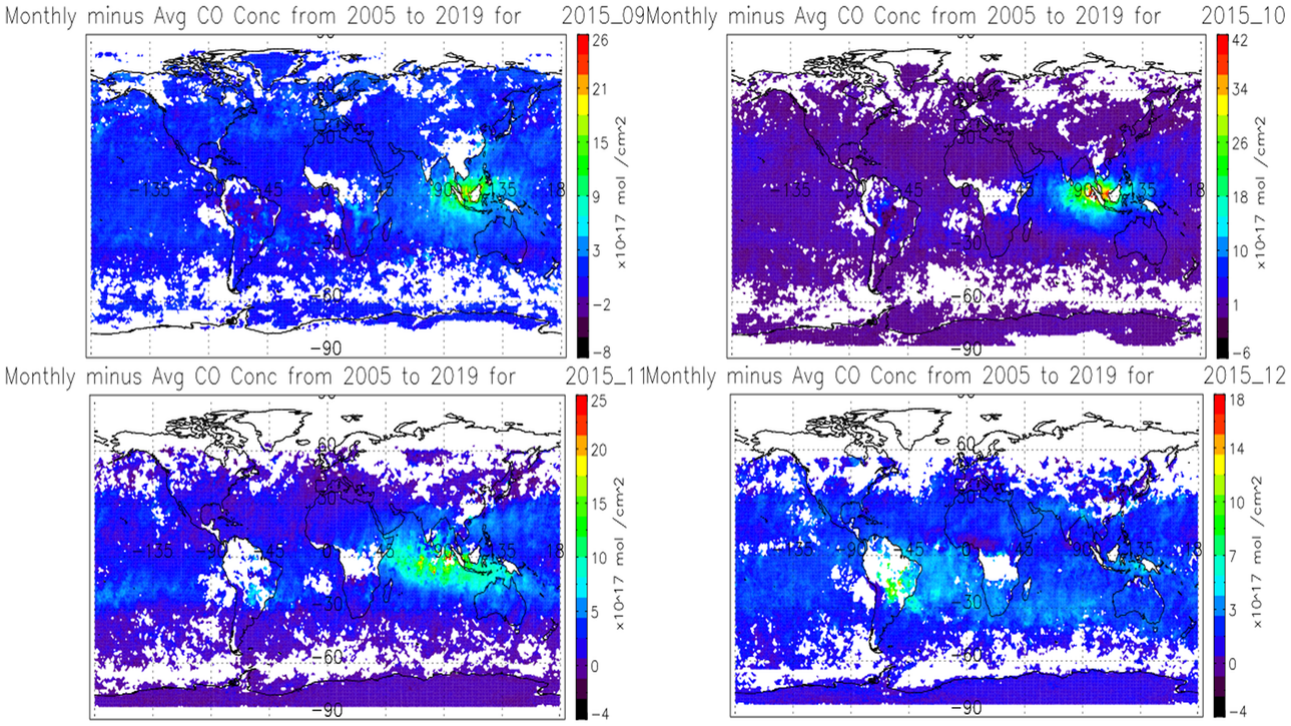

Figure 34: CO emissions fluctuations for the last four months of 2015

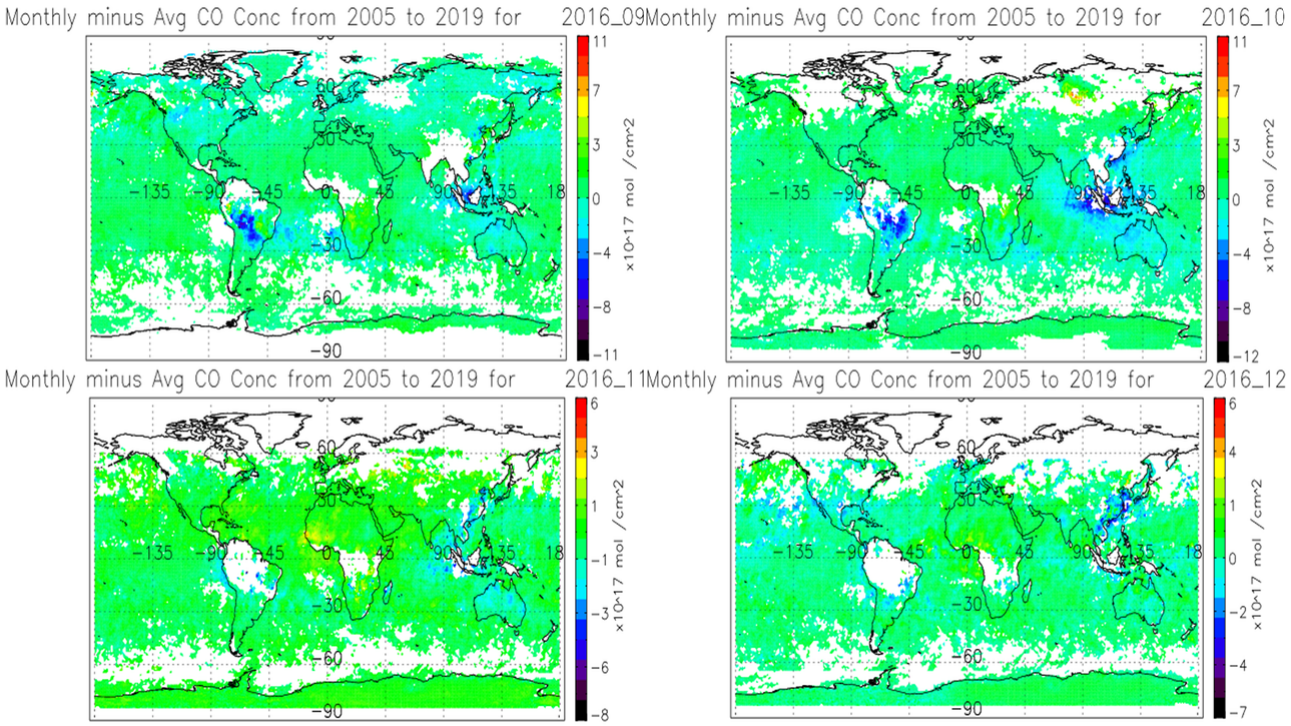

Figure 35: CO emissions fluctuations for the last four months of 2016

Figure 30 shows the SST fluctuations from September to December 2015, measured in degrees Celsius. The mean temperature in the Niño 3.4 region can be seen to be more than 1.5 degrees above average, hence showing a strong El Niño phase. Figure 31 shows the SST fluctuations during the last quarter of 2016. The mean temperature in the Niño 3.4 region can be seen to have dropped below average. This is because the El Niño phase dissipated around May-June 2016 [166]. Temperature in the region can be seen to have dropped by more than 0.5

degrees Celsius below average, suggesting the occurrence of the 2016-17 weak La Niña phase [167].
Figures 32 and 33 show the precipitation fluctuations from September to December of both 2015 and 2016, measured in mm/day. Precipitation levels in 2015 can be seen to be near or below-average for the most part in the South America, southern Africa, and Austrlia. However, some parts in southern Africa, particularly near the equator, can be seen to have reached above-average levels by up to 9 mm/day. In 2016, precipitation levels South of the equator seem to have risen, likely due to the fact that the La Niña phase is already occuring at that time. Figures 34 and 35 show the CO fluctuations also from September to December of both 2015 and 2016, measured in mol/cm^2. In 2015, Southern Hemisphere CO levels can be seen to be consistently above-average, as expected during El Niño, and in 2016, they have fallen below-average, as La Niña is already occuring. The warming of the El Niño 3.4 region significantly impacts global weather patterns, including rainfall. El Niño events alter precipitation patterns in the Southern Hemisphere, usually resulting in higher precipitation in some areas.

In South America, El Niño leads to increased rainfall in the central and southern regions. El Niño events frequently result in above-average rainfall in Peru, Ecuador, and parts of Brazil. This can result in flooding, landslides, and other water-related risks. The 1997-1998 El Niño event, for example, led to severe flooding in Peru and Ecuador, inflicting substantial damage and disruption [168]. The higher rainfall is due to a shift in atmospheric circulation patterns, which improves moisture transport and convective activity in these areas.
Due to the complex interplay between oceanic and atmospheric conditions that influence the Australian climate, the effects of El Niño on precipitation in the region can be quite variable. They generally lead to drier-than-average conditions in the northern and eastern parts of the country. However, some parts of southern Australia can experience increased rainfall during El Niño events. The 2015-2016 El Niño event, for instance, resulted in higher-than-average rainfall to parts of southern Australia, even as the northern regions experienced drought conditions [169].
El Niño is accompanied by the decease in rainfall in much of southern Africa, especially in the southeastern part of the region (Malawi, Zambia, and Zimbabwe) and in South Africa. This can significantly affect agricultural productivity in some regions. The 2015-16 caused the worst drought in Southern Africa in 35 years, with effects lasting into 2017, with reduced rainfall and hot temperatures negatively affecting crop growth [66, 160, 170].

As previously stated, El Niño is characterized by warmer-than-average sea surface temperatures in the central and eastern equatorial Pacific Ocean. The temperature must be at least 0.5 degrees Celsius higher than average for at least 9 to 12 months, peaking around December [46, 65].
El Niño also has significant effects on the frequency and intensity of wildfires, which are the main natural source of CO. El Niño is frequently linked to warmer, drier weather in parts of all three regions (Australia, Southern Africa, and South America), which can lead to a rise in the frequency of wildfires. Increased biomass burning results in increased CO emissions from wildfires. For example, several regions such as the Amazon Forest of Brazil, Swaziland, and more recently, in the Republic of Congo, experienced high CO emissions during strong El Niño periods, due to widespread fires. El Niño raises the likelihood of higher temperatures and less rainfall in eastern and northern Australia, although it does not guarantee that the conditions will be warmer and drier [66].
Additionally, an El Niño event does not exclusively imply drier conditions in the SH, particularly in parts of South America, as seen previously. Places such as Ecuador and northern Peru sometimes experience intense increases in rainfall, causing to coastal flooding and erosion [159].

4.5 The El Niño Effect on Burned area

Westward-blowing trade winds become weaker around the Equator during an El Niño event. Warm surface water moves eastward down the Equator from the western Pacific to the coast of northern South America as a result of these variations in air pressure and wind speed. The thermocline, the ocean depth that divides warm surface water from cooler water below, is pushed down by these warm surface waves. The thermocline can drop by as much as 152 meters during an El Niño event [171].

Recall that for a climatic phenomenon to qualify as an El Niño event, there must be a Sea Surface Temperature (SST) anomaly, that is, a rise of 0.5°C or more over five consecutive overlapping three-month periods, centered on the equatorial Pacific Ocean in the Niño-3.4 region (5°N–5°S, 120°W–170°W), relative to a baseline period of 1971–2000. El Niño event are characterized as weak (0.5 to 0.9°C SST anomaly), Moderate (1.0 to 1.4°C), Strong (1.5 to 1.9°C) and Very Strong (more than 1.9°C). Between 2005 and 2019, 5 El Niño events have been registered, notably in 2004-05, 2006-07, 2009-10, 2014-16, and 2019; with the strongest one in that time span being the one in 2014-16 (very strong), a moderate one in 2009-10, and the rest being relatively weak [172, 173].

As previously stated in Chapter 2, El Niño events have been shown to have a potential to significantly influence global temperatures and regular rainfall patterns. Warmer temperatures than usual leading to droughts and reduced precipitations, and increased fire occurrences and fire emissions have all been associated with El Niño. However, impacts can differ throughout continents. For instance, southern South America frequently sees wetter weather conditions, whilst northern and central-east regions endure drought [138]. The impact of El Niño on burned areas in the SH (South America, Southern Africa and Australia) will be looked at in this section. The burned areas are measured in square meters (m^2).

4.5.1 South America

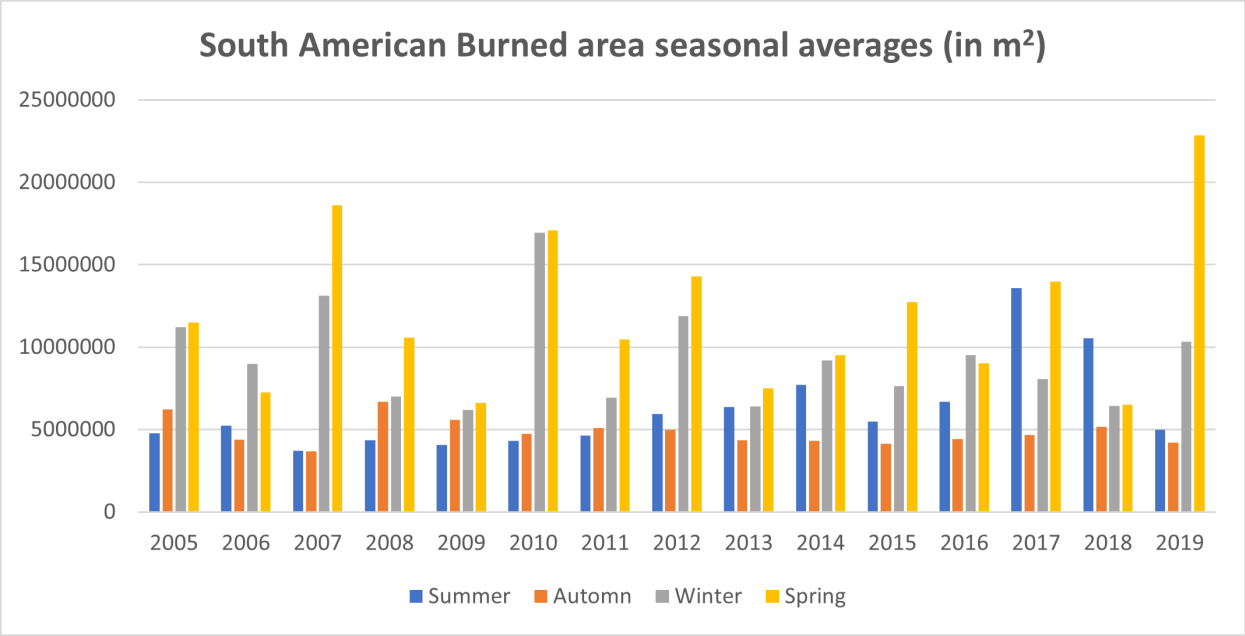

Figure 36: South American average Burned area seasonal averages from 2005 to 2019 measured in m^2. The El Niño years (2005, 2007, 2010, 2015-16 and 2019) can be seen to have generally higher average burned areas

Figure 36 represent the average South American burned area in seasonal averages from 2005 to 2019 measured in m^2. Although the figure include South America as a whole, which does not allow to differentiate the Northern and Southern regions, it still makes it possible to draw a clear distinction between El Niño and non-El Niño years in terms of burned areas. The El Niño years (2005, 2007, 2010, 2015-16 and 2019) can be seen to have generally higher average burned areas.

A case study of the 2015-16 El Niño showed that it caused a drop in soil moisture and precipitation and a rise in temperature in the northern part of the South American continent, and that these hotter, drier conditions have been associated with an increase in fires and are characteristic of the expected effects of a strong El Niño [172].

4.5.2 Southern Africa

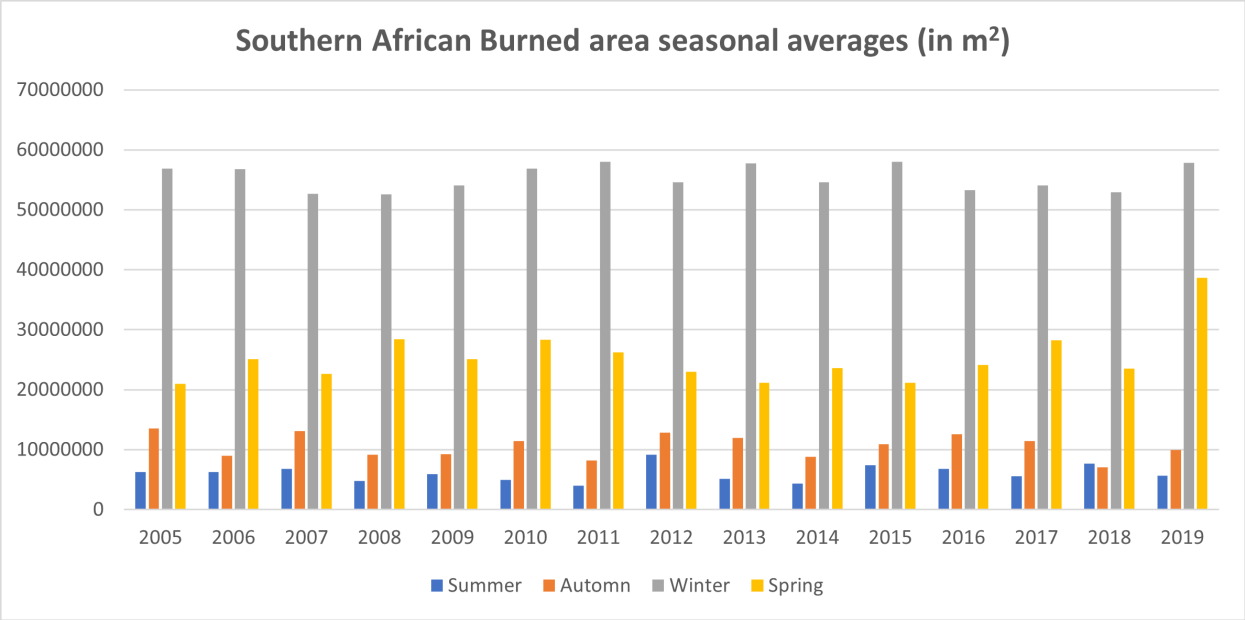

Figure 37: Southern African average Burned area seasonal averages from 2005 to 2019 in m^2. El Niño years can once again be seen to have higher average burned areas than normal years.

Figure 37 illustrates the average Burned area seasonal averages from 2005 to 2019 in Southern Africa. Overall, El Niño years can be seen to have on average higher burned areas than non-El Niño years, with the highest yearly average of 2.80×10^7 m^2 in 2019, and the lowest of 2.28×10^7 m^2 in 2018. A La Niña event occurred in 2018, which may be a reason for that low burned area value [174].

Through its wide-ranging teleconnections, the El Niño Southern Oscillation (ENSO) phenomenon largely regulates the variation in rainfall in this region. Teleconnections are persistent climate anomalies or patterns that span wide geographic areas and are correlated with one another. Numerous previous research works have linked El Niño to the rise in wildfire activity in Southern Africa during drought circumstances. This correlation is such that strong El Niño events alter rainfall patterns and cause the region's vegetation to become drier, which makes the vegetation more prone to wildfires. For instance, during strong El Niño events, many areas, including Swaziland and more recently the Republic of Congo, saw extensive wildfires [66, 175].

4.5.3 Australia

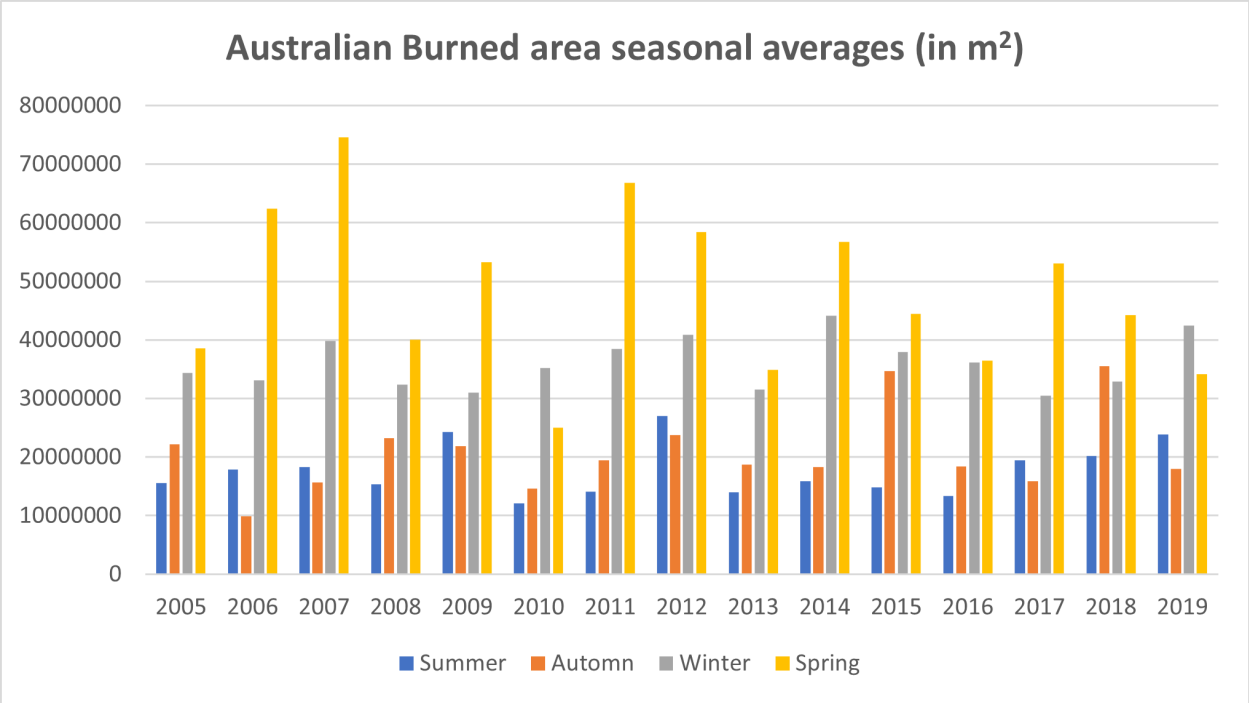

Figure 38: Australian average Burned area seasonal averages from 2005 to 2019 in m^2. Burned areas can be seen to be higher after an El Niño year

Figure 38 illustrates the average Burned area seasonal averages from 2005 to 2019 in Australia. Higher burned areas can be seen during the years following El Niño year, except for the year 2007 which can be seen to have fairly high average burned area of 3.71×10^7 m^2, which is in fact the second highest. the highest yearly average of 3.75×10^7 m^2 in 2012, and the lowest of 2.77×10^7 m^2 in 2005, which was an El Niño year.

Similarly to South America and Southern Africa, Australia has as well been impacted by El Niño events, by experiencing hotter than average temperatures (Eastern Australia), and drier winter-spring seasons (Central Australia). It has also been found by previous studies that in Australia, particularly in the south-east region, the likelihood of a major fire danger season increases dramatically following an El Niño year, especially when coupled with a positive Indian Ocean dipole (IOD) event, which is determined by the sea surface temperature differences between the eastern and western Indian Ocean. Additionally, although an El Niño event brings hotter than average temperatures and drier conditions, the intensity of the rainfall deficits over Australia does not always correlate with the strength of an El Niño. There have been weak events in the past that have resulted in substantial drought, as well as strong ones that haven't brought about such dire circumstances [176].

5 Conclusion

In this study we have investigated the monthly averages of CO concentrations, their seasonal variations, burned areas, the global wind circulations and their impact on CO distributions, and the El Niño effect and its impact on burned areas. Burned areas were compiled as total average burned areas, and as average burned areas in vegetation classes. The vegetation classes were Forest, Cropland, Grassland and Shrubland. The region focused on in this study was the Southern Hemisphere, namely South America, Southern Africa and Australia; the time frame was from 2005 to 2019.

The findings presented here indicate that there is a difference in monthly and regional CO concentrations. In South America, the maximum concentration is reached in September, and the minimum in May. Southern Africa's maximum happens in August and its minimum around April-May, whereas Australia's maximum is reached in October and its minimum in March. Likewise, there is a difference in seasonal CO concentrations. Overall, winter has higher concentrations than summer. Spring also shows considerably high concentrations.

Biomass burning, both natural and antropogenic, was found to be the major source of CO emissions in the SH. The correlation between burned areas and CO concentrations was visible. It was shown that Biomass burning generally peaks in winter months and is at its lowest in summer because the dry seasons experience a decline in rainfall which favours the buildup of fuel load, making those seasons more suitable for wildfires and agricultural burning among other things. In term of vegetation classes, forest and shrubland have the most burning, especially in South America and Australia.

Statistical analysis using the Pearson correlation coefficient and p-value appeared to show a general consistency, which seemed to endorse the theoretical expectations of a positive correlation between CO emissions and burned areas. Weak correlations had higher than accepted p-values, and strong correlations had accepted p-values. However, not all accepted correlations were positive, as can be seen in the Australian cropland. This may be explained by different factors, such as wind circulation.

It was also shown in this study how the global wind circulation affect CO distributions in the Southern Hemisphere. CO is transported westward in lower latitude in mid-winter from Southern Africa over the Atlantic ocean, and by mid-spring, the transport is towards the east from South America to Africa to Australia over the Atlantic and Indian oceans, especially in the higher latitudes (21°S and above)

Additionally, two specific La Niña and El Niño phases were identified and compared with their transitional (neutral) phase in terms of their CO and precipitation levels. The El Niño was mostly found to cause drier conditions which led to below-average rainfall and above-average CO levels, and La Niña was mostly found to cause wetter conditions which led to above-average rainfall and below-average CO levels. The neutral phase was found to have stable or near-average conditions, as expected.

Finally, the El Niño effect was shown to have an impact on burned areas. As an El Niño event is characterised by a raise in temperatures, depending on its strength, regions in the SH experience higher than average temperatures during El Niño years, causing dryer winter seasons that increase the frequency of wildfires due to an increase in fuel load.

Furthermore, although this study to a degree gave some detailed information about the spatial and temporal variation of CO concentrations and its cause in the SH region, there are still many questions that need answers. For example, are there any other phenomena that affect CO concentrations (or distributions) and the frequency of biomass burning? What are the other sources of CO in the atmosphere? There are many other questions than these that give room to more research to better understand this atmospheric dynamic. Also, biomass burning is the source of many other gases such as CO_2 and CH_4 that give a vast array of aspects to look at and help to improve the understanding of our nature.

References

[1] Carbon monoxide poisoning. (2019). *Mayo Clinic*. (Accessed May 26, 2023). Link

[2] Raub, J. A. and Benignus, V. A. (2002). Carbon monoxide and the nervous system. *Neuroscience & Biobehavioral Reviews*, 26(8), 925-940.

[3] National Research Council. (2002). The ongoing challenge of managing carbon monoxide pollution in Fairbanks, Alaska: Interim Report. *National Academies Press*.

[4] Przyborski, P and Levy, R. (2017) Carbon monoxide. *NASA*. (Accessed July 20, 2023). Link

[5] Carbon monoxide. (2017). *UCAR, Center for Science Education*. (Accessed July 20, 2023). Link

[6] Thompson, A. M., Balashov, N. V., Witte, J. C., Coetzee, J. G. R., Thouret, V. and Posny, F. (2014). Tropospheric ozone increases over the southern Africa region: bellwether for rapid growth in Southern Hemisphere pollution?. *Atmospheric Chemistry and Physics*, 14(18), 9855-9869.

[7] Paton-Walsh, C., Emmerson, K.M., Garland, R.M., Keywood, M., Hoelzemann, J.J., Huneeus, N., Buchholz, R.R., Humphries, R.S., Altieri, K., Schmale, J. and Wilson, S.R. (2022). Key challenges for tropospheric chemistry in the Southern Hemisphere. *Elem Sci Anth*, 10(1), 00050.

[8] Worden, J., Kulawik, S. S., Shephard, M. W., Clough, S. A., Worden, H., Bowman, K. and Goldman, A. (2004). Predicted errors of tropospheric emission spectrometer nadir retrievals from spectral window selection. *Journal of Geophysical Research: Atmospheres*, 109(D9).

[9] Huijnen, V., Wooster, M.J., Kaiser, J.W., Gaveau, D.L., Flemming, J., Parrington, M., Inness, A., Murdiyarso, D., Main, B. and van Weele, M. (2016). Fire carbon emissions over maritime southeast Asia in 2015 largest since 1997. Scientific reports, 6(1), 26886.

[10] Edwards, D.P., Emmons, L.K., Hauglustaine, D.A., Chu, D.A., Gille, J.C., Kaufman, Y.J., Pétron, G., Yurganov, L.N., Giglio, L., Deeter, M.N. and Yudin, V. (2004). Observations of carbon monoxide and aerosols from the Terra satellite: Northern Hemisphere variability. Journal of Geophysical Research: Atmospheres, 109(D24).

[11] Bowman, D. M., Williamson, G. J., Abatzoglou, J. T., Kolden, C. A., Cochrane, M. A. and Smith, A. M. (2017). Human exposure and sensitivity to globally extreme wildfire events. Nature ecology & evolution, 1(3), 0058.

[12] Levy, R. C., Mattoo, S., Munchak, L. A., Remer, L. A., Sayer, A. M., Patadia, F. and Hsu, N. C. (2013). The Collection 6 MODIS aerosol products over land and ocean. Atmospheric Measurement Techniques, 6(11), 2989-3034.

[13] Duncan, B.N., Prados, A.I., Lamsal, L.N., Liu, Y., Streets, D.G., Gupta, P., Hilsenrath, E., Kahn, R.A., Nielsen, J.E., Beyersdorf, A.J. and Burton, S.P. (2014). Satellite data of atmospheric pollution for US air quality applications: Examples of applications, summary of data end-user resources, answers to FAQs, and common mistakes to avoid. Atmospheric environment, 94, 647-662..

[14] Wargan, K., Labow, G., Frith, S., Pawson, S., Livesey, N. and Partyka, G. (2017). Evaluation of the Ozone Fields in NASA's MERRA-2 Reanalysis. Journal of Climate, 30(8), 2961-2988.

[15] Cai, W., Wu, L., Lengaigne, M., Li, T., McGregor, S., Kug, J.S., Yu, J.Y., Stuecker, M.F., Santoso, A., Li, X. and Ham, Y.G. (2019). Pantropical climate interactions. Science, 363(6430), eaav4236.

[16] Narsey, S., Brown, J. R., Delage, F., Boschat, G., Grose, M., Colman, R. and Power, S. (2022). Storylines of South Pacific Convergence Zone changes in a warmer world. Journal of Climate, 35(20), 6549-6567.

[17] Russell, A. R., Valin, L. C., Bucsela, E. J., Wenig, M. O. and Cohen, R. C. (2010). Space-based constraints on spatial and temporal patterns of NOx emissions in California, 2005-2008. Environmental science & technology, 44(9), 3608-3615. 044017.

[18] Environmental Handbook Volume III: Compendium of Environmental Standards. (1995). World Environmental Library. (Accessed September 26, 2023). Link

[19] US EPA. (1997). Procedures for Preparing Emission Factor Documents. United States Environmental Protection Agency, EPA-454/R-95-015. (Accessed September 15, 2023). Link

[20] Carbon monoxide. (2009). National Pollutant Inventory. (Accessed June 12, 2023). Link

[21] Higins, C. (2005). Causes and clinical significance of increased carboxyhemoglobin. Acute Care Testing.

[22] Borbon, A., Gilman, J.B., Kuster, W.C., Grand, N., Chevaillier, S., Colomb, A., Dolgorouky, C., Gros, V., Lopez, M., Sarda-Esteve, R. and Holloway, J. (2013). Emission ratios of anthropogenic VOC in northern mid-latitude megacities: observations vs. emission inventories in Los Angeles and Paris. J. Geophys. Res, 118, 2041-2057.

[23] Anderson, D. C., Lindsay, A., DeCarlo, P. F. and Wood, E. C. (2021). Urban emissions of nitrogen oxides, carbon monoxide, and methane determined from ground-based measurements in Philadelphia. Environmental Science & Technology, 55(8), 4532-4541.

[24] Hampson, N. B., Piantadosi, C. A., Thom, S. R. and Weaver, L. K. (2012). Practice recommendations in the diagnosis, management, and prevention of carbon monoxide poisoning. American journal of respiratory and critical care medicine, 186(11), 1095-1101.

[25] Ernst, A. and Zibrak, J. D. (1998). Carbon monoxide poisoning. New England journal of medicine, 339(22), 1603-1608.

[26] Rose, J. J., Wang, L., Xu, Q., McTiernan, C. F., Shiva, S., Tejero, J. and Gladwin, M. T. (2017). Carbon monoxide poisoning: pathogenesis, management, and future directions of therapy. American journal of respiratory and critical care medicine, 195(5), 596-606.

[27] Carbon Monoxide's Impact on Indoor Air Quality. (2023). United States Environment Protection Agency. (Accessed October 3, 2023) Link

[28] Ryter, S. W., Ma, K. C. and Choi, A. M. (2018). Carbon monoxide in lung cell physiology and disease. American Journal of Physiology-Cell Physiology, 314(2), C211-C227.

[29] Weaver, L.K., Hopkins, R.O., Chan, K.J., Churchill, S., Elliott, C.G., Clemmer, T.P., Orme Jr, J.F., Thomas, F.O. and Morris, A.H. (2002). Hyperbaric oxygen for acute carbon monoxide poisoning. New England Journal of Medicine, 347(14), 1057-1067.

[30] Prockop, L. D. and Chichkova, R. I. (2007). Carbon monoxide intoxication: an updated review. Journal of the neurological sciences, 262(1-2), 122-130.

[31] Lin, C.H., Su, W.H., Chen, Y.C., Feng, P.H., Shen, W.C., Ong, J.R., Wu, M.Y. and Wong, C.S. (2018). Treatment with normobaric or hyperbaric oxygen and its effect on neuropsychometric dysfunction after carbon monoxide poisoning: A systematic review and meta-analysis of randomized controlled trials. Medicine, 97(39).

[32] Choi, S., Han, S., Nah, S., Lee, Y.H., Cho, Y.S., Lim, H., Kim, M.S. and Kim, G.W., 2021. Effect of ethanol in carbon monoxide poisoning and delayed neurologic sequelae: A prospective observational study. PLoS one, 16(1), e0245265.

[33] National Center for Biotechnology Information (2024). PubChem Compound Summary for CID 281, Carbon Monoxide. (Accessed October 3, 2023). Link.

[34] Quinn, D. K., McGahee, S. M., Politte, L. C., Duncan, G. N., Cusin, C., Hopwood, C. J. and Stern, T. A. (2009). Complications of carbon monoxide poisoning: a case discussion and review of the literature. Primary Care Companion to the journal of clinical Psychiatry, 11(2), 74.

[35] Raub, J. A., Mathieu-Nolf, M., Hampson, N. B. and Thom, S. R. (2000). Carbon monoxide poisoning—a public health perspective. Toxicology, 145(1), 1-14.

[36] Watt, S., Prado, C. E. and Crowe, S. F. (2018). Immediate and delayed neuropsychological effects of carbon monoxide poisoning: a meta-analysis. Journal of the International Neuropsychological Society, 24(4), 405-415.

[37] Goldammer, J. G. (2013). Vegetation fires and global change: Challenges for concerted international action. A white paper directed to the united nations and international organizations. Kessel. Max Planck Institute for Chemistry.

[38] Andreae, M. O. and Merlet, P. (2001). Emission of trace gases and aerosols from biomass burning. Global Biogeochemical Cycles, 15(4), 955-966.

[39] Yokelson, R. J., Bertschi, I. T., Christian, T. J., Hobbs, P. V., Ward, D. E. and Hao, W. M. (2003). Trace gas measurements in nascent, aged, and cloud-processed smoke from African savanna fires by airborne Fourier transform infrared spectroscopy (AFTIR). Journal of Geophysical Research: Atmospheres, 108(D13).

[40] Akagi, S.K., Yokelson, R.J., Wiedinmyer, C., Alvarado, M.J., Reid, J.S., Karl, T., Crounse, J.D. and Wennberg, P.O. (2011). Emission factors for open and domestic biomass burning for use in atmospheric models. Atmospheric Chemistry and Physics, 11(9), 4039-4072.

[41] Carbon Monoxide-2008-2011. (2015). Science On a Sphere. (Accessed July 20, 2021). Link

[42] Voiland, A. (2015). Fourteen Years of Carbon Monoxide from MOPITT. NASA.

[43] Reay, D. (2006) Other Indirect Greenhouse Gases-Carbon monoxide. Greenhouse Gases Online. (Accessed July 20, 2021). Link

[44] Bowman, D.M., Balch, J.K., Artaxo, P., Bond, W.J., Carlson, J.M., Cochrane, M.A., D'Antonio, C.M., DeFries, R.S., Doyle, J.C., Harrison, S.P. and Johnston, F.H. (2009). Fire in the Earth system. science, 324(5926), 481-484.

[45] Giglio, L., Randerson, J. T. and Van Der Werf, G. R. (2013). Analysis of daily, monthly, and annual burned area using the fourth-generation global fire emissions database (GFED4). Journal of Geophysical Research: Biogeosciences, 118(1), 317-328.

[46] Trenberth, K. E. (1997). The definition of El Niño. Bulletin of the American Meteorological Society, 78(12), 2771-2777.

[47] Van der Werf, G.R., Randerson, J.T., Giglio, L., Collatz, G.J., Mu, M., Kasibhatla, P.S., Morton, D.C., DeFries, R.S., Jin, Y.V. and van Leeuwen, T.T. (2010). Global fire emissions and the contribution of deforestation, savanna, forest, agricultural, and peat fires (1997–2009). Atmospheric chemistry and physics, 10(23), 11707-11735.

[48] Van Der Werf, G.R., Randerson, J.T., Giglio, L., Van Leeuwen, T.T., Chen, Y., Rogers, B.M., Mu, M., Van Marle, M.J., Morton, D.C., Collatz, G.J. and Yokelson, R.J. (2017). Global fire emissions estimates during 1997–2016. Earth System Science Data, 9(2), 697-720.

[49] Pivello, V. R. (2011). The use of fire in the Cerrado and Amazonian rainforests of Brazil: past and present. Fire ecology, 7, 24-39.

[50] Page, S. E., Siegert, F., Rieley, J. O., Boehm, H. D. V., Jaya, A. and Limin, S. (2002). The amount of carbon released from peat and forest fires in Indonesia during 1997. Nature, 420(6911), 61-65.

[51] Field, R.D., Van Der Werf, G.R., Fanin, T., Fetzer, E.J., Fuller, R., Jethva, H., Levy, R., Livesey, N.J., Luo, M., Torres, O. and Worden, H.M. (2016). Indonesian fire activity and smoke pollution in 2015 show persistent nonlinear sensitivity to El Niño-induced drought. Proceedings of the National Academy of Sciences, 113(33), 9204-9209.

[52] Justice, C.O., Townshend, J.R.G., Vermote, E.F., Masuoka, E., Wolfe, R.E., Saleous, N., Roy, D.P. and Morisette, J.T. (2002). An overview of MODIS Land data processing and product status. Remote sensing of Environment, 83(1-2), 3-15.

[53] Brennan, J., Gómez-Dans, J. L., Disney, M. and Lewis, P. (2019). Theoretical uncertainties for global satellite-derived burned area estimates. Biogeosciences, 16(16), 3147-3164.

[54] Tonbul, H., Colkesen, I. and Kavzoglu, T. (2022). Pixel-and Object-Based ensemble learning for forest burn severity using USGS FIREMON and Mediterranean condition dNBRs in Aegean ecosystem (Turkey). Advances in Space Research, 69(10), 3609-3632.

[55] Roy, D. P., Boschetti, L., Justice, C. O. and Ju, J. (2008). The collection 5 MODIS burned area product—Global evaluation by comparison with the MODIS active fire product. Remote sensing of Environment, 112(9), 3690-3707.

[56] Agbeshie, A. A., Abugre, S., Atta-Darkwa, T., and Awuah, R. (2022). A review of the effects of forest fire on soil properties. Journal of Forestry Research, 33(5), 1419-1441.

[57] Cochrane, M. A. and Laurance, W. F. (2008). Synergisms among fire, land use, and climate change in the Amazon. AMBIO: A Journal of the Human Environment, 37(7), 522-527.

[58] United Nations Framework Convention on Climate Change (UNFCCC). (n.d.). (Accessed December 19, 2023). Link

[59] Gordon, A., Grace, W., Byron-Scott, R. and Schwerdtfeger, P. (2016). Dynamic meteorology. Routledge.

[60] Global Atmospheric Circulations. Physical Geography, College Sidekick. (Accessed November 09, 2023). Link

[61] Global circulation patterns. (2013) Met Office. (Accessed November 09, 2023). Link

[62] Edwards, D.P., Emmons, L.K., Hauglustaine, D.A., Chu, D.A., Gille, J.C., Kaufman, Y.J., Pétron, G., Yurganov, L.N., Giglio, L., Deeter, M.N. and Yudin, V. (2004). Observations of carbon monoxide and aerosols from the Terra satellite: Northern Hemisphere variability. Journal of Geophysical Research: Atmospheres, 109(D24).

[63] Lelieveld, J. O. S., Crutzen, P. J. amd Dentener, F. J. (1998). Changing concentration, lifetime and climate forcing of atmospheric methane. Tellus B, 50(2), 128-150.

[64] Chandra, S., Ziemke, J. R., Duncan, B. N., Diehl, T. L., Livesey, N. J. and Froidevaux, L. (2009). Effects of the 2006 El Niño on tropospheric ozone and carbon monoxide: implications for dynamics and biomass burning. Atmospheric Chemistry and Physics, 9(13), 4239-4249.

[65] Null, J. (2023). El Niño and La Niña Years and Intensities. Golden Gate Weather Services. (Accessed December 13, 2023). Link

[66] Shikwambana, L., Kganyago, M. and Xulu, S. (2022). Analysis of wildfires and associated emissions during the recent strong ENSO phases in Southern Africa using multi-source remotely-derived products. Geocarto international, 37(27), 16654-16670.

[67] Van Der Werf, G. R., Randerson, J. T., Collatz, G. J., and Giglio, L. (2003). Carbon emissions from fires in tropical and subtropical ecosystems. Global Change Biology, 9(4), 547-562.

[68] Zheng, B., Chapman, S., and Chenu, K. (2018). The value of tactical adaptation to El Niño–Southern Oscillation for East Australian wheat. Climate, 6(3), 77.

[69] Cai, W., McPhaden, M.J., Grimm, A.M., Rodrigues, R.R., Taschetto, A.S., Garreaud, R.D., Dewitte, B., Poveda, G., Ham, Y.G., Santoso, A. and Ng, B. (2020). Climate impacts of the El Niño–southern oscillation on South America. Nature Reviews Earth & Environment, 1(4), 215-231.

[70] Zhang, Y. (2011). Mean global and regional distributions of MOPITT carbon monoxide during 2000–2009 and during ENSO. Atmospheric environment, 45(6), 1347-1358.

[71] Kaiser, J.W., Heil, A., Andreae, M.O., Benedetti, A., Chubarova, N., Jones, L., Morcrette, J.J., Razinger, M., Schultz, M.G., Suttie, M. and Van Der Werf, G.R. (2012). Biomass burning emissions estimated with a global fire assimilation system based on observed fire radiative power. Biogeosciences, 9(1), 527-554.

[72] Deeter, M. N., Edwards, D. P., Francis, G. L., Gille, J. C., Martínez-Alonso, S., Worden, H. M. and Sweeney, C. (2017). A climate-scale satellite record for carbon monoxide: the MOPITT Version 7 product. Atmospheric Measurement Techniques, 10(7), 2533-2555.

[73] Worden, H. M., Deeter, M. N., Edwards, D. P., Gille, J. C., Drummond, J. R. and Nédélec, P. (2010). Observations of near-surface carbon monoxide from space using MOPITT multispectral retrievals. Journal of Geophysical Research: Atmospheres, 115(D18).

[74] Rienecker, M.M., Suarez, M.J., Gelaro, R., Todling, R., Bacmeister, J., Liu, E., Bosilovich, M.G., Schubert, S.D., Takacs, L., Kim, G.K. and Bloom, S. (2011). MERRA: NASA's modern-era retrospective analysis for research and applications. Journal of climate, 24(14), 3624-3648.

[75] Ichoku, C., Remer, L. A., Kaufman, Y. J., Levy, R., Chu, D. A., Tanré, D. and Holben, B. N. (2003). MODIS observation of aerosols and estimation of aerosol radiative forcing over southern Africa during SAFARI 2000. Journal of Geophysical Research: Atmospheres, 108(D13).

[76] Manikandan, S. (2011). Measures of central tendency: The mean. Journal of pharmacology & pharmacotherapeutics, 2(2).

[77] Gravetter, F.J., and Wallnau, L.B., (2000). Statistics for the behavioral sciences, 5th ed. Belmont: Wadsworth – Thomson Learning.

[78] McClave, J. T., Benson, P. G., and Sincich, T. (2008). Statistics for business and economics. Pearson Education.

[79] Bobbitt, Z. (2023). Advantages & Disadvantages of Using Mean in Statistics. Statology. (Accessed August 8, 2024). Link

[80] Gilbert-Kawai, E. T., and Wittenberg, M. D. (2014). Essential Equations for Anaesthesia. Cambridge University Press.

[81] Kumar, P. K., Araki, T., Rajan, J., Laird, J. R., Nicolaides, A., and Suri, J. S. (2018). State-of-the-art review on automated lumen and adventitial border delineation and its measurements in carotid ultrasound. Computer methods and programs in biomedicine, 163, 155-168.

[82] Komaroff, E. (2020). Relationships between p-values and Pearson correlation coefficients, type 1 errors and effect size errors, under a true null hypothesis. Journal of Statistical Theory and Practice, 14(3), 49.

[83] Gösset, W. S. (1908). The probable error of a mean. Biometrika, 6(1), 1-25.

[84] Cohen, J. (2013). Statistical power analysis for the behavioral sciences. routledge.

[85] Fisher, R. A. (1950). Methods for research workers.

[86] Kim, T. K. (2015). T test as a parametric statistic. Korean journal of anesthesiology, 68(6), 540-546.

[87] Kock, N. (2015). One-tailed or two-tailed P values in PLS-SEM?. International Journal of e-Collaboration (IJeC), 11(2), 1-7.

[88] Cho, H. C., and Abe, S. (2013). Is two-tailed testing for directional research hypotheses tests legitimate?. Journal of Business Research, 66(9), 1261-1266.

[89] Casanova, T. (1939). A test of the assumptions of linearity and homoscedasticity made in estimating the correlation in one range from that obtained in a different range. The Journal of Experimental Education, 7(3), 245-250.

[90] Baguley, T. (2009). Standardized or simple effect size: What should be reported?. British journal of psychology, 100(3), 603-617.

[91] Wu, H. (2017). Non-Normality and Heteroscedasticity in Regression and ANOVA.

[92] Armstrong, R. A. (2019). Should Pearson's correlation coefficient be avoided?. Ophthalmic and Physiological Optics, 39(5), 316-327.

[93] Essam, F., El, H., and Ali, S. R. H. (2022). A comparison of the pearson, spearman rank and kendall tau correlation coefficients using quantitative variables. Asian J. Probab. Stat, 36-48.

[94] Ozer, D. J. (1985). Correlation and the coefficient of determination. Psychological bulletin, 97(2), 307.

[95] Barrett, J. P. (1974). The coefficient of determination—some limitations. The American Statistician, 28(1), 19-20.

[96] Saunders, L. J., Russell, R. A., and Crabb, D. P. (2012). The coefficient of determination: what determines a useful R2 statistic?. Investigative ophthalmology & visual science, 53(11), 6830-6832.

[97] Nevil, S. (2023). Coefficient of Determination: How to calculate it and interpret the result. Investopedia.

[98] Fernando, J. (2024). R-Squared: Definition, Formula, Uses, and Limitations. Investopedia.

[99] R^2 of unpaired and paired t test results. (2024). GraphPad Software. (Accessed July 29, 2024). Link

[100] Edwards, D.P., Emmons, L.K., Gille, J.C., Chu, A., Attié, J.L., Giglio, L., Wood, S.W., Haywood, J., Deeter, M.N., Massie, S.T. and Ziskin, D.C. (2006). Satellite-observed pollution from Southern Hemisphere biomass burning. Journal of Geophysical Research: Atmospheres, 111(D14).

[101] Edwards, D. P., Pétron, G., Novelli, P. C., Emmons, L. K., Gille, J. C. and Drummond, J. R. (2006). Southern Hemisphere carbon monoxide interannual variability observed by Terra/Measurement of Pollution in the Troposphere (MOPITT). Journal of Geophysical Research: Atmospheres, 111(D16).

[102] Van Der Werf, G.R., Randerson, J.T., Giglio, L., Van Leeuwen, T.T., Chen, Y., Rogers, B.M., Mu, M., Van Marle, M.J., Morton, D.C., Collatz, G.J. and Yokelson, R.J. (2017). Global fire emissions estimates during 1997–2016. Earth System Science Data, 9(2), 697-720.

[103] Ichoku, C., Remer, L. A., Kaufman, Y. J., Levy, R., Chu, D. A., Tanré, D. and Holben, B. N. (2003). MODIS observation of aerosols and estimation of aerosol radiative forcing over southern Africa during SAFARI 2000. Journal of Geophysical Research: Atmospheres, 108(D13).

[104] van Marle, M.J., Field, R.D., van der Werf, G.R., Estrada de Wagt, I.A., Houghton, R.A., Rizzo, L.V., Artaxo, P. and Tsigaridis, K. (2017). Fire and deforestation dynamics in Amazonia (1973–2014). Global biogeochemical cycles, 31(1), 24-38.

[105] Commonwealth Scientific and Industrial Research Organisation (CSIRO). (2019). State of the Climate 2018. (Accessed December 15, 2023). Link

[106] Duncan, B.N., Logan, J.A., Bey, I., Megretskaia, I.A., Yantosca, R.M., Novelli, P.C., Jones, N.B. and Rinsland, C.P. (2007). Global budget of CO, 1988–1997: Source estimates and validation with a global model. Journal of Geophysical Research: Atmospheres, 112(D22).

[107] Granier, C., Darras, S., van Der Gon, H.D., Jana, D., Elguindi, N., Bo, G., Michael, G., Marc, G., Jalkanen, J.P., Kuenen, J. and Liousse, C. (2019). The Copernicus atmosphere monitoring service global and regional emissions (April 2019 version) (Doctoral dissertation, Copernicus Atmosphere Monitoring Service).

[108] Bremer, H., Kar, J., Drummond, J.R., Nichitu, F., Zou, J., Liu, J., Gille, J.C., Deeter, M.N., Francis, G., Ziskin, D. and Warner, J. (2004). Spatial and temporal variation of MOPITT CO in Africa and South America: A comparison with SHADOZ ozone and MODIS aerosol. Journal of Geophysical Research: Atmospheres, 109(D12). (Accessed December 4, 2023), Link

[109] Archibald, S., Roy, D. P., van Wilgen, B. W. and Scholes, R. J. (2009). What limits fire? An examination of drivers of burnt area in Southern Africa. Global Change Biology, 15(3), 613-630.

[110] Lehsten, V., Tansey, K., Balzter, H., Thonicke, K., Spessa, A., Weber, U., Smith, B. and Arneth, A. (2009). Estimating carbon emissions from African wildfires. Biogeosciences, 6(3), 349-360.

[111] Van der Werf, G.R., Randerson, J.T., Giglio, L., Collatz, G.J., Mu, M., Kasibhatla, P.S., Morton, D.C., DeFries, R.S., Jin, Y.V. and van Leeuwen, T.T. (2010). Global fire emissions and the contribution of deforestation, savanna, forest, agricultural, and peat fires (1997–2009). Atmospheric chemistry and physics, 10(23), 11707-11735.

[112] Archibald, S., Roy, D. P., van Wilgen, B. W. and Scholes, R. J. (2009). What limits fire? An examination of drivers of burnt area in Southern Africa. Global Change Biology, 15(3), 613-630.

[113] Le Page, Y., Morton, D., Bond-Lamberty, B., Pereira, J. M. C. and Hurtt, G. (2015). HESFIRE: a global fire model to explore the role of anthropogenic and weather drivers. Biogeosciences, 12(3), 887-903.

[114] Roy, D. P., Jin, Y., Lewis, P. E. and Justice, C. O. (2005). Prototyping a global algorithm for systematic fire-affected area mapping using MODIS time series data. Remote sensing of environment, 97(2), 137-162..

[115] Korontzi, S., McCarty, J., Loboda, T., Kumar, S. and Justice, C. (2006). Global distribution of agricultural fires in croplands from 3 years of Moderate Resolution Imaging Spectroradiometer (MODIS) data. Global Biogeochemical Cycles, 20(2).

[116] Silva, L. C., Hoffmann, W. A., Rossatto, D. R., Haridasan, M., Franco, A. C. and Horwath, W. R. (2013). Can savannas become forests? A coupled analysis of nutrient stocks and fire thresholds in central Brazil. Plant and Soil, 373, 829-842.

[117] Lehsten, V., Tansey, K., Balzter, H., Thonicke, K., Spessa, A., Weber, U., Smith, B. and Arneth, A. (2009). Estimating carbon emissions from African wildfires. Biogeosciences, 6(3), 349-360.

[118] Chen, Y., Morton, D.C., Jin, Y., Collatz, G.J., Kasibhatla, P.S., van der Werf, G.R., DeFries, R.S. and Randerson, J.T. (2013). Long-term trends and interannual variability of forest, savanna and agricultural fires in South America. Carbon Management, 4(6), 617-638.

[119] Aragão, L.E., Anderson, L.O., Fonseca, M.G., Rosan, T.M., Vedovato, L.B., Wagner, F.H., Silva, C.V., Silva Junior, C.H., Arai, E., Aguiar, A.P. and Barlow, J. (2018). 21st Century drought-related fires counteract the decline of Amazon deforestation carbon emissions. Nature communications, 9(1), 536.

[120] Morton, D. C., Collatz, G. J., Wang, D., Randerson, J. T., Giglio, L. and Chen, Y. (2013). Satellite-based assessment of climate controls on US burned area. Biogeosciences, 10(1), 247-260.

[121] Cochrane, M. A., Alencar, A., Schulze, M. D., Souza Jr, C. M., Nepstad, D. C., Lefebvre, P. and Davidson, E. A. (1999). Positive feedbacks in the fire dynamic of closed canopy tropical forests. Science, 284(5421), 1832-1835.

[122] Achard, F., Eva, H. D., Stibig, H. J., Mayaux, P., Gallego, J., Richards, T. and Malingreau, J. P. (2002). Determination of deforestation rates of the world's humid tropical forests. Science, 297(5583), 999-1002.

[123] Ferrelli, F. and Casado, A. (2023). Influence of climate variability on fire generation: Myths and facts in southern Pampas (Argentina). Cuadernos de Investigación Geográfica.

[124] Britannica, T. Editors of Encyclopaedia (2015). the Pampas. Encyclopedia Britannica. (Accessed November 30, 2023). Link

[125] Aragao, L. E. O., Malhi, Y., Barbier, N., Lima, A., Shimabukuro, Y., Anderson, L. and Saatchi, S. (2008). Interactions between rainfall, deforestation and fires during recent years in the Brazilian Amazonia. Philosophical Transactions of the Royal Society B: Biological Sciences, 363(1498), 1779-1785.

[126] Cochrane, M. A., Alencar, A., Schulze, M. D., Souza Jr, C. M., Nepstad, D. C., Lefebvre, P. and Davidson, E. A. (1999). Positive feedbacks in the fire dynamic of closed canopy tropical forests. Science, 284(5421), 1832-1835.

[127] Achard, F., Eva, H. D., Stibig, H. J., Mayaux, P., Gallego, J., Richards, T., and Malingreau, J. P. (2006). Determination of deforestation rates of the world's humid tropical forests. Science, 297(5583), 999-1002.

[128] Achard, F., Eva, H. D., Stibig, H. J., Mayaux, P., Gallego, J., Richards, T. and Malingreau, J. P. (2002). Determination of deforestation rates of the world's humid tropical forests. Science, 297(5583), 999-1002.

[129] Zeballos, S., Acosta, A., Agüero, W.D., Ahumada, R.J., Almiron, M., Argibay, D., Arroyo, D.N., Blanco, L.J., Biurrun, F.N., Cantero, J. and Márquez, J. (2023). Vegetation types of the Arid Chaco in Central-Western Argentina. International Association for Vegetation Science. (Accessed December 1, 2023). Link

[130] Aragão, L. E. and Shimabukuro, Y. E. (2010). The incidence of fire in Amazonian forests with implications for REDD. Science, 328(5983), 1275-1278.

[131] Vidal-Riveros, C., Souza-Alonso, P., Bravo, S., Laino, R. and Ngo Bieng, M.A. (2023). A review of wildfires effects across the Gran Chaco region, Forest Ecology and Management, 549, (Accessed December 4, 2023). Link.

[132] Marengo, J.A., Liebmann, B., Grimm, A.M., Misra, V., Silva Dias, P.D., Cavalcanti, I.F.A., Carvalho, L.M.V., Berbery, E.H., Ambrizzi, T., Vera, C.S. and Saulo, A.C. (2012). Recent developments on the South American monsoon system. International Journal of Climatology, 32(1), 1-21.

[133] Jolly, W., Cochrane, M., Freeborn, P., Holden, Z.A., Brown, T. J., Williamson, G. J. and Bowman, D. M. J. S. (2015). Climate-induced variations in global wildfire danger from 1979 to 2013. Nat Commun 6, 7537. (Accessed December 4, 2023). Link

[134] Stavi I. (2019). Wildfires in Grasslands and Shrublands: A Review of Impacts on Vegetation, Soil, Hydrology, and Geomorphology. Water, 11(5):1042. (Accessed December 4, 2023). Link

[135] Boer, M. M., Resco de Dios, V. and Bradstock, R. A. (2020). Unprecedented burn area of Australian mega forest fires. Nature Climate Change, 7(7), 547-548.

[136] Cary, G.J., Flannigan, M.D., Keane, R.E., Bradstock, R.A., Davies, I.D., Lenihan, J.M., Li, C., Logan, K.A. and Parsons, R.A. (2009). Relative importance of fuel management, ignition management and weather for area burned: evidence from five landscape–fire–succession models. International Journal of Wildland Fire, 18(2), 147-156.

[137] Russell-Smith, J., Yates, C., Edwards, A., Allan, G.E., Cook, G.D., Cooke, P., Craig, R., Heath, B. and Smith, R. (2003). Contemporary fire regimes of northern Australia, 1997–2001: change since Aboriginal occupancy, challenges for sustainable management. International Journal of Wildland Fire, 12(4), 283-297.

[138] Archibald, S., Lehmann, C.E., Belcher, C.M., Bond, W.J., Bradstock, R.A., Daniau, A.L., Dexter, K.G., Forrestel, E.J., Greve, M., He, T. and Higgins, S.I. (2018). Biological and geophysical feedbacks with fire in the Earth system. Environmental Research Letters, 13(3), 033003.

[139] Rabin, S. S., Magi, B. I., Shevliakova, E. and Pacala, S. W. (2015). Quantifying regional, time-varying effects of cropland and pasture on vegetation fire. Biogeosciences, 12(22), 6591-6604.

[140] Liu, T., Mickley, L. J. and McCarty, J. L. (2021). Global search for temporal shifts in fire activity: potential human influence on southwest Russia and north Australia fire seasons. Environmental Research Letters, 16(4), 044023.

[141] Yin, E. (2023). Australian Bushfire Summer Forecast - 2023. Crisis 24. (Accessed December 15, 2023). Link

[142] NVIS Fact sheet MVG 17 - Other shrublands. (2017). Australian Government: Department of the Environment and Energy, 17. (Accessed December 15, 2023). Link

[143] Bushfire. (2019). Australian Institute for Disaster Resilience. (Accessed December 15, 2023). Link

[144] Turner, D., Lewis, M. and Ostendorf, B. (2011). Spatial indicators of fire risk in the arid and semi-arid zone of Australia. Ecological Indicators, 11(1), 149-167.

[145] Buchholz, R. R., Hammerling, D., Worden, H. M., Deeter, M. N., Emmons, L. K., Edwards, D. P., and Monks, S. A. (2018). Links between carbon monoxide and climate indices for the southern hemisphere and tropical fire regions. Journal of Geophysical Research: Atmospheres, 123(17), 9786-9800.

[146] Worden, H.M., Deeter, M.N., Frankenberg, C., George, M., Nichitiu, F., Worden, J., Aben, I., Bowman, K.W., Clerbaux, C., Coheur, P.F., and De Laat, A.T.J. (2013). Decadal record of satellite carbon monoxide observations. Atmospheric Chemistry and Physics, 13(2), 837-850.

[147] Zheng, B., Chevallier, F., Yin, Y., Ciais, P., Fortems-Cheiney, A., Deeter, M.N., Parker, R.J., Wang, Y., Worden, H.M., and Zhao, Y. (2019). Global atmospheric carbon monoxide budget 2000–2017 inferred from multi-species atmospheric inversions. Earth System Science Data, 11(3), 1411-1436.

[148] Andela, N., Morton, D.C., Giglio, L., Chen, Y., van der Werf, G.R., Kasibhatla, P.S., DeFries, R.S., Collatz, G.J., Hantson, S., Kloster, S., and Bachelet, D. (2017). A human-driven decline in global burned area. Science, 356(6345), 1356-1362.

[149] Ahn, D. H., Choi, T., Kim, J., Park, S. S., Lee, Y. G., Kim, S. J., and Koo, J. H. (2019). Southern Hemisphere mid-and high-latitudinal AOD, CO, NO_2, and HCHO: spatiotemporal patterns revealed by satellite observations. Progress in Earth and Planetary Science, 6, 1-16.

[150] Hille, B. K. (2017). NASA Airborne Mission Chases Air Pollution Through the Seasons. NASA. (Accessed December 5, 2023). Link

[151] Toihir, A. M., Venkataraman, S., Mbatha, N., Sangeetha, S. K., Bencherif, H., Brunke, E. G. and Labuschagne, C. (2015). Studies on CO variation and trends over South Africa and the Indian Ocean using TES satellite data. South African Journal of Science, 111(9-10), 01-09. (Accessed December 5, 2023). Link

[152] Sinha, P., Jaeglé, L., Hobbs, P. V. and Liang, Q. (2004). Transport of biomass burning emissions from southern Africa. Journal of Geophysical Research, 109 (D20), 01-15. (Accessed December 5, 2023). Link

[153] Gloudemans, A. M. S., Krol, M. C., Meirink, J. F., de Laat, A. T. J., van der Werf, G. R., Schrijver, H., van den Broek, M. M. P., and Aben, I. (2006). Evidence for long-range transport of carbon monoxide in the Southern Hemisphere from SCIAMACHY observations. Geophysical Research Letters, 33(16), 01-05. (Accessed December 5, 2023). Link

[154] What are El Nino and La Nina?. Rainbow Resesrvoirs. (Accessed July 9, 2024). Link

[155] Meyers, G., McIntosh, P., Pigot, L., and Pook, M. (2007). The years of El Niño, La Niña, and interactions with the tropical Indian Ocean. Journal of Climate, 20(13), 2872-2880.

[156] Ummenhofer, C. C., Sen Gupta, A., England, M. H., Taschetto, A. S., Briggs, P. R., and Raupach, M. R. (2015). How did ocean warming affect Australian rainfall extremes during the 2010/2011 La Niña event?. Geophysical Research Letters, 42(22), 9942-9951.

[157] What are El Niño and La Niña?. National Oceanic and Atmospheric Administration. (Accessed July 9, 2024). Link

[158] Glantz, M. H. (2002). La Nina: An overview of the process. La Niña and Its Impacts: Facts and Speculation, 3-24.

[159] Rollenbeck, R., Orellana-Alvear, J., Bendix, J., Rodriguez, R., Pucha-Cofrep, F., Guallpa, M., Fries, A. and Celleri, R., (2022). The Coastal El Niño event of 2017 in Ecuador and Peru: A weather radar analysis. Remote Sensing, 14(4), p.824.

[160] Howard, E., Washington, R., and Hodges, K. I. (2019). Tropical lows in southern Africa: Tracks, rainfall contributions, and the role of ENSO. Journal of Geophysical Research: Atmospheres, 124(21), 11009-11032.

[161] Zhang, Y. (2011). Mean global and regional distributions of MOPITT carbon monoxide during 2000–2009 and during ENSO. Atmospheric environment, 45(6), 1347-1358.

[162] Detmers, R.G., Hasekamp, O., Aben, I., Houweling, S., Van Leeuwen, T.T., Butz, A., Landgraf, J., Köhler, P., Guanter, L. and Poulter, B., (2015). Anomalous carbon uptake in Australia as seen by GOSAT. Geophysical Research Letters, 42(19), 8177-8184.

[163] Shikwambana, L., and Kganyago, M. (2023). Seasonal comparison of the wildfire emissions in Southern African region during the strong ENSO events of 2010/11 and 2015/16 using trend analysis and anomaly detection. Remote Sensing, 15(4), 1073.

[164] La Niña. (2023). National Geographic. (Accessed July 9, 2024). Link

[165] What is ENSO?. National Weather Service. (Accessed July 3, 2024). Link

[166] Cook, A., Watkins, A. B., Trewin, B., and Ganter, C. (2016). El Niño is over, but has left its mark across the world. The Conversation, 26.

[167] Ferrer, N., Folch, A., Lane, M., Olago, D., Odida, J., and Custodio, E. (2019). Groundwater hydrodynamics of an Eastern Africa coastal aquifer, including La Niña 2016–17 drought. Science of the total environment, 661, 575-597.

[168] Glantz, M. H. (2001). Currents of change: impacts of El Niño and La Niña on climate and society. Cambridge University Press.

[169] What is El Niño's impact on Australia's weather and climate?. (2023). Climate Extremes. (Accessed July 3, 2024). Link

[170] Mason, S. J., and Jury, M. R. (1997). Climatic variability and change over southern Africa: a reflection on underlying processes. Progress in physical geography, 21(1), 23-50.

[171] Santoso, A., Hendon, H., Watkins, A., Power, S., Dommenget, D., England, M.H., Frankcombe, L., Holbrook, N.J., Holmes, R., Hope, P. and Lim, E.P. (2019). Dynamics and predictability of El Niño–Southern Oscillation: An Australian perspective on progress and challenges. Bulletin of the American Meteorological Society, 100(3), 403-420.

[172] Burton, C., Betts, R. A., Jones, C. D., Feldpausch, T. R., Cardoso, M. and Anderson, L. O. (2020). El Niño Driven Changes in Global Fire 2015/16. Frontiers in Earth Science, 8. (Accessed December 13, 2023). Link

[173] Null, J. (2023). El Niño and La Niña Years and Intensities. Golden Gate Weather Services. (Accessed December 13, 2023). Link

[174] L'Heureux, M. (2018). Overview of the 2017-18 La Niña and El Niño Watch in Mid-2018. Science and Technology Infusion Climate Bulletin, NOAA's National Weather Service, 43. (Accessed December 13, 2023). Link

[175] Verhegghen, A., Eva, H., Ceccherini, G., Achard, F., Gond, V., Gourlet-Fleury, S. and Cerutti, P.O. (2016). The Potential of Sentinel Satellites for Burnt Area Mapping and Monitoring in the Congo Basin Forests. Remote Sensing, 8(12):986. (Accessed December 13, 2023). Link

[176] Hyde, M. (2023) Australia now in El Niño climate pattern, increasing bushfire risk, BOM says. The Guardian. (Accessed December 13, 2023). Link